POLITECNICO DI MILANO
DEPARTMENT OF MATHEMATICS
DOCTORAL PROGRAMME IN
MATHEMATICAL MODELS AND METHODS IN ENGINEERING

STABILITY ANALYSIS IN SUSPENSION BRIDGES THROUGH SOME NEW MATHEMATICAL MODELS

Doctoral Dissertation of:
Alessio Falocchi

Supervisor:
Prof. Filippo Gazzola

Tutor:
Prof. Irene Maria Sabadini

The Chair of the Doctoral Program:
Prof. Irene Maria Sabadini

2018 – Cycle XXXI

Abstract

THE main object of study of this work is the mathematical modeling of suspension bridges. The motivations are multiple, first of all the fact that these structures manifested and manifests anomalous oscillations. Many observations throughout history have recorded that torsional instability afflicts suspension bridges, leading in some cases to the collapse of the structure. The most famous case, here studied in deep, is the collapse of the Tacoma Narrows Bridge in 1940, in which a sudden change from vertical to torsional oscillations led to the failure. In the scientific community there is not an unanimously accepted explanation about the origin of instability; there are many theories from vortex shedding to flutter, from structural instability to parametric resonance.

In this work we present three new isolated models for suspension bridges aiming to show that the torsional instability arises suddenly due to the nonlinear configuration of the structures. The energy given by the wind excitation is introduced in the system through the initial conditions, avoiding to consider the wind as an explicit external force and dealing with the problem from a different point of view. In general we proceed writing the total energy of the system and deriving from variational principles two nonlinear partial differential equations in space and time. Our unknowns are the vertical displacement and the torsional rotation of the deck, corresponding respectively to a harmless oscillation and to a very dangerous one. The system of differential equations is studied at first in terms of existence and uniqueness of a solution and subsequently performing numerical analysis on the approximated solution; as we will see the existence and uniqueness topic is not trivial at all due to the nonlinearities, hence we provide the full proofs in the most interesting cases.

Since the dynamics of a bridge is affected by many factors, like the oscillation of the deck, the slackening of the hangers, the displacements of the main cables..., we proceed step by step considering models with simplifications. At first we suggest a new nonlinear model in which the cables are fixed and the hangers are extensible to focus on the slackening mechanisms of the hangers; in particular, we model this phenomenon through nonlinearities as the positive part function and some variants. We find numerically the solution of the dynamical system, highlighting the instability phenomena with

respect to the modes and the mechanical parameters.

Then, inspired by the Melan equation we propose a second model for suspension bridges with two deformable cables linked to a deck, through inextensible hangers; in this case we overturn the simplification related to the first model. We prove existence and uniqueness of a weak solution and we perform some numerical experiments on the approximated solution; moreover, we propose a sensitivity analysis of the system by mechanical parameters in terms of torsional instability.

Aiming to propose more refined models we conclude this work presenting a third model for suspension bridges in which both the cables and the hangers are deformable, imposing the convexification of the cables. More precisely we show that, by inserting a convexity constraint on the cables of a suspension bridge, the torsional instability of the deck appears at lower energy thresholds. Since this constraint is suggested by the behavior of real cables, this model appears more reliable than the classical ones. Moreover, it has the advantage to reduce to two the number of degrees of freedom, avoiding to introduce the slackening mechanism of the hangers as an independent variable. The drawback is that the resulting energy functional is extremely complicated, involving the convexification of unknown functions. For these reasons the chapter devoted to this model is divided in two main parts. The first part focuses on the study of these functionals and provides some new results from calculus of the variations. The second part applies this study to the suspension bridge model with convexified cables, giving the proofs related to existence and uniqueness of a solution and performing different numerical experiments.

Our results display that there are specific thresholds of torsional instability with respect to the initial amplitude of the longitudinal mode excited, suggesting that the origin of the instability is hidden in the nonlinear behavior of structures.

Contents

CHAPTER 1

Introduction

SOME *fortuitous condition* is the justification invoked by Scanlan [68, p.209] to explain how in suspension bridges longitudinal oscillations suddenly switch into torsional ones. This explanation is quite emblematic of the uncertainties surrounding the strange behavior manifested by these structures. Their particular configuration seems to be prone to develop torsional oscillations of the deck, which can be catastrophic for the bridge; the most famous example is the collapse of the Tacoma Narrows Bridge occurred in 1940, known also thanks to the video on line [73]. This event burst a spark in the scientific community, that from the next years started to formulate hypothesis and theories on the incident.

The theme raises interest not only in the engineering community, but also among mathematicians and physicists. As we will see in Chapter 2, already two centuries ago, Navier studied the suspension bridges. Hence, a topic that may seem purely of civil engineering's interest, actually has notable mathematical implications. In the present work we will deal with problems of existence and uniqueness of a solution, problems of convexification and issues related to the stability of the solution; thus, topics often referable to the abstract sphere of the mathematics, here find on the background the modeling of a suspension bridge, through partial differential equations.

The setup of a reliable model appears quite demanding, because it has to be on the one hand simple enough to be mathematically tractable and on the other hand sufficiently accurate to describe the real bridge behavior. The modeling approach presented in this thesis has to be intended as a process that begins from simple situations and, step by step, goes towards more refined. We refer to the next sections to better understand our motivations and point of view.

1.1 Motivations

Bridges have always been a strategical infrastructure for the owners, facilitating social and economic development, as much as during the wars the destruction of a bridge could represent the isolation of a community, implying its decadence. For their importance and their sizes the bridges had a strong impact on the society and on the environment; although the remarkable progresses of the civil engineering in the nineteenth and twentieth centuries, the bridges also today collapse, manifesting problems often difficult to understand.

In [41] the author reports a database of collapses of bridges from 1444 to 2004, listing 347 cases of rail, road and foot bridges fallen; from this study it emerges that the 32% of the collapses happened during the construction stage, highlighting that most designers consider the in-service performance as the most important period, not studying enough the construction stage. Between the causes of the collapses the most common is the natural hazard (29.3%), followed by design errors (20.9%), large impacts (17.7%), overloading (9.9%), human errors (9.9%), limited knowledge (9.6%), deterioration (2.3%) and vandalism (0.6%), see [41] for details; the Tacoma Narrows Bridge case, that we will study in deep, see Section 2.3, is included in the category "limited knowledge", referring to the engineering lacunae on the topic. It is interesting to note that the overloading is a cause of failure common in the past, but nowadays very rare; this fact reveals the tendency to overbuild the bridges, in particular suspension bridges, after the shock provoked by the collapse of Tacoma. Obviously this database does not include all the bridges' failures, probably there are secret cases or events lost in the history, but it is alarming to see that the percentage of collapses due to human error and errors in design is similar in the past as today; it is worrying that 58 bridges on 237 collapsed between 1991 and 2004. These data and recent episodes, e.g. the collapse of Morandi Bridge in Genova (Italy) in August 2018, reveal how the problem is current and how the research has a fertile field of study.

The aim of this thesis is not to study in general bridges, but a particular kind: the suspension bridge; moreover, we study these structures from a mathematical point of view, proposing models able to simulate torsional instability phenomena, like those seen during Tacoma collapse. First of going in the details let us describe the structure of a suspension bridge in order to introduce the different models and the assumptions on which they are based.

1.2 The configuration of a suspension bridge

The main elements composing a suspension bridge are four towers, a rectangular deck, two sustaining cables and some hangers, see Figure 1.1. The hangers link the deck to the main cables, obtaining a structural configuration optimal to bear the weight of decks having long span. The most common suspension bridges have two minor side spans and a central main span; in this thesis we will focus on the behavior of the main span, that is usually juxtaposed independently to the others.

Such bridges are economical for span greater than 300m, while for shorter span is preferable to use cable-stayed bridges; this last have multiple inclined taut cables and they work in a considerably different way with respect to suspension bridges [62, §15.3]. The lightness, due to relatively small dead load, is one of the relevant economic

Figure 1.1: *The Golden Gate bridge.*

feature of the suspension bridges; as a result they are more suitable for highways rather than heavy railroads. At the same time the lightness could represent a drawback; in fact, structures very flexible are susceptible to vibrations and large deflections under live loads. This problem is considerable as much as many of these structures collapsed, revealing impressive oscillations. The study of such phenomena is a purpose of this thesis, that we pursue setting up three mathematical models.

1.3 Three isolated models for suspension bridges

It is out of doubt that in suspension bridges the wind is one of the principal source of disturb, provoking oscillations of the deck. Hence, the wind action may be a candidate of external forcing term in a model for suspension bridge; nevertheless our models are isolated, so that no forcing and damping are considered. The idea to neglect both structural and aerodynamic damping was suggested by Irvine [42, p.176] and was adopted for instance in [4,5,10]. In particular we suppose that the wind introduces energy in the structure through the initial conditions, without appearing explicitly. With these models we are able to show that longitudinal oscillations may switch rapidly into torsional ones, see Figure 1.2. The delicate choice to consider isolated model is motivated in

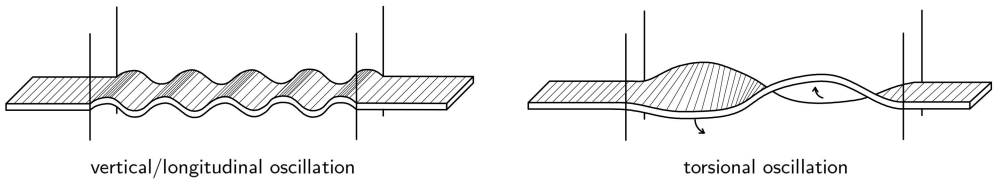

Figure 1.2: *Comparison between longitudinal and torsional oscillations of the deck.*

Section 3.1.

The set up of the models was conducted by a deep analysis of some collapses of suspension bridges. In Chapter 2 is reported a brief history of the suspension bridges and some meaningful collapses or episodes involving these structures. We give many information on the Tacoma's collapse, since on it there is a huge literature and we often use its mechanical parameters for the numerical simulations. Some precious witnesses and information are reported in Section 2.3; we will often refer to them to justify some

assumptions in modeling.

In this work we present three dynamical models for suspension bridges. Since they have some common features we devoted Chapter 3 to introduce and discuss the general approach and the common assumptions on the three models. In Section 3.2 we describe the so-called *fish-bone* model and we focus on the different choices of the cable shape at rest. We always consider two degrees of freedom, the vertical displacement and the torsional rotation and we highlight some questions related to the approximation of the nonlinearities. In particular, due to the geometric bridge configuration we face with the problem of the trigonometric functions' linearization. Especially in the engineering community this simplification is very common and is based on the assumption of the smallness of the torsional angle, see for instance [68]. In this work we do not perform this linearization and we comply with the real geometry of the problem.

In Section 3.2.2 we explain our general approach to the problem; for each model we write the total energy of the system and we derive from variational principles a system of nonlinear partial differential equations in space and time. We study existence and uniqueness of a solution and we seek a numerical approximation adopting the Galerkin procedure; we complete the numerical experiments finding the thresholds of torsional instability. We underline that a new mathematical explanation for the origin of torsional oscillations was given in [3] through the introduction of suitable Poincaré maps: these oscillations appear whenever there is a large amount of energy within the bridge and this happens due to the nonlinear behavior of structures. Due to the complexity of the equations that we do not linearize, in this work we do not follow strictly the theoretical definition of instability, but we consider a physical quantitative approach, referring to a definition introduced in [32], see Section 3.3.5.

The main results of the thesis are reported in Chapters 4, 5 and 6, corresponding respectively to the three different models for suspension bridge.

During the Tacoma bridge's collapse, the slackening mechanisms in the hangers were recorded. These phenomena assume a great importance with respect to the torsional instability of the bridge. Motivated by this fact in Chapter 4 we propose a new simplified nonlinear model for suspension bridges, in which we consider

the main cables fixed and the hangers extensible.

This choice is performed to concentrate our attention on the slackening mechanisms, modeling with different nonlinearities (positive part function and some variants) the elastic restoring force due to the hangers. We will see how the presence of deformable hangers affects the dynamic response of the suspension bridge in terms of instability; we perform different numerical experiments, carrying out a sensitivity analysis of the system by the mechanical parameters. These results are published in [28].

We point out that the choice to consider fixed cables is pretty unrealistic, but it represents our first necessary step in order to define a more complex and realistic model. In engineering literature is more common to consider the cables deformable and the hangers rigid, e.g. see [46]. As we will see also this assumption does not give totally realistic behavior, but we decided to study it in order to obtain some useful information. Hence, Chapter 5 is devoted to the study of a new nonlinear model in which

the main cables are deformable and the hangers are inextensible.

This model is inspired by the Melan equation and leads to a nonlinear nonlocal system of partial differential equations. In this case we state the results related existence and uniqueness of a weak solution, giving the complete version of the proof. In fact the presence of the nonlinearities makes challenging the uniqueness problem, that is proved in a wider functional space. In particular we obtain the latter result in a non-standard way, testing the equations with the "potential", i.e. with the Green function applied to the time derivative of the solutions. Then we found numerically thresholds of torsional instability, depending on the initial amplitude of the longitudinal mode excited, and we perform an analysis of sensitivity of the system by the parameters; these results are published in [27].

All these preliminary studies allowed us to set up a realistic model in which

the main cables are deformable and the hangers are extensible.

This model is presented in Chapter 6 and it can be considered as a final result of this modeling process step by step. The results in Chapter 6 are presented in [25].

The models in Chapter 4 and 5 manifested some drawbacks, for instance the cable shape in Chapter 5 may show nonconvex sections; this unrealistic behavior becomes more and more evident if the energy in the system (the amplitude of oscillation) is increased. In real bridges it is more probable that the slackening of the hangers occurs instead of the cables convexity's lost. Moreover, a nonconvex configuration would increase the energy and the tension of the cable, against the variational principle of minimization of the energy. For these reasons we assume here that the actual shape of the cables coincides with its *convexified shape*, namely the shape minimizing its length at the same loading condition.

Acting only on this geometric feature, we are able to maintain two degrees of freedom in the model and to consider the slackening of the hangers indirectly. The great advantage is that we do not need to find a nonlinearity simulating the slackening mechanisms. The drawback is that the convexity constraint leads to some technical mathematical difficulties. For these reasons the Chapter 6 is divided in two parts: the first is devoted to the study of functionals containing convexifications; the second part applies this study to the suspension bridge model with convexified cables.

In particular, in Section 6.1 we state some preliminary results related to convexification of functions in one variable. In Theorem 6.1.8 we compute the variation of functionals containing convexifications. This characterization is new and, in our opinion, of independent interest with possible applications to more general variational problems. The convexification makes the energy function non-differentiable: its variation yields a weak form of a *system of partial differential inclusions* (see (6.23) in Section 6.3.2) for which the uniqueness of the solution is not expected. However, by exploiting the peculiarity of the model, we are able to show that Galerkin approximation of the problem admits a unique classical solution, because the obstruction to the differentiability of the energy is ruled out in a finite dimensional phase space. This suggests to introduce the class of *approximable solutions* of the problem, namely solutions that are the limit of the Galerkin subsequences. This class of solutions will be physically justified and it will be shown that they are representative of the full problem; moreover, within this class we are able to obtain existence results. This requires some particular attention due to the convexification and to the unusual behavior of test functions.

A further purpose is to study the torsional instability of the deck through the model with convexified cables. To this end, we proceed numerically by introducing a new algorithm dealing with the convexification at the beginning of each temporal iteration. We then numerically show that the slackening mechanism hidden in the convexification of the cables yields energy thresholds of instability for high modes significantly smaller than in models where slackening is neglected. This means that *the slackening of the hangers must be taken into account because it gives lower thresholds of torsional instability*.

CHAPTER 2

Historical notes on suspension bridges

THE mathematical modeling of suspension bridges is a challenging topic that has to take roots in real observations. The reproduction of scaled models in laboratory is a way, but some simplifications are necessary, first of all the rescaling of the structure and of the actions applied; this is a drawback with respect to the study of physical phenomena that can be exactly reproduced in lab experiments. For large and complex structures such as suspension bridges, the history is surely an important source from which to draw information.

It is undeniable that these engineering works always aroused a strong appeal in humans, so that on the topic are available reports, paintings, reliefs and videos; each witness is aligned with the means of its time and tells us something that can be useful for the mathematical modeling purpose.

In this chapter we survey several historical events, focusing mainly on the Tacoma Narrows Bridge (TNB) collapse, that represents a key event in the study of the instability phenomena afflicting suspension bridges; many information like videos, reports, precise measurements are available on the TNB and the scientific community provided different theories and hypothesis on its collapse.

We refer to [34] for a detailed survey on the history of suspension bridges and meaningful collapses.

2.1 Evolution of the cable-suspended structure

The origin of the concept of bridging spans with cables, sustaining the deck through their strength in tension, is lost in the history. Early cable-suspended bridges were made by ropes formed twisting vines, whose ends were attached to trees or other fixed elements located on the edges of the obstruction to cross. The deck hung to the cables,

was probably in rough plank. We found this kind of structures in remote ages in China, Japan, India, Tibet and New Guinea; it was used by the Aztecs of Mexico and the Inca of Peru, but these first examples were unknown to western civilizations until the end of the medieval period, when the well known explorations started [62].

The Venetian engineer Fausto Veranzio (1551-1617), also trained in mathematics at the University of Padua, is considered by C. L. M. H. Navier [56] the inventor of the modern suspension bridge. In 1595 he published the treatise *Machinae Novae*, anticipating scientific and technological advances that will characterize the Industrial Revolution; in the work we find the paintings of an iron bridge, *Pons Ferreus*, representing a mixture between a suspension bridge and a cable-stayed bridge, and of the *Pons Canabeus*, a bridge with two cables and some hangers linked to a deck, very similar to the modern suspension bridges.

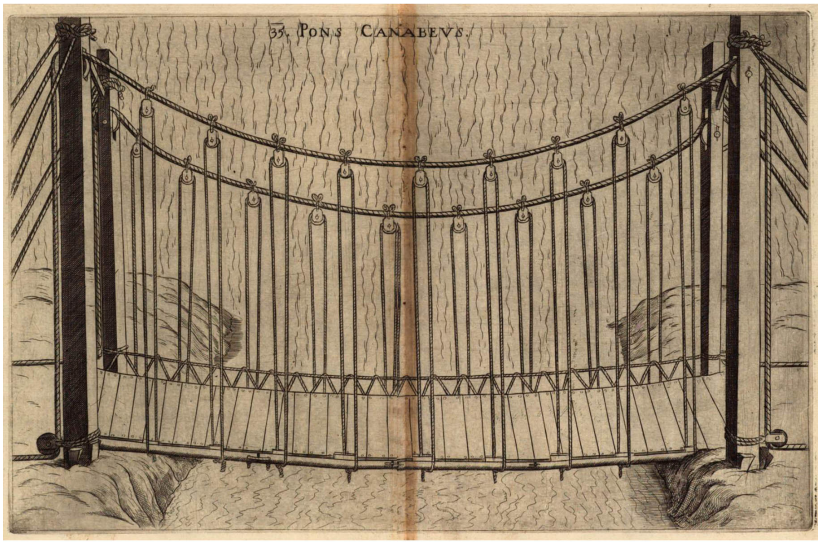

Figure 2.1: *Design of Pons Canabeus, in which the pulleys sustain with ropes the wooden deck.*

The designs of Veranzio were not built and we have to wait until 1734 to see the first metal suspension bridge in Europe; the project was realized by the Saxon army, using iron chains, to cross the Oder River at Glorywitz for military reasons.

The first metal suspension bridge in North America was the Jacob Creek Bridge, erected in Pennsylvania in 1801 by the Irish engineer Finley (1756-1828), inspired by Veranzio's drawings; in this case wrought iron chains were used to sustain the span of about 21 meters in timber planks with anchorages and towers completing the structure as in modern bridges. Finley became a pioneer in this field and its innovations were taken up and extended in Britain by Samuel Brown, a retired naval captain, who introduced the most efficient shape for the iron links in a cable for suspension bridge [19]. Brown became a leading builder of these structures and, consequently, during the nineteenth century several suspension bridges were built in Great Britain.

The importance of the Great Britain in this field is manifest when the prestigious *École des Ponts et Chaussées*, encouraged by the French government to study the development of suspension bridge technology, looked to Britain. For these reasons Navier, that was professor at the *École des Ponts et Chaussées*, visited Britain twice in 1821 and 1823. From these investigations he wrote the book [56], in which we found for the first

time the analytical and abstract approach of the mathematician to the topic. In 1823 he designed the *Pont des Invalides*, the first monumental suspension bridge in Paris, see Figure 2.2; the bridge had not a lucky ending, indeed, it developed a crack just before

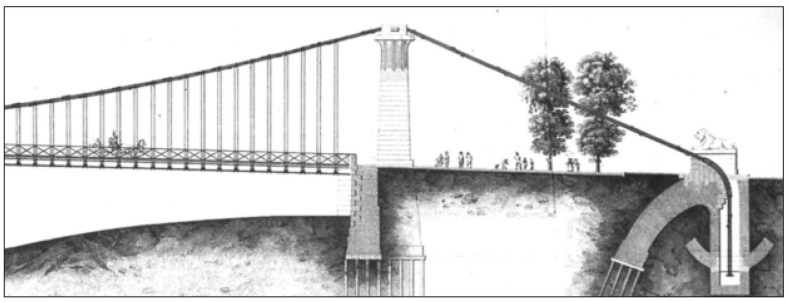

Figure 2.2: *Anchorage details of the Pont des Invalides designed by Navier. Source: [56].*

the opening, and Navier was accused to be *too much of a theoretical mathematician* and not *practical* as British builders, for details see [19, 58].

To be honest also British suspension bridges presented some problems; from 1818 and 1889 ten suspension bridges manifested damages or collapsed due to windstorms or overloading, see [29, Table 1, p.13]. We point out that in these years cable-stayed bridge or hybrid solutions between suspension and stayed arose, but these bridges had as much problems that Navier, in [56], condemned the use of cable stays; hence, the conventional suspension bridge was dominant until the latter half of the twentieth century.

In 1825 the Séguin brothers experimented the cables instead of the chains and they applied this technique to the *Pont de Saint-Antoine* in Geneva. L. J. Vicat studied the Séguin's technique analytically for the *École des Ponts et Chaussées* and with a publication in 1831, he inaugurated the golden age for suspension bridges in France, recommending to use wires instead of iron bars for the cables; in the next ten years one hundred of these structures were built in France [31]. The idea of drawn wires spread out quickly and it was adopted to solve problems of vibration in the Menai Straits Bridge (1826), the longest span bridge in the world at the time, interlinking Wales and Anglesey island. In 1842 J. Roebling registered a patent to produce cables twisting wires and he retrieved the principle of using stays to support the vertical hangers in the bridge superstructure. Roebling's technique is evident in the Niagara River Railway Carriage Bridge (1847), the first bridge capable to carry rail traffic, and in the Brooklyn Bridge in New York (1883), having the supremacy for the longest main span (486.3m) for 20 years.

Between the 19th and 20th century, thanks to the improvement of the technologies, materials and constructive techniques, the suspension bridges increased their length more and more. We mention the Golden Gate Bridge in San Francisco (1937) still present nowadays, that maintained for 27 years the record of the longest main span (1282m), representing the prototype of suspension bridge in the North American tradition. In the recent years other countries achieved excellent results in building suspension bridges; we refer to Scandinavian countries, intentioned to connect Norway coastal fjords with an ambitious program based on many suspension bridges, and eastern countries like China and Japan. The world records in the length of main span is

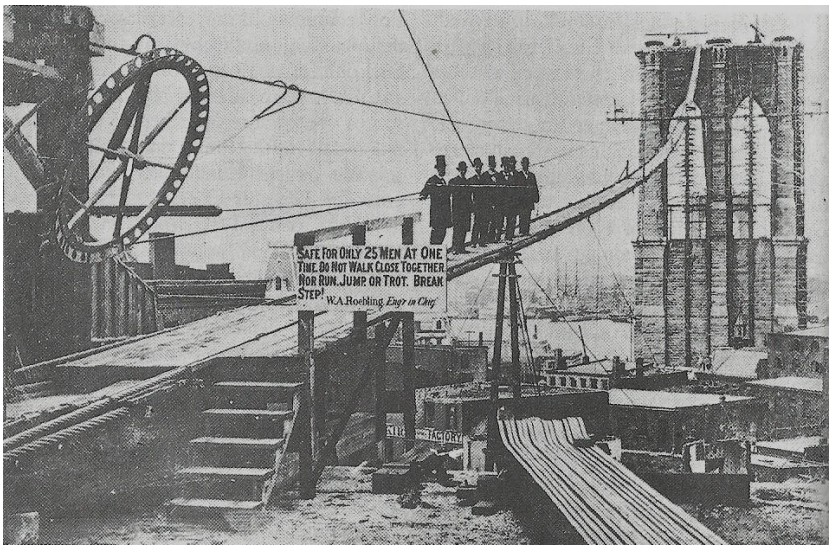

Figure 2.3: *Brooklyn Bridge, during the stage of wires' twisting in 1877. Source: [31].*

held today by Akashi Kaikyo Bridge in Japan (1991m) concluded in 1998, that broke the Danish record of the Storebæltsforbindelsen bridge of 1624m.

Altough nowadays the suspension bridges are quite safe, their performing configuration is the result of past errors, continuous improvements and experiments with different materials and technologies. From one hand these big structures continues to exert attraction in the human due to the engineering challenge implied, on the other, during the history, humans had to deal with their strange behavior, sometime unintelligible; the case of the Tacoma Narrows Bridge is emblematic and the debate to find the explanation of the collapse is still open. The next section is devoted to the description of collapses of some bridges through direct witnesses, very useful to set up the mathematical modeling.

2.2 Some collapses of suspension bridges

In literature there are many examples of collapses of suspension bridges; in this section we comment some cases, relevant from our point of view. The reasons of the collapses can be different, from windstorms to external resonance etc.

Theoretically we have external resonance if the natural frequency of the structure coincides with the frequency of the forcing term; in [34, p.4] the author observes that this phenomenon can occur if the external *force is somehow able to adapt itself to already existing oscillations*. If the wind is the forcing term is very unlikely that there is a perfect matching between the frequency of the structure and the continuously variable frequency of the wind. This circumstance can be realistic if we have other forcing terms, for instance the men's step with a certain rhythm.

In 1831 the Broughton Suspension Bridge, close to Manchester, collapsed after only 5 years from the building, due to the resonance caused by troops marching in step over the bridge. Although there were not victims, 40 men fell into the river and the British Army imposed that troops have to *break step* when passing over a bridge. This warning must have had effect on the successive generations of bridge builders, as much as we

found it in the signboard applied by Roebling on the catwalk for the building of the Brooklyn Bridge, see Figure 2.3.

A battalion of French soldiers caused the collapse of the Angers Suspension Bridge in 1850, killing 226 of them and inducing the abandon of the suspension bridges in France in the following years. In this case the bridge was oscillating due to thunderstorm and the troops involuntarily marched with the same cadence of the structure, developing the resonance effect.

The history is rich of examples of bridges having problems due to the pedestrian motion until today; in 2000 all the newspapers spoke about the closure of the London Millennium Bridge during its inauguration, since it started to sway when the crowd passed over it. As for the Angers Bridge, the pedestrians fell spontaneously into step with the oscillations of the structure, acting as negative dampers, i.e. injecting energy in the bridge. The problem was solved adding positive dampers that mitigated the swaying.

Surely the wind is, in the most of the cases, the major problem for the suspension bridges. The Brighton Chain Pier, built in 1823, was destroyed by windstorms twice

Figure 2.4: *J. M. W. Turner, Brighthelmston, Sussex, 1824, watercolor on paper, Royal Pavillon & Museums, Brighton & Hove.*

in 1833 and in 1836, after the rebuilding; it was one of the earliest bridges in Great Britain and it was designed by Brown to provide a landing stage for larger vessels crossing the Channel to Dieppe. As other suspension bridges aroused admiration in the contemporary society at the point that two of the most influent romantic painters, John Constable (1776-1837) and William Turner (1775-1851), sketched it in different views, see Figure 2.4. About the second collapse there is an important witness of the British Royal engineer Col. William Reid, who assisted at the event and wrote about different oscillations, including a torsional one. Figure 2.5 is a meaninful sketch of the engineer representing the moment before and after of the disaster.

The Menai Straits Bridge is coeval to the Brighton bridge and the project, due to Thomas Telford, had a huge impact on the English engineering, determining the birth of the *Structural Engineering*. Anyway in 1839 a hurricane destroyed it, provoking unexpected oscillations; about the episode Provis [64] wrote about an oscillation combining vertical and torsional motions:

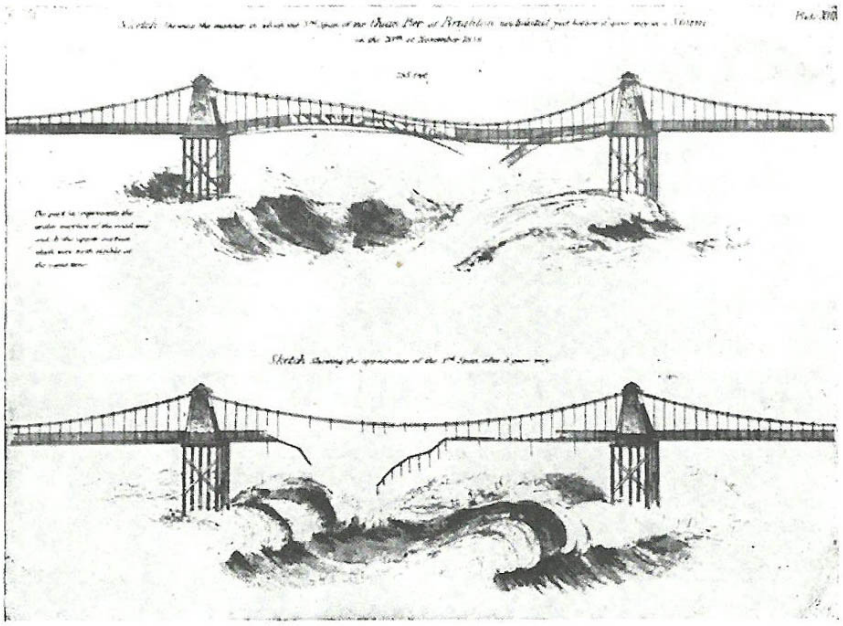

Figure 2.5: *The failure of the Brighton Chain Pier (1836) reproduced by W. Reid.*

> The movement of this undulatory wave, however, was oblique with the lines of the bearers and their suspending rods as well as with the general direction of the bridge.

In his report Provis pointed out that the bridge would have withstood to vertical oscillations, but during the collapse there were also other kind of oscillations: the torsional ones; he attributed to the vertical and torsional oscillations respectively the adjective *expected* and *unexpected*.

Another collapse due to windstorm concerns the Wheeling Suspension Bridge, erected in West Virginia in 1849 and destroyed 5 years later. We mention this bridge because there is an interesting description of the event on "The Intelligencer" of May 18-th, 1854; here, there is a clear reference to a torsional (*twisted and writhed*) motion and to a temporal time lapse of *only two minutes*, related to the sudden change in the oscillation. From this description we get an information that will be crucial for our simulations:

the change from vertical to torsional oscillations is sudden.

This anomalous behavior is also common for more recent bridges, for instance, the Tacoma Narrows or the Matukituki Bridge, collapsed respectively in 1940 and 1977. The Matukituki Bridge was a small suspension footbridge built in New Zealand that was destroyed by a gale; in [42] the author reported about its collapse that

> ...the deck persisted in lurching and twisting wildly until failure occurred, and for part of the time a node was noticeable at midspan,

highlighting a torsional oscillation following the second torsional mode, i.e. the mode manifesting a node in midspan, see Section 2.3.

About the Tacoma Narrows Bridge collapse we devote the next full section to the description of its failure, since it is emblematic in this research field and the amount of information is relevant for our modeling choices.

2.3 The Tacoma Narrows Bridge case

The Tacoma Narrows Bridge (TNB) was a suspension bridge with a center span of 853.44m and two sides span of 335.28m. The two towers of 128.2m in height were grounded on two piers, having a size in plan of about 20mx36m, while each cable of 43.49cm of diameter, consisted of 19 strands of cold drawn galvanized wires. The cables were hung in correspondence of the towers at 78.36m of height and had a sag of 70.71m, so that the sag-span ratio was equal to 1/12; the hangers were spaced of 15.24m and each one consisted of 4 ropes having 3.18cm of diameter. The deck of total width of about 12m was composed by steel stiffening girder with traverse floorbeams, 5 lines of longitudinal stringers spaced 1.75m and a roadway slab on the top of 13.34cm, see Figure 2.6 and [2, p.11-13].

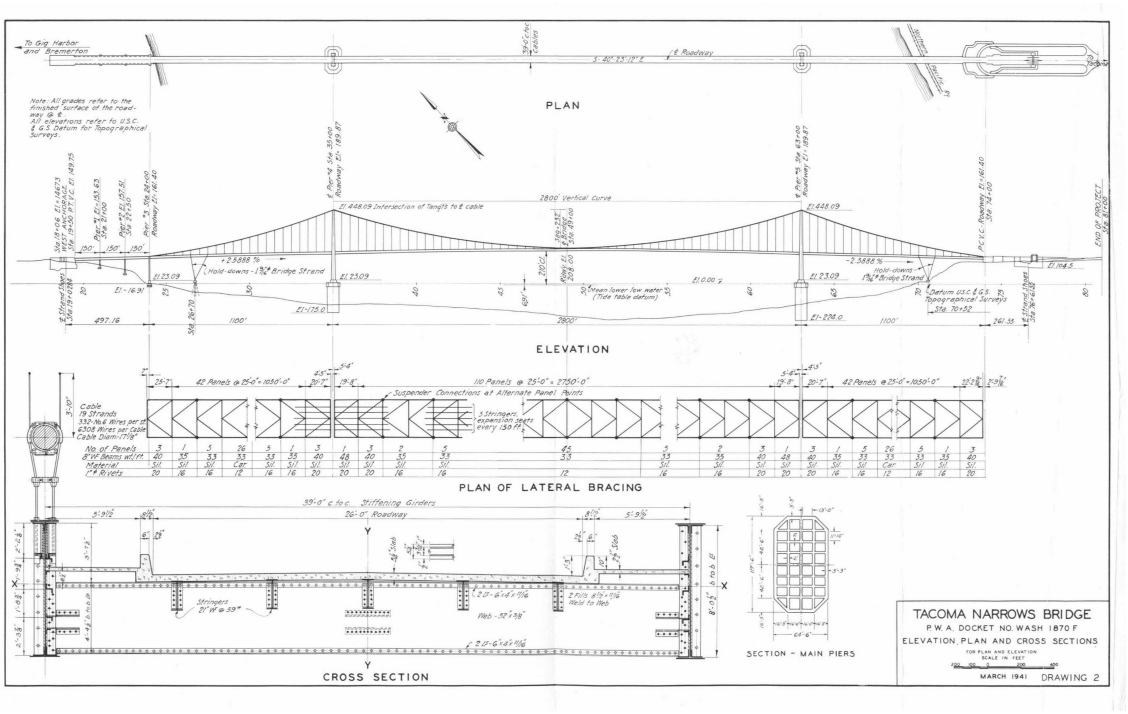

Figure 2.6: *Sketches of TNB. From above the plan, the front elevation, the scheme of the deck's girder, the cross section of the deck and the pier. Source: [2].*

The bridge was designed by Leon Solomon Moisseiff to cross the Tacoma channel dividing the cities of Tacoma and Gig Harbor in the state of Washington; it was built from 1938 and 1940 and collapsed just a few months after its opening. The structure began to oscillate even during the last stages of the construction, so that it was renamed *Galloping Gertie*. To mitigate this phenomenon were introduced oblique wires at the center linking the deck to the cables and hydraulic jacks connecting the deck to the towers. Nevertheless it never stopped to oscillate, also after the opening on July 1st, 1940; in order to stabilize the bridge were carried out some experiments in the wind tunnel, while the structure was monitored with a series of readings. The results of monitoring were annotated in a systematic way, so that many information are available on this bridge; most of them are reported in [2], the Official Report produced for Public Works Administration by the engineers O.H. Ammann, T. von Kármán and G.B. Woodruff,

representing our main source.

In the sequel we refer some meaningful witnesses related to the TNB collapse; when we speak about the n-th mode, we refer to a motion with $(n-1)$ nodes, in which the latter are the zeros of the corresponding sine function $\sin\left(\frac{n\pi}{L}x\right)$ for $x \in (0, L)$ and L is the main span of the bridge. In Figure 2.7 is reported a drawing attached to [2] in which the different oscillations of the bridge were annotated and classified; in the picture the nodes are highlighted.

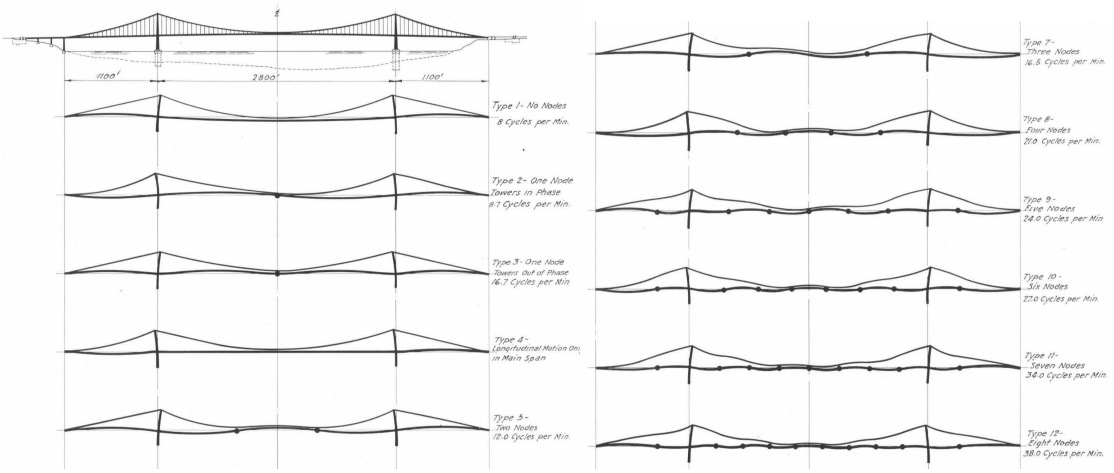

Figure 2.7: *Different oscillations recorded at the TNB with the nodes in evidence. Source: [2].*

From [2, p.28] we know that

> seven different motions have been definitely identified on the main span of the bridge [...]. (W1)

The most common appears to be the 2 nodes mode, like a $\sin\left(\frac{3\pi}{L}x\right)$. From the letter of Mr Durkee, project engineer, [2, p.28] we know that the days before the collapse

> Motions of considerable magnitude, having amplitudes as high as 48"[1.22m] with frequencies of 16 per minute, have been observed [...]. Amplitudes as high as 60" [1,52m] [...], have been observed. (W2)

November 7th, 1940, the morning of the failure around 8:30 a.m. the bridge appeared to behave in the customary way, but around 10:00 a.m. a violent torsional movement started, see Figure 2.8. That day the wind velocity was about 80km/h [29, p.23], almost one half the wind velocity of design (161 km/h). In [2, p.29] the authors wrote

> the center span was oscillating with either 8 or 9 nodes [...]. There appears to have been no instrumental measurement of the amplitudes [...], at 10:00 A.M. the center span developed a torsional movement with a node at mid span. [...] At the quarter points, the angle of rotation was observed as nearly 45 degrees each way. (W3)

Farquharson, a witness of the collapse, confirmed the presence of the second torsional mode [2, V-2]

> a violent change in the motion was noted. [...] the motions, which a moment before had involved a number of waves (nine or ten) had shifted almost instantly to two [...] the node was at the center of the main span and the structure was subjected to a violent torsional action about this point. (W4)

Figure 2.8: *Torsional oscillation of TNB seen from a tower. Source: [2].*

In [71, p.21] a detailed analysis on the TNB was performed by Smith-Vincent that wrote

> The only torsional mode which developed under wind action on the bridge or on the model is that with a single node at the center of the main span. (W5)

The torsional oscillation developed suddenly from vertical oscillations, it reached an amplitude of 45 degrees that led to the collapse, without victims, around 11:00 a.m., see Figure 2.9. From this description we learn that

vertical and torsional oscillations are not independent.

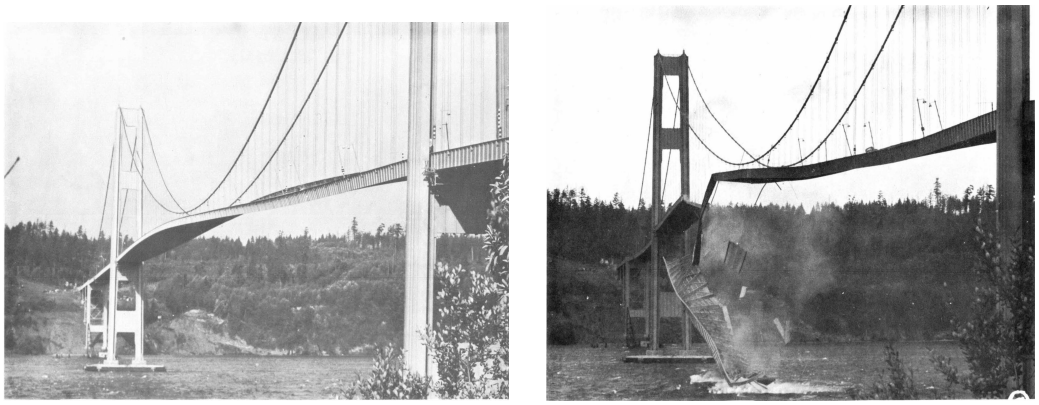

Figure 2.9: *Torsional oscillations of TNB on the left and the collapse of the main span on the right. Source: [2].*

We point out that Rocard in [65, p.99] wrote

> the oscillation of the Tacoma Bridge then corresponded exactly to Lt.-Col- Reid's description of the Brighton Chain Pier,

confirming a general attitude of suspension bridges to develop torsional instability.

Beyond the excited modes, the report gives us further information related to the modeling of the hangers, which are typically designed to withstand only traction; we

will see that the possibility of hangers' slackening is relevant in torsional instability phenomena. We report some comments focusing on this issue; Arkin [2, V-12] wrote that

> However, at two points one of the four suspenders in its group was permanently slack. (W6)

and again in [2, p.31]

> This slackness permitted greater amplitudes of the relative motions between the cable and the suspended structure. (W7)

The collapse of TNB provoked a strong shock in the engineering community; the Moisseiff's design was analyzed, but relevant mistakes were not found. The Official Report [2] did not provide a definitive explanation on the collapse and it reported that

> The Tacoma Narrows Bridge was well designed and built to resist safely all the static forces, including wind, usually considered in the design of similar structures.

This fact revealed that something in the behavior of suspension bridges was not understood, so that many scientists began to study the phenomenon proposing different theories.

2.4 After the Tacoma Narrows Bridge

The TNB collapse triggered different reactions in the research field and in the design practice of suspension bridges. In the first case there were many attempts to explain the anomalous behavior recorded the day of the collapse, while in the design practice a tendency to overbuild structures diffused to get rid of the problem. We organize these different topics in the following subsections. We refer to [34, pp.21-36] to further details.

2.4.1 Some explanations on the Tacoma Narrows Bridge collapse

The main supposed causes of the TNB collapse are essentially 5: structural failure, external resonance, vortices, flutter and parametric resonance.

Structural failure

We have already said that Moisseiff, the designer of TNB, is not deemed guilty for the disaster. Its project was son of its time and of the lack of knowledge in dealing with dynamical phenomena. Nevertheless several people considered structural the cause of failure.

They accused a cable band that slipped out of place at mid span to be responsible of the twisting, since its loosening generated lateral asymmetry, see [48, 60, 61]. In particular, W.F. Miles of the Pacific Bridge Company [2, V-14] noted during the collapse that the diagonal ties attached to the north midspan cable band were alternately slack and taut, provoking snap loads to the cable band, see Figure 2.10.

This explanation was not unanimously accepted, because the structural failure is viewed as a consequence of the dynamical instability, instead of the primarily cause

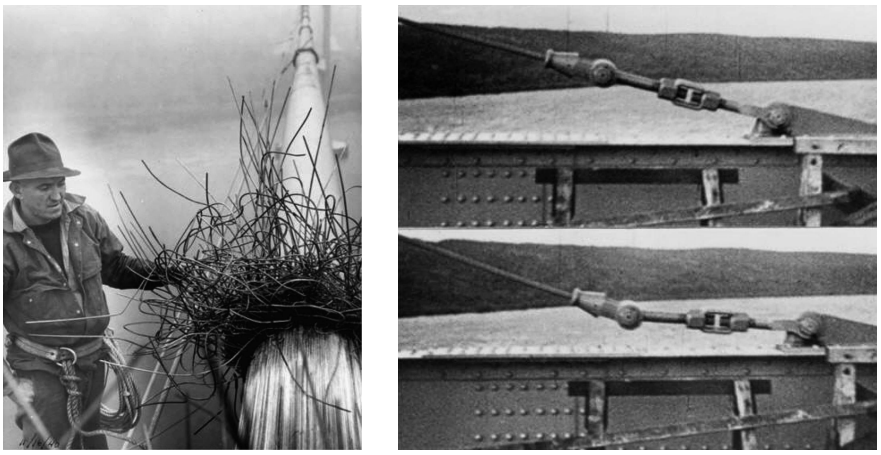

Figure 2.10: *On the left broken cable's wires at north cable band. On the right taut (top) and slack (bottom) of midspan tie just before torsion. Source: [60].*

[65]. Moreover it is not probable that a particular event of such type affected other suspension bridges that showed torsional instability, see Section 2.2.

External resonance

Resonance is the motivation attributed to the collapse by New York Times of November 9-th, 1940, comparing the TNB to a pendulum. From a physical point of view to reach the resonance condition it is necessary a perfect match between the natural frequency of the wind and that of the structure. But the wind is a random action, acting generally without precise rules,

> ..."gusts" and "gale" do not connote any well-defined periodicity,

wrote Billah-Scanlan [12, p.119]. In [44] the mathematicians Lazer-McKenna stated that

> the phenomenon of linear resonance is very precise. Could it really be such precise conditions existed in the middle of the Tacoma Narrows, in an extremely powerful storm?

Surely the media and society interest on the TNB encouraged the diffusion of wrong information as the attribution of the collapse to resonance effects. Anyway, if in bridges destroyed by the marching of the troops this principle may have a sense, see Section 2.2, for the TNB is very unlikely.

Vortices

In fluid dynamics, vortex shedding is a possible candidate in the periodicity of the wind. It takes place when a fluid flows past a bluff body, as TNB deck's cross section, at certain velocities, depending on the size and shape of the body; the term bluff must be understood as opposite of streamlined. Von Kármán vortex street arises when the wakes are characterized by alternating low-pressure vortices on the roadway's downwind side, generating consequently a movement of the bridge towards the low-pressure zone, the so-called vortex-induced vibration. The oscillations become self sustaining and the structure begins to resonate when the frequency of vortex shedding are equal to that of the bridge.

Vor Kármán deemed that the TNB collapse was due to these vortices, but Billah-Scanlan [12] demonstrated that the torsion oscillation of the bridge was wholly out of sync with the vortex shedding frequency. Moreover, the vortex trail is considered as a consequence of the motion, since the wind would modify its behavior following the oscillation of the deck, see [12, 65].

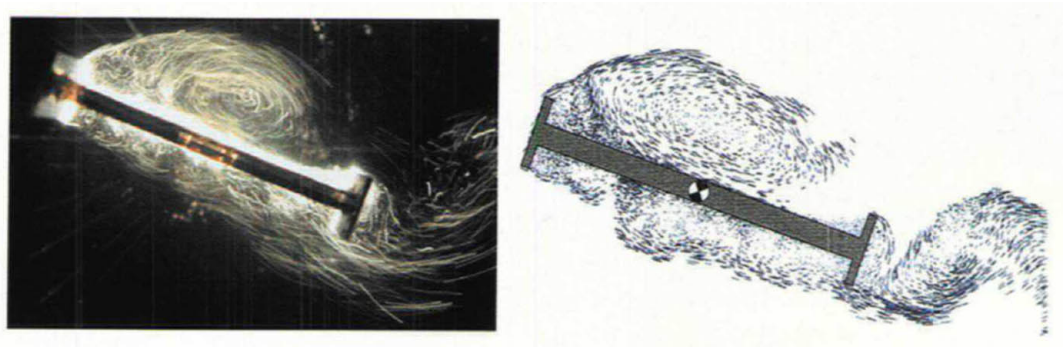

Figure 2.11: *Vortices on TNB deck's cross section. Comparison of water-tunnel experiments (hydrogen-bubble visualization) and numerical simulation performed by Larsen. Source: [43].*

This theory was recently reintroduced by Larsen [43], rousing great success in engineering community. In [43, p.245] he wrote

> The key to the torsion instability mechanism is the formation and drift of large-scale vortices on the cross section. A discrete vortex simulation of the flow around a simplified model of the Tacoma Narrows section shape, in which the angle of attack changes stepwise from 0 to 10°, highlights the cortex dynamics involved.

Although the Larsen's work received the "Outstanding Paper Award" by IABSE Journal Structural Engineering International, some doubts on it raised; the main criticisms struck the limited range of wind speeds considered and the range of variation of the wind's angle of attack.

Flutter

Flutter is a form of dynamic instability that involves elastic structure in a fluid flow; the first studies on flutter instability were performed on aircraft wings. To have a simple idea of the phenomenon we can think to the waving of a flag, that occurs over a certain wind velocity. Bleich found a connection between suspension bridges and aircraft wings and he defined the flutter speed in this way [13, pp.246-247].

> With increasing wind speed the external force necessary to maintain the motion at first increases and then decreases until a point is reached where the air forces alone sustain a constant amplitude of oscillation. The corresponding velocity is called the critical velocity or flutter speed.

In a linear system, the flutter point is when the structure undergoes a simple harmonic motion, in which the net damping is zero. Net damping is understood as the sum of the structural positive damping and that negative of the aerodynamic force. If net damping decreases a self-oscillation arises, leading possibly to the failure.

A precise way to calculate the critical speed of the wind was suggested by Rocard, that applied its procedure to TNB, finding a good agreement between the theoretical value of flutter speed and the wind recorded the day of the collapse, see [65, p. 158].

Other formulas were proposed by different authors to compute the critical velocity; some time before, Theodorsen suggested the circulation function [75] to determine flutter coefficients. Bleich commented that Theodorsen's results were obtained assuming small oscillations and concluded to apply them to find flutter speed [13, p.248]. Also Scanlan [67, p.841] and other authors were interested in studying the phenomenon assuming small torsional oscillations, even if the witnesses on the TNB collapse always described **large torsional oscillations**, see [73].

Anyway the main trouble in studying flutter is that is given by a combination of many phenomena, so that the set up of a generally valid formula is not thinkable. Today the flutter speed is determined by experiments in wind tunnel on scale models.

Parametric resonance

Around 1960 the Russian mathematicians Malkin, Krein and Yakubovich introduced the so-called parametric resonance, that it was applied by Yakubovich and Pittel to TNB [59]. They described the bridge with two degrees of freedom, the vertical displacement and the torsional angle, and then they set up two equations coupled through the wind speed; in correspondence of a particular value of this velocity, i.e. the flutter speed, the torsional and vertical frequencies are coincident, so that the parametric resonance occurs. This phenomenon stands out from external resonance because the wind's chaotic action is regularized within vortices, dealing with a periodic forcing.

Yakubovich [78, Chap. VI] concluded that an explanation to the TNB problem was found, but other scientists did not agree; Scanlan [67], for instance, wrote that the parametric resonance added further confusion to the explanations on the TNB collapse.

2.4.2 New tendencies in suspension bridge design

After the collapse of the TNB the tendency to design light decks was abandoned and the stiffened decks were preferred. Steimann in [72] wrote

> It is more scientific to eliminate the cause than to build up the structure to resist the effect.

The new TNB is an example, see Figure 2.12 on the left; today is a twin bridge with stiffened trusses, in which to the first bridge, opened 1950, was added further lanes in 2007.

We point out that the deck's stiffening technique gave good results also before the collapse of the TNB; for instance, the Golden Gate Bridge opened in 1937 is still present and has a strongly stiffened girder, see Figure 2.12 on the right. Although showed important oscillations during its life, the Golden Gate Bridge is largely considered one of the most important example of applied engineering. The Golden Gate case witnesses that the trusses do not solve completely the problem. Anyway, to see large and dangerous torsional oscillations might be necessary an *optimal wind for a sufficient period of time*, see [29, p.13], i.e. a very large (unrealistic?) input of energy.

The return to flexible solution for the decks occurred after that aerodynamics improved its knowledge in structural engineering; more recently the bridge designers adopts aerodynamic decks, in which the optimal shape is obtained also through tests in wind tunnel.

Anyway McKenna in [51, p.2] wrote

> ...to remove the offending behavior is not the same as mathematically understanding its cause.

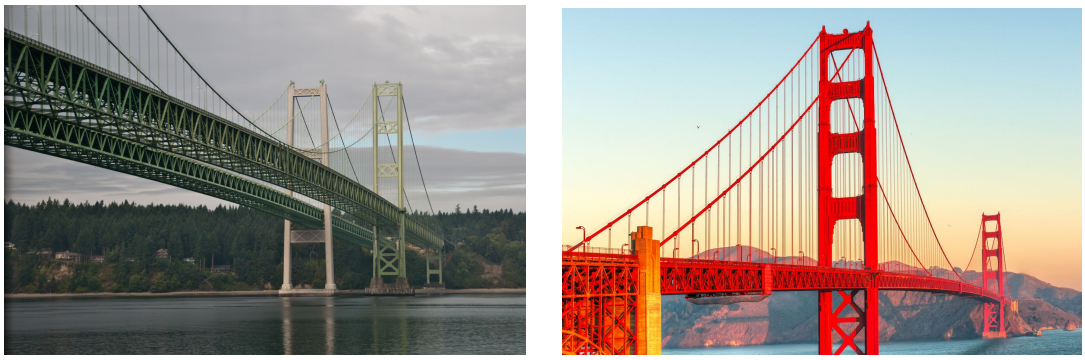

Figure 2.12: *The new twins Tacoma Bridges (1950 and 2007) on the left and the Golden Gate Bridge (1937) on the right.*

This sentence is meaningful from our point of view and for the aim of the thesis; hence, we devote the next section to outline some issues, concerning the previous information, fundamental for our mathematical models.

2.5 A new approach to deal with the problem

From the events described in Sections 2.1, 2.2 and 2.3 we learn that in suspension bridges large torsional oscillations can arise, almost instantaneously, from large vertical oscillations. In Section 2.4 we revised some explanations, but none of them is considered unanimously conclusive and the question "why do vertical oscillations switch suddenly into torsional oscillations?" remains.

A new mathematical explanation for the origin of torsional oscillations was given in [3–5, 34], using in an alternative way the previous information and assuming a different point of view in the modeling; the authors attributed the origin of the torsional instability to the **nonlinear configuration** of the suspension bridge's structure. In [3] they studied an isolated simplified model through the introduction of suitable Poincaré maps: these oscillations appear whenever there is a large amount of energy within the bridge. The very same conclusion was subsequently reached in more sophisticated models [4, 5, 10, 20] and also in the models that we present in this thesis [25, 27, 28].

It is clear that in absence of wind, the deck does not move, but, when the wind hits a bluff body, asymmetric vortices appear; this asymmetry produces a forcing lift and the rise of vertical oscillations, manifesting the so-called vortex shedding. We underline that the phenomenon related to vortex shedding is shared by the whole scientific community, e.g. see [43].

Hence, it is possible to consider isolated systems for a sufficient small interval of time, so that the structural damping balances the forcing term; then, we introduce the wind energy through the initial conditions. More precisely, we initially apply a certain amplitude of oscillation on a vertical component to see if there is a transfer of energy on the torsional components, assumed initially small. In this way our models include the wind through the vortex effect not as a traditional forcing term, but as a source of energy, that does not appear explicitly. In Chapter 3 we will come back on the topic, providing more details to better understand this modeling approach.

CHAPTER 3

Main features and assumptions on the models

In this chapter we present some common features of the three models, to avoid repetitions in the sequel. The most relevant assumptions are highlighted in bold. Since our models are isolated, we better motivate this fundamental assumption, relating the issue to the numerical experiments that we carry out.

In general, the analysis of each dynamical model is performed following the next steps:

- Introduction of mathematical or engineering preliminaries;
- Definition of the degrees of freedom (DOF) of the model;
- Computation of the total energy of the system;
- Derivation of a system of partial differential equations (PDEs) from variational principles;
- Study of existence and uniqueness of a solution;
- Search of an approximated solution through numerical methods, in the finite dimensional setting (Galerkin procedure) and definition of the instability thresholds;
- Comments on the instability thresholds and comparison with other models.

Throughout the thesis we denote the derivatives of a function $f = f(t)$ (depending only on t), of a function $g = g(x)$ (depending only on x) and the partial derivatives of a function $w = w(x,t)$, respectively by

$$\dot{f} = \frac{df}{dt}, \qquad g' = \frac{dg}{dx}, \qquad w_x = \frac{\partial w}{\partial x}, \quad w_t = \frac{\partial w}{\partial t},$$

and similarly for higher order derivatives.

3.1 The reasons why we deal with isolated models

In this section we argue the choice to consider isolated systems, without forcing and damping terms, that represents the basic idea of our models. First of all let us recall some issues on the wind.

The classical theories distinguish the wind action in steady and unsteady forces, in which the first ones act on the structure in a uniform wind stream, while the second ones result from the variation of the velocity and the direction of the wind or from a non uniform motion of the structure. The modeling difficulties are related to this latter contribute, also known as dynamic component of the wind, that, due to the natural turbulences, is difficult to predict both in terms of angle of attack both in terms of peaks of the velocity fluctuations. From [2] we know that in the design of the TNB the static wind forces were considered, so that the bridge would have borne the wind in the horizontal direction until about 48 m/s; the day of the TNB collapse a sensor on the bridge measured the wind with a velocity very lower, equal to 19 m/s.

This fact rouse great amazement and suggested that something else had to be considered in the dynamics of the suspension bridges. A more sophisticated modeling of the wind action? Surely, maybe not only. In Section 2.4 we quoted the different theories presented on this topic, not with the aim to discuss them, but simply highlighting how many uncertainties and open questions there are on the aerodynamic of suspension bridges.

Our aim is to use this information in an alternatively way. As a first-hand approach let us simplify extremely the problem, assuming that the bridge is an elastic oscillator following the differential equation

$$m\ddot{w}(t) + c\dot{w}(t) + kw(t) = A\sin\omega t \qquad \text{for } t \in (0,\infty) \tag{3.1}$$

in which $w(t)$ is the displacement, m the mass, $c \in (0, 2\sqrt{km})$ the damping, $k > 0$ the elastic coefficient of the oscillator and $A\sin\omega t$ the forcing term identified in the wind, in which $A > 0$ is the amplitude and $\frac{\omega}{2\pi}$ the frequency of the wind. We exclude the very improbable situation of perfect resonance between the wind and the oscillator, confirmed also by [12], i.e. $\omega \neq \overline{\omega} := \frac{\sqrt{c^2-4km}}{2}$; hence we obtain as solution

$$w(t) = e^{-\frac{ct}{2m}}(c_1\sin\overline{\omega}t + c_2\cos\overline{\omega}t) + c_3\sin\omega t + c_4\cos\omega t, \tag{3.2}$$

in which the constants c_1, c_2, c_3, c_4 depend on the initial conditions. From (3.2) we see that as $t \to \infty$ the solutions have a sinusoidal behavior, in which the damped part tends to vanish and the oscillator achieves the so-called steady motion.

We consider the oscillator during its steady motion and we evaluate its behavior on a certain interval of time $[0, T]$ with $T > 0$, on which the structural damping balances perfectly the forcing term; in this case (3.1) becomes

$$m\ddot{w}(t) + kw(t) = 0 \qquad \text{for } t \in (0, T] \tag{3.3}$$

i.e. the equation of the correspondent isolated system, that has solutions similar to (3.2) during the steady motion, with possible different frequencies.

Since our aim is to study the stability of a system, this kind of approach gives some hints, hence

we consider the suspension bridge as an isolated system on $[0, T]$,

see also [42]. We point out that in this way we avoid the arduous choice of the wind forcing term and of the damping of the system; this latter is quite difficult to obtain with precision for big structures as suspension bridges, since it is necessary to investigate scale models in the wind-tunnel. About the wind forcing term we have discussed the uncertainties around the topic and the choice of a periodic excitation as in (3.1) seems to trivialize the problem.

If from one hand we have these advantages, on the other a perfect balance between damping and wind is thinkable on intervals $[0, T]$ for sufficiently small $T > 0$; for these reasons we consider numerical simulations on intervals of about 2 minutes, that represent small intervals compared to 70 minutes of violent oscillations recorded during the TNB collapse, see [73].

This approach requires also a focus on the initial conditions, overall on $w(0)$; if (3.1) can be studied starting by $w(0) = 0$, (3.3) needs an initial condition $w(0) = w_0$, where w_0 is the amplitude of the oscillation during the steady motion. Supposing in this extreme simplification that (3.3) models the TNB, then w_0 is the vertical amplitude recorded in [2] before the rise of the torsional oscillations, and is linked to the energy introduced by the wind in the system through the vortex shedding, see Section 2.5.

In the sequel we present isolated models for suspension bridge with the aim to see if the isolated structure by itself can lead to the torsional instability phenomena; if the bridge were like the oscillator (3.3) nothing would happen, but the geometrical configuration of a suspension bridge is more complex, involving different nonlinearities.

3.2 Description of the suspension bridge's model

In Section 1.2 we introduced the main elements of a suspension bridge; here we describe in details the modeling of such elements.

We consider the portion of the deck between the towers as a degenerate plate occupying at rest the planar position $(0, L) \times (-\ell, \ell) \subset \mathbb{R}^2$, composed by a central beam of length L in its midline and cross sections of length $2\ell \ll L$, whose midpoints lie on the beam. Each cross section is free to rotate around the beam and to leave the horizontal equilibrium position. The hangers link the endpoints of the cross sections (the longer edges of the degenerate plate) to the cables. This model is called *fish-bone* in [10] and a preliminary linear version of it was suggested in [78, p.458, Chapter VI].

We introduce a reference system (O, x, w) with origin in correspondence of a tower at the level of the deck, assuming w **positive if directed downward** and x along the main span of the bridge, see Figure 3.1.

We suppose that the two main cables have the same mechanical properties and that the hangers are uniformly distributed along the two free edges of the deck. The sag-span ratio $\frac{f}{L}$ assumes an important role in the bridge behavior, affecting the horizontal component of the cable force; in the design practice [62, §15.17]

$$\frac{f}{L} = \frac{1}{12} \div \frac{1}{8}. \tag{3.4}$$

A primary source of nonlinearity for the problem is given by the cable shape that assumes different configurations with respect to the loading conditions; we devote the next section to cable statics, underlying which case we assume for our models.

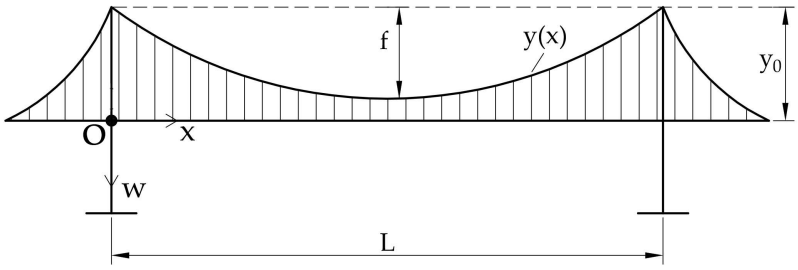

Figure 3.1: *Sketch of the side view of the suspension bridge with the quotes assumed positive.*

3.2.1 Cable statics

The static equation of a cable is different if this element is subjected to its own weight ($m > 0$) or to a distributed load ($M > 0$), e.g. see [62, §15.15] and Figure 3.2. Let

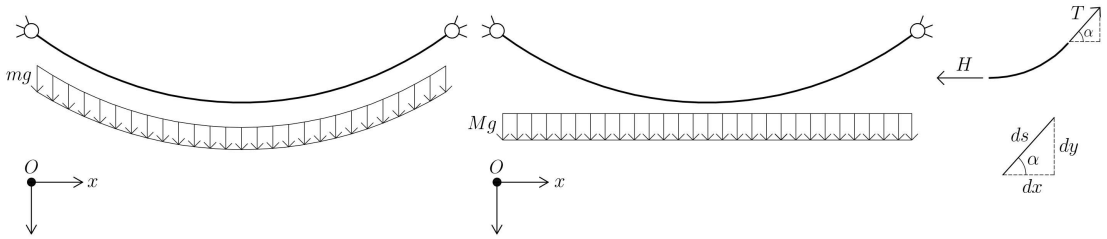

Figure 3.2: *Cable subjected to its own weight and to distributed load. On the right the equilibrium of a portion of cable and the cable's infinitesimal segment.*

us analyze these situations, assuming a perfect flexible and inextensible cable, having a shape given by $y(x)$ for $x \in [0, L]$. For geometrical reasons the length of the cable is given by

$$L_c = \int_0^L \sqrt{1 + (y')^2} dx. \tag{3.5}$$

Cable under its own weight ($m > 0, M = 0$)

Referring to Figure 3.2 on the left, we consider the mass of the cable m constant and we denote by g the intensity of the gravitational acceleration. In absence of external horizontal force, the horizontal tension $H_0 > 0$ remains constant and we write the equilibrium of a cable's segment as

$$T \cos \alpha = H_0, \qquad T \sin \alpha = mgs.$$

Here, $T := T(x)$ is the generic tension in the cable, $\alpha := \alpha(x)$ is the angle between T and the horizontal direction and $s := s(x)$ is the curvilinear abscissa related to the cable for $x \in [0, L]$, see Figure 3.2 on the right; hence, we end up with the intrinsic equation of the catenary

$$s = \frac{H_0}{mg} \tan \alpha. \tag{3.6}$$

Observing that $\tan\alpha = -\frac{dy}{dx}$ and $\frac{ds}{dx} = \sqrt{1+(y')^2}$, we differentiate (3.6) with respect to x so that

$$\begin{cases} H_0 y''(x) = -mg\sqrt{1+[y'(x)]^2} & \forall x \in (0,L) \\ y(0) = y(L) = -y_0 & (y_0 > 0), \end{cases} \tag{3.7}$$

where L is the length of the main span and y_0 is the height of the towers. The solution of (3.7) gives the well known catenary shape, i.e.

$$y(x) = -\frac{H_0}{mg}\left[\cosh\left(\frac{mg}{2H_0}(2x-L)\right) - \cosh\left(\frac{mgL}{2H_0}\right)\right] - y_0 \qquad \forall x \in [0,L].$$

By (3.5) the length of the cable L_c is

$$L_c = \frac{2H_0}{mg}\sinh\left(\frac{mgL}{2H_0}\right).$$

A typical engineering approach to find H_0 is to fix the length of the cable L_c.

Cable under a uniformly distributed load ($M > 0, m = 0$)

In this case we neglect the cable mass and we suppose that there is only a uniform distributed load, e.g. the linear density of the deck mass M, see Figure 3.2. As suggested in [77], the cable at rest take the shape $y(x)$, where y solves the following differential equation

$$\begin{cases} H y''(x) = -q & \forall x \in (0,L) \\ y(0) = y(L) = -y_0 & (y_0 > 0). \end{cases} \tag{3.8}$$

Here, $q > 0$ is the dead load, $H > 0$ is the horizontal tension of the cable, L is the length of the bridge span and y_0 is the height of the towers. Since we will deal with models having two cables to support the same deck, we assume that each cable sustains a dead load $q = \frac{Mg}{2}$. Since q is constant we find that the cables take the shape of a parabola given by

$$y(x) = -\frac{Mg}{4H}x^2 + \frac{MgL}{4H}x - y_0 \qquad \forall x \in [0,L]. \tag{3.9}$$

As suggested in [62, §15.16.1], from the elastic theory and (3.4), the parabolic shape of the cables implies that, in a situation of equilibrium,

$$H = \frac{qL^2}{8f} = \frac{MgL^2}{16f} = (1.00 \div 1.50)\frac{MgL}{2}, \tag{3.10}$$

where f is the cable sag as in Figure 3.1. Then an equivalent way to write (3.9) is

$$y(x) = -\frac{4f}{L^2}x^2 + \frac{4f}{L}x - y_0 \qquad \forall x \in [0,L]. \tag{3.11}$$

By (3.5) we compute the length of the cable L_c as

$$L_c = \frac{L}{2}\sqrt{1+\left(\frac{4f}{L}\right)^2} + \frac{L^2}{8f}\sinh^{-1}\left(\frac{4f}{L}\right) = (1.018 \div 1.040)L,$$

in which the last relation comes from (3.4).

Cable under uniformly distributed load and its own weight $(M, m > 0)$

In [4, p.214] the authors obtain the differential equation in the general case where both the distributed load and the weight of the cable are considered. Given the horizontal tension of the cable $H_1 > 0$, the derivation is analogous as before and leads to

$$\begin{cases} H_1 y''(x) = -(\frac{M}{2} + m\sqrt{1 + [y'(x)]^2})g & \forall x \in (0, L) \\ y(0) = y(L) = -y_0 & (y_0 > 0). \end{cases} \tag{3.12}$$

Existence and uniqueness of a solution of (3.12) symmetric with respect to $x = L/2$ is proved [4]; the equation has not simple explicit solution, but we can find it numerically. To this aim we use (3.12) and the symmetry of the solution to compute the length of the cable by (3.5)

$$L_c = -\frac{1}{2mg}\int_0^L \big(2H_1 y''(x) + Mg\big)dx = \frac{4H_1 y'(0) - MgL}{2mg}.$$

Fixing L_c we obtain the horizontal tension as

$$H_1 = \frac{(2mL_c + ML)}{4y'(0)}g;$$

hence we solve (3.12) introducing an arbitrary value of $y'(0) \neq 0$ and repeating the numerical procedure until the boundary condition $y(L) = -y_0$ is satisfied. In particular

$$\begin{cases} (2mL_c + ML)y'' = -4y'(0)\left(\dfrac{M}{2} + m\sqrt{1 + y'^2}\right) & \forall x \in (0, L) \\ y(0) = -y_0 & (y_0 > 0) \\ y'(0) = \alpha. \end{cases} \tag{3.13}$$

As first attempt we choose $\alpha = 4f/L$, deriving from the parabolic case (3.11); increasing slightly α we found $y(L) = -y_0$ with an error less than $1 \cdot 10^{-4}$.

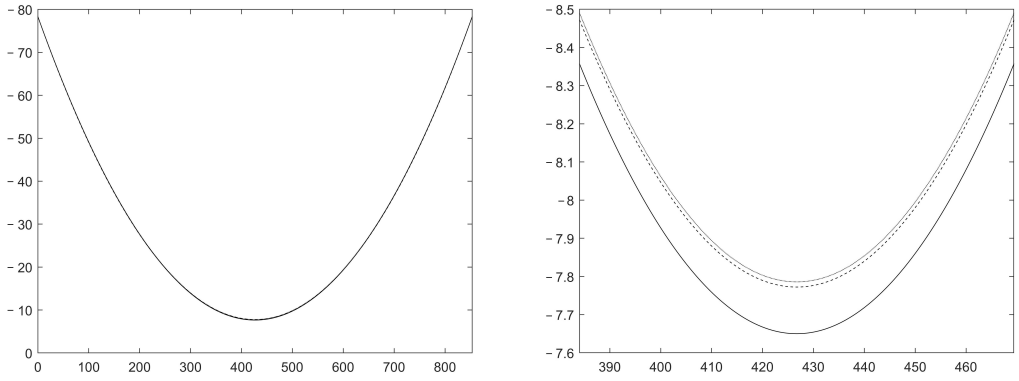

Figure 3.3: *On the left the three cables' shape for the TNB, scale in meters. On the right a zoom on* $[\frac{9}{20}L, \frac{11}{20}L]$*, in which from below we have the parabola, the catenary (dashed) and the numerical solution (dotted).*

In Figure 3.3 we plot the cables' shape in the three cases discussed, applying the mechanical parameters of the TNB, see Table 3.1. As we can see, it is difficult to

distinguish the three plots on the right, because the curves are very close. On the left we show a zoom on the interval $[\frac{9}{20}L, \frac{11}{20}L]$ to appreciate the differences near $x = L/2$. The catenary (dashed line) and the solution of (3.13) are quite close (dotted line), so that we have respectively f =70.59m and f =70.57m. The parabolic shape (continuous line) assumes the greatest deformation showing f =70.71m. We point out that, although the vertical loads are greater in the case $M, m > 0$, the horizontal tensions follow the relation $H_1 > H > H_0$; therefore, assuming the same length of the cables, it is possible that a cable sustaining a heavier load, has lower sag, due to the higher horizontal tension. Indeed, in the limit case where this tension tends to infinity the cable will assume horizontal position, independently by the vertical loads.

It is out of doubt that the most realistic shape is represented by the numerical solution of (3.13); anyway, the three shapes are very close (maximum difference for the TNB of 14cm at midspan). This important datum and the immediacy of (3.11) with respect to the involved solution of (3.12) have led to the following assumption for our models:

the cable's mass is neglected and we assume parabolic cable shape (3.11)**.**

Throughout the thesis we will deal with the local length $\sqrt{1+y'^2}$ of the cables. For these reasons we introduce for all $x \in [0, L]$ the bounded and positive function

$$\xi(x) := \sqrt{1+y'(x)^2}, \qquad 1 \le \xi(x) \le \xi_M := \sqrt{1+\left(\frac{4f}{L}\right)^2}, \tag{3.14}$$

in which, by (3.4), its maximum value, assumed for $x \in \{0, L\}$, is

$$\xi(0) = \xi(L) = \xi_M \in \left[\frac{\sqrt{10}}{3}, \frac{\sqrt{5}}{2}\right] = [1.05, 1.11]. \tag{3.15}$$

3.2.2 Degrees of freedom and the debate on the nonlinearities

In Figure 3.4 we sketch a generic cross section of the bridge, highlighting the degrees of freedom of the problem given by $w := w(x,t)$ and $\theta := \theta(x,t)$, representing respectively the downward displacement and the torsional angle of the barycentric line of the deck. Throughout the thesis we will deal with models having

two degrees of freedom, w **and** θ**,**

always depending by two independent variables: the space x, referring to the position on $[0, L]$ of the bridge's section, and the time t as usual in dynamic problems.

A torsional rotation of the deck immediately involves, for geometric reasons, the trigonometric functions. In our models we will maintain the dependence from $\sin\theta$ (and $\cos\theta$), avoiding the assumption $\sin\theta \approx \theta$ (and $\cos\theta \approx 1$). This issue is very sensitive within the debate on the stability of suspension bridges. In engineering literature the linearization on the positions of the two free edges

$$w \pm \ell \sin\theta \approx w \pm \ell\theta \tag{3.16}$$

has been often performed, simplifying considerably the problem, see [68].

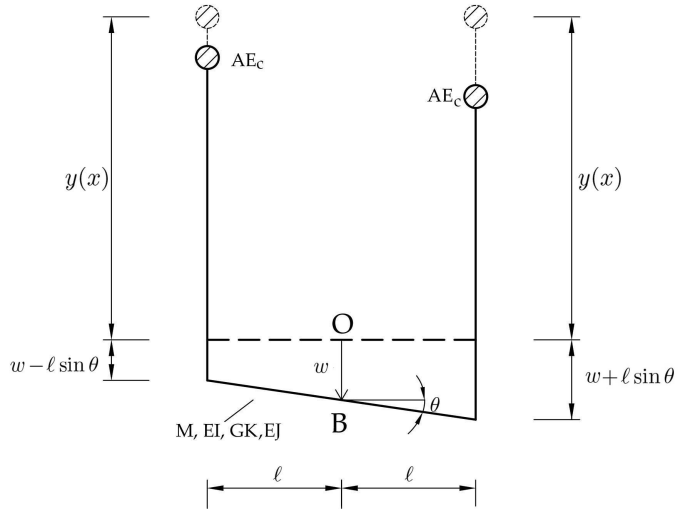

Figure 3.4: *A cross section of the bridge.*

In [51] McKenna presents a rod model for suspension bridges showing that the key to understand the large torsional oscillations of the TNB is linked to the presence of the trigonometric functions. In particular the linearization (3.16) is an error for wide oscillations, i.e. if large torsional forcing terms or large initial conditions on θ are assumed; he wrote [51, p.2]

> the 'small-angle' linearisations can remove a large class of large-amplitude nonlinear solutions that can be sustained by extremely small periodic forcing term.

We point out that, when the interest is focused on very small torsional oscillations, (3.16) is correct; for instance, in the design practice, the linearized theory may have sense, because the new bridges are designed to avoid large torsional oscillations.

In our case we do not consider forcing terms and we will apply small initial data on θ, but we avoid this simplification to have more precise results and to observe the growth of θ even for large rotations, hence

we do not linearize the trigonometric functions $\sin\theta$ and $\cos\theta$.

Needless to say, the presence of the trigonometric functions increases the computational burden, but we think that it better models the real problem. In Section 4.2.2 we compare numerically the solution of the problem to the homologous obtained assuming (3.16).

An other nonlinearity strongly discussed by engineer and mathematicians is $\xi(x)$ see (3.14), that is very close to 1. Its presence has implications on the system, since generally it becomes very difficult to find explicit solutions; in classical literature ξ is usually approximated with 1, gaining often the possibility to solve by hand the differential equations. Biot and von Kármán [77, p.277] warn the reader by writing

> ...whereas the deflection of the beam may be considered small, the deflection of the string, i.e. the deviation of its shape from a straight line, has to be considered as of finite magnitude.

Hence, they accept the assumption on small rotations and displacements, while no approximation of $y'(x)$ should be taken. Nevertheless, subsequently [77, (5.14)] the authors decide to neglect $y'(x)^2$ in comparison with unity, putting in fact $\xi(x) \equiv 1$. In [35]

the authors underline how this choice may significantly change the response of the system.

3.2.3 Mechanical parameters

In this section we describe briefly the mechanical parameters that will appear in the sequel, without repeating those already introduced previously; they belong to the classical science of construction, see for instance [39]. The comprehension of this work lies outside the deep knowledge of them. The use of such parameters allow us to discuss more reliable models, dealing with real physical quantities.

The deck's deformations comes up, as for a beam, from bending and torsion, due to some energy input; according to the de Saint Venant theory a simple beam has a bending stiffness depending on E, the Young modulus, and I, the linear density of the moment of inertia of the cross section. On the other hand the beam opposes to torsional movements with a torsional stiffness proportional to G, the shear modulus, and K, the torsional constant of the section; we point out that the pure torsion, depending on the GK-term, occurs only when the warping can take place freely. The presence of welding at the supports, typical of steel structures, changes in the beam section or imposed torsional moment restrain the warping in some points of the beam [69]. In 1940, Vlasov [76] developed a torsion theory in which constrained warping was included; in particular, to the pure torsional term of de Saint Venant, Vlasov added a new differential term of the fourth order, proportional to E and J, the warping constant of the section. The choice to include or not the Vlasov term will be specified case by case in the description of the three models.

In Table 3.1 we summarize the notations and the specific values related to the TNB [2], useful for the numerical simulations. The torsional constant K is given in a small range of variation because in literature is computed in different ways, so that both the values are used, e.g. see [60, p.625]; we will specify case by case which value we use.

We suppose that

the hangers are massless and continuously spanned onto the span.

To compute their Hooke constant k_0 we observe that each hanger is composed by four steel ropes having circular shape, see for instance Figure 2.8. Hence we obtain

$$\kappa_0 = \frac{n_h \pi \phi^2}{4 l_h} E_h, \tag{3.17}$$

where $n_h = 4$ is the number of ropes for each hanger, $\phi = 31.75$mm is the diameter of the rope, E_h is the elastic modulus of the hangers and $l_h = 15.24$m is the distance between consecutive hangers.

We point out that we tested our models also considering different parameters with respect to those in Table 3.1, e.g. values belonging to other suspension bridges. We refer to Sections 4.5 and 5.3 for some analysis of sensitivity of the systems by the mechanical parameters; this approach allows us to define models having general validity for any suspension bridge.

Notation	TNB Value	Mechanical parameter
L	853.44m	Length of the main span
ℓ	6m	Half width of the deck
L_c	868.815m	Initial length of the cables, see (3.5)
f	70.71m	Sag of the cable
f/L	$\approx 1/12$	Sag-span ratio
y_0	78.36m	Length of the longest hanger
I	0.154m^4	Moment of inertia of the deck cross section
A	0.1228m^2	Area of the cables section
K	$(6.07 \div 6.44) \cdot 10^{-6}\text{m}^4$	Torsional constant of the deck
J	5.44m^6	Warping constant of the deck
M	7198kg/m	Mass linear density of the deck
m	918kg/m	Mass linear density of the cable
H	45 413kN	Initial tension in the cables, see (3.10)
E	200GPa	Young modulus of the deck (steel)
E_h	200GPa	Hangers' Young modulus (steel)
E_c	185GPa	Young modulus of the cables (steel)
G	81GPa	Shear modulus of the deck (steel)
κ_0	$4.16 \cdot 10^7$N/m	Hooke constant of the hangers

Table 3.1: *TNB mechanical features. Source: [2]*

3.3 The general approach to the problem

In this section we give a general and synthetic scheme of analysis that we use for the three models. Since we study variational problems, we first define the energy of the system, useful to derive the Euler-Lagrange equations. Then, we perform some numerical experiments on the approximated solutions; here, we present our numerical approach, highlighting what we mean for torsional instability.

3.3.1 Energy of the system

The total energy of the system is given by the energy of the deck, the energy of the cables and the energy of the hangers. Let us begin by computing the energy of the deck that represents a common contribute for all our models. We refer to Sections 3.2 for the description of the mechanical parameters involved.

The energy of the deck is given by the kinetic, the gravitational and the deformation contributions. The first depends on the vertical displacement and the rotation of the

deck, i.e.

$$E_k = \frac{M}{2}\int_0^L w_t^2\,dx + \frac{M\ell^2}{6}\int_0^L \theta_t^2\,dx.$$

The gravitational energy is due to dead loads and is negative because w is positive downwards,

$$E_g = -Mg\int_0^L w\,dx.$$

The deformation energy comes form the bending energy and the torsional energy. To be precise the first is given by the square of the curvature times half the flexural rigidity, i.e.

$$E_b = \frac{EI}{2}\int_0^L \frac{w_{xx}^2}{(1+w_x^2)^3}\sqrt{1+w_x^2}.$$

As highlighted in [34]

> this energy is not convex and it fails to be coercive in any reasonable functional space so that standard methods of calculus of variations do not apply.

Therefore, a common approach is to assume an asymptotic expansion of E_b, neglecting the higher order infinitesimals [4] and simply taking

$$E_b = \frac{EI}{2}\int_0^L w_{xx}^2.$$

The torsional energy of the deck is given by

$$E_t = \frac{GK}{2}\int_0^L \theta_x^2\,dx + \frac{EJ}{2}\int_0^L \theta_{xx}^2\,dx.$$

Here we include also the EJ-term introduced by Vlasov [76], but, as explained before, we will specify case by case if we consider it or not.

Otherwise the energetic contributes related to the cables and the hangers will be computed in the specific chapters, since they feature the novelty of the different models. At this stage we include them into the generic functional

$$J(w,\theta) = \int_0^L \mathcal{L}(w,\theta,w_x,\theta_x)dx + \frac{1}{2}\left(\int_0^L \mathcal{T}(w_x,\theta_x)dx\right)^2,$$

so that we find the total energy of the system

$$\begin{aligned}\mathcal{E}(t) := &\int_0^L \left(\frac{M}{2}w_t^2 + \frac{M\ell^2}{6}\theta_t^2 + \frac{EI}{2}w_{xx}^2 + \frac{EJ}{2}\theta_{xx}^2 + \frac{GK}{2}\theta_x^2 - Mgw\right)dx \\ &+ \int_0^L \mathcal{L}(w,\theta,w_x,\theta_x)dx + \frac{1}{2}\left(\int_0^L \mathcal{T}(w_x,\theta_x)dx\right)^2.\end{aligned} \tag{3.18}$$

We recall that our system is isolated, see Section 3.1, so that this energy is conserved in time. We point out that the integral square terms depending on $\mathcal{T}$, in the models will be two, since they represent the deformation energy of the two cables; anyway, in this general framework we consider only one to avoid weighting the notation.

3.3.2 The system of evolution partial differential equations

In Section 3.1 we pointed out that, physically speaking, it has sense to consider the system isolated for $t \in [0, T]$ with $T > 0$; anyway, we write the system for $t \in [0, \infty)$, since it is correct from a mathematical point of view, while in the sequel we study its stability on a sufficiently small interval $[0, T]$.

We proceed formally denoting by $\mathcal{L}_w = \dfrac{\partial \mathcal{L}}{\partial w}$, $\mathcal{L}_{w_x} = \dfrac{\partial \mathcal{L}}{\partial w_x}$, $\mathcal{L}_\theta = \dfrac{\partial \mathcal{L}}{\partial \theta}$, $\mathcal{L}_{\theta_x} = \dfrac{\partial \mathcal{L}}{\partial \theta_x}$ and similarly for $\mathcal{T}$. From (3.18) we derive the autonomous system of partial differential equations

$$\begin{cases} Mw_{tt} = -EIw_{xxxx} + Mg - \mathcal{L}_w + (\mathcal{L}_{w_x})_x + \left(\displaystyle\int_0^L \mathcal{T}(w_x, \theta_x)dx\right)(\mathcal{T}_{w_x})_x \\ \frac{M\ell^2}{3}\theta_{tt} = -EJ\theta_{xxxx} + GK\theta_{xx} - \mathcal{L}_\theta + (\mathcal{L}_{\theta_x})_x + \left(\displaystyle\int_0^L \mathcal{T}(w_x, \theta_x)dx\right)(\mathcal{T}_{\theta_x})_x \\ w(0,t) = w(L,t) = w_{xx}(0,t) = w_{xx}(L,t) = 0 \qquad \text{for } t \in (0,\infty) \\ \theta(0,t) = \theta(L,t) = \theta_{xx}(0,t) = \theta_{xx}(L,t) = 0 \qquad \text{for } t \in (0,\infty) \\ w(x,0) = w^0(x), \quad \theta(x,0) = \theta^0(x) \qquad \text{for } x \in (0,L) \\ w_t(x,0) = w^1(x), \quad \theta_t(x,0) = \theta^1(x) \qquad \text{for } x \in (0,L). \end{cases} \tag{3.19}$$

The boundary conditions refer the fact that the main span of the bridge is hinged at the endpoints, see Figure 3.1. The occurrence of θ_{xx} equal to zero in $x = \{0, L\}$ depends on the presence of the EJ-Vlasov torsional term; indeed, possible welding at the supports may constrain the free rotation, see Section 3.2.3.

Our general approach consists then in finding a weak formulation of (3.19) and in giving existence and uniqueness results. To this aim we consider the Hilbert spaces $L^2(0, L)$, $H_0^1(0, L)$, $H^2 \cap H_0^1(0, L)$ endowed respectively with the scalar products

$$(u, v)_2 = \int_0^L uv, \quad (u, v)_{H^1} = \int_0^L u'v', \quad (u, v)_{H^2} = \int_0^L u''v'' \tag{3.20}$$

and we denote by $H^{-1}(0, L)$ and $H^*(0, L)$ the dual spaces respectively of $H_0^1(0, L)$ and $H^2 \cap H_0^1(0, L)$ with the corresponding duality $\langle \cdot, \cdot \rangle_1$ and $\langle \cdot, \cdot \rangle_*$. Moreover we introduce an orthogonal base $\{e_k\}_{k=1}^\infty$ for the these spaces, in which

$$e_k(x) = \sqrt{\frac{2}{L}} \sin\left(\frac{k\pi x}{L}\right) \quad (k \geq 1) \tag{3.21}$$

where $\sqrt{\frac{2}{L}}$ is a pure number with no unit of measure. Note that $\|e_k\|_2 = 1$, $\|e_k\|_{H^1} = k\pi/L$ and $\|e_k\|_{H^2} = k^2\pi^2/L^2$.

However, since the existence and uniqueness topic is highly dependent on the specific choices of $\mathcal{L}$ and $\mathcal{T}$, we deal with it in the next chapters case by case.

3.3.3 Numerical analysis

Assured the well posedeness of the problem we apply a finite dimensional approximation; in fact, civil structures typically oscillate on low modes since higher modes do not appear in realistic situations, due to very large bending energy; [13, p.23] says that

> ... out of the infinite number of possible modes of motion in which a suspension bridge might vibrate, we are interested only in a few, to wit: the ones having the smaller numbers of loops or half waves.

Therefore, mathematically

we project an infinite dimensional space on a finite dimensional subspace, using the Galerkin approximation.

This procedure is widely accept in engineering literature, see for instance [13, 71]. In particular, given the boundary conditions, we seek approximate solutions in the form

$$w(x,t) = \sum_{q=1}^{n} w_q(t)e_q(x), \qquad \theta(x,t) = \sum_{r=1}^{\nu} \theta_r(t)e_r(x), \tag{3.22}$$

for some integers $n, \nu \geq 1$, in which e_k is given in (3.21). The choice of the integers n and ν to whom truncating the Fourier sum (3.22) will be discussed model by model, also with respect to the witnesses recorded during bridges' collapses, see Sections 2.2 and 2.3.

For brevity we denote the nonlocal term of (3.19) by $\Gamma := \int_0^L \mathcal{T}(w_x, \theta_x)dx$; hence, plugging (3.22) into (3.19) and projecting onto the space spanned respectively by the first n and ν Fourier components, we find

$$\begin{cases} M\ddot{w}_k(t) + EI\dfrac{k^4\pi^4}{L^4}w_k(t) = Mg\sqrt{2L}\dfrac{(1-(-1)^k)}{k\pi} - \left(\mathcal{L}_w, e_k\right)_2 - (\mathcal{L}_{w_x} + \Gamma\mathcal{T}_{w_x}, e_k')_2 \\ \dfrac{M\ell^2}{3}\ddot{\theta}_i(t) + \left(EJ\dfrac{i^4\pi^4}{L^4} + GK\dfrac{i^2\pi^2}{L^2}\right)\theta_i(t) = -(\mathcal{L}_\theta, e_i)_2 - (\mathcal{L}_{\theta_x} + \Gamma\mathcal{T}_{\theta_x}, e_i')_2 \end{cases} \tag{3.23}$$

$$\text{for } k = 1, \dots, n \quad i = 1, \dots, \nu,$$

with the initial conditions

$$\begin{aligned} &w_k(0) = w_k^0 = (w^0, e_k)_2, && \dot{w}_k(0) = w_k^1 = (w^1, e_k)_2, && \forall k = 1, \dots, n \\ &\theta_i(0) = \theta_i^0 = (\theta^0, e_i)_2, && \dot{\theta}_i(0) = \theta_i^1 = (\theta^1, e_i)_2 && \forall i = 1, \dots, \nu. \end{aligned} \tag{3.24}$$

In this way we deal with a system of $(n + \nu)$ second order ordinary differential equations (ODEs), easily transformable to a system of $2(n + \nu)$ first order ODEs; this last passage is useful to apply numerical methods of resolution and to study theoretically the stability. In the sequel we name the unknowns of (3.23) following the

Definition 3.3.1. *We call* $\overline{w}_k(t) := \sqrt{\frac{2}{L}}w_k(t)$ ***k-th longitudinal mode*** *and* $\overline{\theta}_i(t) := \sqrt{\frac{2}{L}}\theta_i(t)$ ***i-th torsional mode***.

By the Definition 3.3.1, we put $\overline{w}_k^0 := \sqrt{\frac{2}{L}} w_k^0$, $\overline{w}_k^1 := \sqrt{\frac{2}{L}} w_k^1$ and similarly for the θ initial conditions.

Recalling Section 3.1, we study the isolated system (3.23) on an interval $[0, T]$ for sufficiently small $T > 0$, enough to see the possible sudden transfer of energy between modes. Our initial conditions reflect the system during its steady motion, in which the oscillation of a j-th longitudinal mode prevails. Therefore, we concentrate the energy on the amplitude of the j-th longitudinal mode, perturbing all the other modes with an initial condition K-times smaller, i.e. in dimensionless form

$$\overline{w}_k^0 = K \cdot \overline{w}_j^0 \quad \forall k \neq j, \qquad \overline{\theta}_i^0 = \overline{w}_k^1 = \overline{\theta}_i^1 = K \cdot \overline{w}_j^0 \quad \forall k, i. \tag{3.25}$$

The constant K consists in a reduction of $\overline{w}_j^0$ of 3 or 4 orders; we will fix it case by case. Following this approach we say that the initial energy of our system corresponds to that of the longitudinal mode excited and represents, indirectly, the wind energy introduced on the bridge through the so-called vortex shedding [68]. Our aim is to verify if there is a torsional mode that after some time captures energy from the longitudinal modes and becomes larger and larger, i.e. it manifests **torsional instability**. In the next sections we better explain what we mean for such kind of instability.

3.3.4 Instability of ordinary differential equations' systems

The stability of a system can be studied with different techniques with respect to its nature; for instance, in the first order linear homogeneous systems, having constant coefficients, it is enough to verify that the eigenvalues of the coefficients' matrix have negative real part.

In [22] the author presents some stability results for nonlinear systems and he introduces the Floquet theory for linear systems having periodic coefficients. This theory is applied to the Hill's equation, written by George W. Hill in his study of the motion of the moon,

$$\ddot{u} + p(t)u = 0. \tag{3.26}$$

Here $p(t) \in C^0[0, \overline{T}]$ is a periodic coefficient, non constant and such that $p(t + \overline{T}) = p(t)$ for $\overline{T} > 0$. We point out that (3.19) may be led to (3.26) with $u = \theta$, applying proper simplifications; in particular, θ should be linearized ($\sin\theta = \theta$) and it may be assumed that $w(t)$ has periodic motion, so that it acts as $p(t)$.

The Hill equation is stable if $u \equiv 0$ is stable or equivalently all the solutions of (3.26) are bounded in $\mathbb{R}$. A classical stability criterion for (3.26) is given by Lyapunov, Krein and Borg, see [47]; it states that, if $p(t) \geq 0$, then (3.26) is stable if

$$\overline{T} \int_0^{\overline{T}} p(t)dt \leq 4.$$

This very elegant result was generalized by [45], considering $p(t) \in L^\alpha(0, \overline{T})$ for $\alpha \in [1, \infty]$ and stating the stability of (3.26) if

$$\begin{aligned} &\|p(t)\|_\alpha < K(2\alpha^*) && \text{for} \quad \alpha \in (1, \infty] \\ &\|p(t)\|_\alpha \leq K(\infty) = 4/\overline{T} && \text{for} \quad \alpha = 1. \end{aligned}$$

Here $\alpha^* = \alpha/(\alpha-1)$ and $K(\cdot)$ are certain Sobolev constants that the authors compute explicitly. Note that the case $\alpha = 1$ is coincident with that of Lypanuov. We specify that the assumption $p(t) \geq 0$ can be mitigated, we refer to [45] for details.

In literature there are other criteria giving sufficient conditions for the stability of the Hill equation; here we quote a criterion due to Zhukovskii [79] and one due to Burdina [17]. The first states that, if $p(t) \geq 0$ and there exists $m \in \mathbb{N}$ such that

$$\frac{m^2\pi^2}{\overline{T}^2} \leq p(t) \leq \frac{(m+1)^2\pi^2}{\overline{T}^2} \quad \forall t,$$

then (3.26) has stable solution. The second assures the stability if $p(t) > 0$, $a(t)$ admits a unique maximum point and a unique minimum point on $[0, \overline{T})$ and there exist $m \in \mathbb{N}$ such that

$$m\pi < \int_0^{\overline{T}} \sqrt{p(t)}dt - \frac{1}{2}\log\frac{\max p}{\min p} < (m+1)\pi.$$

For particular choices of $p(t)$, these methods can be compared finding numerically instability regions with respect to the initial conditions and the parameters characterizing $p(t)$; in this way it is possible to see which criterion predicts the instability before, see for instance [33].

A particular case of (3.26) is the Mathieu equation [50]

$$\ddot{u} + (a + 2q\cos(2t))u = 0 \quad (q \geq 0), \tag{3.27}$$

for which the stability analysis is well-understood. In the (q, a)-plane it is possible to draw the so-called *resonance tongues*, representing the instability regions, that emanate from the points $(0, m^2)$ with $m \in \mathbb{N}$, see Figure 3.5. The stability regions are defined by *resonance lines*, which are explicitly known [54]. In the Figure 3.5 on the

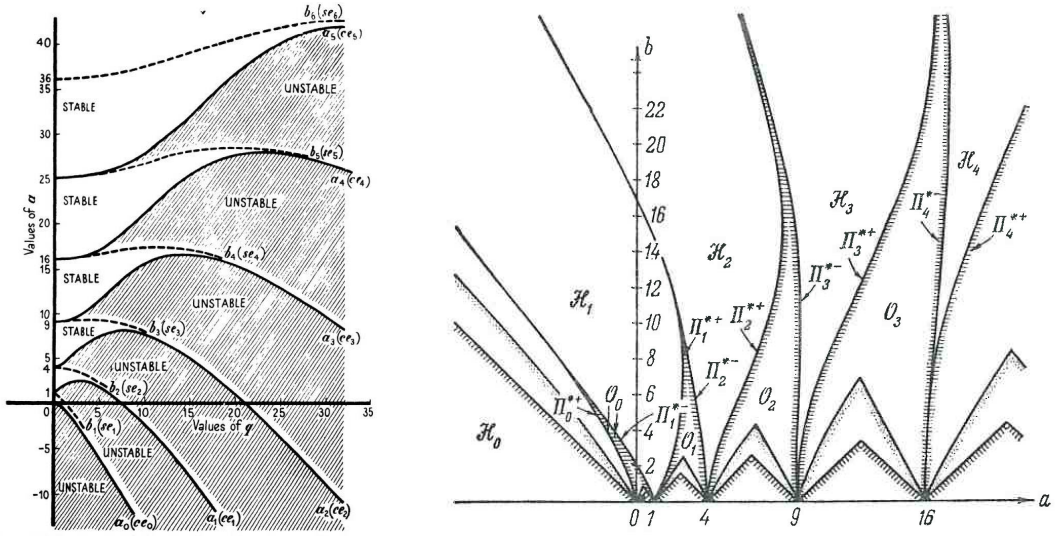

Figure 3.5: *Resonance tongues for the Mathieu equation* (3.27)*. On the left the plot in the* (q, a)*-plane [54], on the right the plot in the* (a, q)*-plane by [78].*

right Starzhinskii and Yakubovich [78, p.707] present the stability regions ($\mathcal{O}_n$) for the

Mathieu equation, inverting the axes (here q is called b); in the plot they also compare the theoretical regions with those obtained through other criteria, e.g. the points belonging to the lowest triangles verify the Zhukovskii's criterion.

The book [34] is rich of simplified models related to suspension bridges, studied leading the problem on the stability to the study of a Hill's equation. It is surprising how the mathematics links through an equation the motion of the moon to that of the suspension bridges!

Another mathematical tool adopted in [3] to study instability phenomena in suspension bridges are Poincaré maps. These were introduced by the French mathematician Henri Poincaré (1854-1912) in [63] to study the celestial mechanics. In not formal way let us explain how to apply the maps to the study of the stability of autonomous systems of differential equations, see [22].

We consider $\dot{u} = f(u)$ in $\mathbb{R}^n$ having periodic orbit Λ; we suppose that for each $\zeta \in \mathbb{R}^n$ the vector function $t \mapsto u(t, \zeta)$ is the solution of the system with initial condition $u(0, \zeta) = \zeta$. If $p \in \Lambda$ and $\Sigma' \subset \mathbb{R}^n$ is a section transverse to $f(p)$ at p then, it is possible to prove that there is an open set $\Sigma \subset \Sigma'$ and a function $T : \Sigma \to \mathbb{R}$ such that for each $\sigma \in \Sigma$ we obtain $u(T(\sigma), \sigma) \in \Sigma'$. T is the time of the first return to Σ', while the map $\mathcal{P}$, given by $\sigma \mapsto u(T(\sigma), \sigma)$ is the Poincaré map corresponding to the Poincaré section Σ, see Figure 3.6. The procedure described can be iterated more

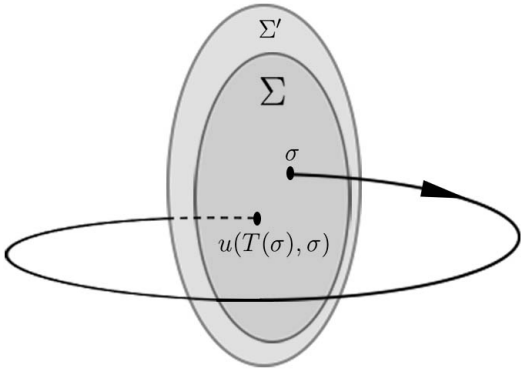

Figure 3.6: *Sketch related to the construction of the Poincaré map.*

and more times. The stability is determined by the stability of the corresponding fixed point of the Poincaré map, i.e. $p \in \Lambda$. In general, the stability of the fixed point of the map is determined by the eigenvalues of its derivative at the fixed point. Proposition 2.122 in [22] states that the system is stable if all the eigenvalues of the derivative of $\mathcal{P}$ in $p \in \Lambda$ have modulus lower than 1; this important result arises because the union of the eigenvalues of the derivative of a Poincaré map at $p \in \Lambda$ and the singleton set $\{1\}$ is the same as the set of the Floquet's characteristic multipliers of the first variational equation $\dot{W} = Df(u(t, p))W$.

Anyway all the stability methods here presented can be applied introducing some linearizations and simplification on (3.23); this approach with interesting results was largely applied to some models in [34]. In the present work we decide to avoid linearizations and simplification, studying the torsional instability in a more pragmatical way.

3.3.5 Torsional instability

From the previous section we learn that the stability of apparently simply linear equations like (3.27) can give very involved diagrams, see Figure 3.5; obviously the plot of the instability regions with respect to the initial conditions and other parameters becomes a hard task dealing with highly nonlinear equations. We point out that to find the *resonance tongues* for the generic (linear) Hill equation (3.26) can be already problematic for a generic $p(t)$. Moreover, is necessary a such kind of analysis to study the torsional instability of suspension bridges?

On the one hand we observe that *resonance tongues* become larger and larger as the initial energy increases, so that beyond certain values almost all the area is unstable; on the other, under certain thresholds we have very thin *resonance tongues*. From a physical point of view the probability to fall in these thin regions is very small, and, even if we were in this situation, it is very probable that the solutions come back to a stability region in a while.

For these reasons we consider the instability not following strictly the theoretical definition, but considering a physical quantitative approach. In [32] the authors give a definition of instability with respect to the time lapse considered $[0, T]$ with $T > 0$, the amplitude of oscillation and its speed of growth. We think that, choosing a proper interval $[0, T]$ and an appropriate rate of growth of the amplitude, such definition can be useful as a **quantitative** indicator of **instability**.

In our simulations we choose T around 2 minutes and, following [32],

we consider the j-th longitudinal mode unstable if at least one torsional mode grows about 1 order in amplitude on $[0, T]$.

Recalling (3.25), from a numerical point of view we define the **threshold of instability** of the j-th longitudinal mode excited as

$$W_j^0 := \left\{ \inf \overline{w}_j^0 : \ \max_i \left\{ \max_{t\in[0,T]} |\overline{\theta}_i(t)| \right\} \geq 10K \cdot \overline{w}_j^0 \right\}; \tag{3.28}$$

this condition allows us to obtain thresholds W_j^0 accurate enough for our purposes.

We know that the wide oscillations at the TNB lasted several hours, but we are focusing on the mechanism related to the transfer of energy between longitudinal and torsional modes and this change happened suddenly. Moreover 2 minutes seem to be a sufficient amount of time to consider the system isolated, in which the injection of energy deriving from the wind and the structural capacity to dissipate it, are balanced, see Section 3.1.

In the three models we find torsional instability thresholds for each longitudinal mode excited; we refer to the next chapters for the specific results.

CHAPTER 4

A model for suspension bridges with fixed cables and extensible hangers

As explained in the introduction, the final aim of this thesis is to set up a realistic model for suspension bridges in which both hangers and cables deformable; since this is a multi step path, we present in this chapter the first "step" model, in which we perform an important simplification:

we consider the cables fixed and the hangers extensible.

This simplification arises because we focus our attention on the slackening of the hangers, differently from other engineering models that usually deal with inextensible hangers and movable cables, see for instance [46].

In this way we suppose ideally that the main cables, after the hooking of the deck, always keep their parabolic position given by (3.11); we know that this is not a model for a real suspension bridge, but our aim is to investigate the stability of the corresponding system with respect to the slackening nonlinearities. The results presented in this chapter are published in [28].

4.1 The dynamical model

4.1.1 Energy involved in the structure

We refer to Chapter 3 for the general setting of the model. In Figure 4.1 we sketch a generic cross section of the bridge, in which are highlighted the DOF and the mechanical parameters related to the deck and the hangers. In this section we mainly focus on the energy of the hangers, in which we concentrate the nonlinearity of the system. We suppose the hangers to behave as stiff nonlinear springs if they are in tension and they

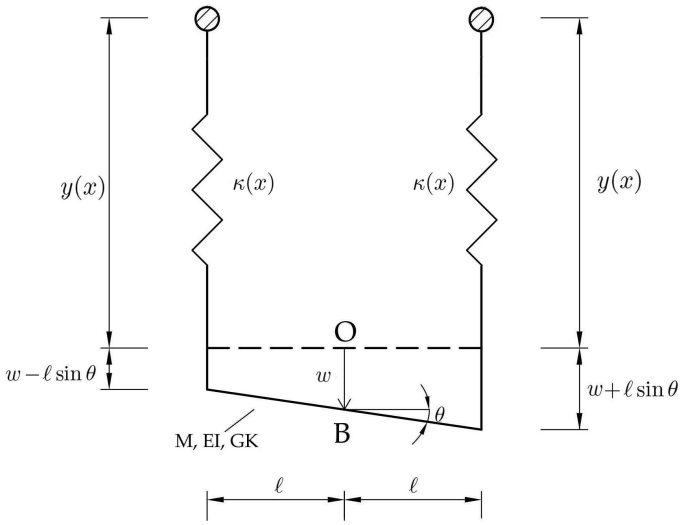

Figure 4.1: *A cross section of the bridge.*

do not apply any force if compressed (*slackening of the hangers*). This assumption is due to observations recorded for instance during the TNB collapse, see (W6)-(W7) in Section 2.3.

We introduce $\lambda = \lambda(x) > 0$ as the length of the unloaded hangers at the position $x \in (0, L)$. After the deck is installed, the hangers are in tension and reach a new length $-y(x) > \lambda(x)$; recall by (3.11) that $y(x)$ is always negative for $x \in [0, L]$, so that $-y(x) > 0$. If no additional loads are introduced, there is equilibrium in correspondence of $(w, \theta) = (0, 0)$. The elastic constant $\kappa(x)$ of the hangers is proportional to the inverse of its unloaded length, i.e.

$$\kappa(x) = \frac{\kappa_0}{\lambda(x)} \qquad (\kappa_0 > 0), \tag{4.1}$$

where κ_0 is the Hooke constant of the hangers. Following [51], we assume that the hangers always remain vertical, even if the deck motion can deflect them slightly with respect to this position. Consequently, we find the elastic forces exerted by them as

$$F_h(w \pm \ell \sin\theta) = \kappa(x)\, f\big(w(x,t) \pm \ell \sin\theta(x,t) - y(x) - \lambda(x)\big) \tag{4.2}$$

which depend on the side of the deck considered and on the choice of the restoring force linked to f. In the next sections we will discuss the behavior of the system for particular choices of f.

It is possible to find $\kappa(x)$ by imposing the static equilibrium after the installation of the deck, when the elastic force of the hangers balances the deck half weight

$$\frac{Mg}{2} = \kappa(x) \cdot f(-y(x) - \lambda(x)). \tag{4.3}$$

Moreover we find the elastic energy in the hangers by introducing $F(s) = \int_0^s f(\sigma)d\sigma$ as

$$E_h(w \pm \ell \sin\theta) = \int_0^L \kappa(x) F\big(w \pm \ell \sin\theta - y(x) - \lambda(x)\big)dx. \tag{4.4}$$

In this model we neglect the Vlasov torsional contribute of the deck, so that from (3.18) the total energy of the system is

$$\begin{aligned}\mathcal{E}(t) := &\int_0^L \left(\frac{M}{2}w_t^2 + \frac{M\ell^2}{6}\theta_t^2 + \frac{EI}{2}w_{xx}^2 + \frac{GK}{2}\theta_x^2 - Mgw\right)dx \\ &+ \int_0^L \kappa(x)F\big(w + \ell\sin\theta - y(x) - \lambda(x)\big)dx \\ &+ \int_0^L \kappa(x)F\big(w - \ell\sin\theta - y(x) - \lambda(x)\big)dx\end{aligned} \tag{4.5}$$

4.1.2 The system of evolution partial differential equations

From the energy balance we derive the following system of PDEs for $(x,t) \in (0,L)\times(0,\infty)$

$$\begin{cases} Mw_{tt} = -EIw_{xxxx} + Mg - \kappa(x)f\big(w + \ell\sin\theta - y - \lambda\big) \\ \qquad\qquad -\kappa(x)f\big(w - \ell\sin\theta - y - \lambda\big) \\ \dfrac{M\ell^2}{3}\theta_{tt} = GK\theta_{xx} - \ell\kappa(x)f\big(w + \ell\sin\theta - y - \lambda\big)\cos\theta \\ \qquad\qquad +\ell\kappa(x)f\big(w - \ell\sin\theta - y - \lambda\big)\cos\theta \end{cases} \tag{4.6}$$

with the boundary and initial conditions, modeling a degenerate plate hinged between the two towers:

$$\begin{aligned} &w(0,t) = w(L,t) = w_{xx}(0,t) = w_{xx}(L,t) = \theta(0,t) = \theta(L,t) = 0 \quad \text{for } t\in(0,\infty) \\ &w(x,0) = w^0(x), \quad \theta(x,0) = \theta^0(x) \quad \text{for } x\in(0,L) \\ &w_t(x,0) = w^1(x), \quad \theta_t(x,0) = \theta^1(x) \quad \text{for } x\in(0,L). \end{aligned} \tag{4.7}$$

In [4] it is proved the existence and uniqueness of the solution for a problem more complex than (4.6), involving deformable cables and 4 degrees of freedom. Some years earlier Holubová and Matas [40] proved for a 2 degrees of freedom problem similar to ours, that there exists a unique weak solution (w,θ) under some assumptions.
We recall in the next proposition the result proved in [40] adapted to (4.6)-(4.7)

Proposition 4.1.1. *Let $T>0$ and F_h in* (4.2) *be continuous locally Lipschitz function with primitive G_h; assume that*

i) $|F_h(\cdot)| \le C(1+|\cdot|^p)$, *for some positive constants C and $p\ge 1$;*

ii) $G_h(\cdot) \ge -D_1 - D_2|\cdot|$, *for some positive constants D_1, D_2.*

If $w^0(x) \in H^2(0,L)\cap H_0^1(0,L)$, $\theta^0(x)\in H_0^1(0,L)$ and $w^1(x),\theta^1(x)\in L^2(0,L)$ then the problem (4.6)-(4.7) has a unique weak solution $w \in C^0\big([0,T];H^2(0,L)\cap H_0^1(0,L)\big)\cap C^1\big([0,T];L^2(0,L)\big)$, $\theta\in C^0\big([0,T];H_0^1(0,L)\big)\cap C^1\big([0,T];L^2(0,L)\big)$.

We will consider cases where the nonlinearity satisfies all the assumptions in Proposition 4.1.1 and, therefore, the problem (4.6)-(4.7) is well posed.

4.1.3 Numerical analysis and torsional stability of the solutions

As explained in Section 3.3.3, we apply the Galerkin procedure to find an approximated solution of (4.6)-(4.7). Recalling (3.22), we introduce for simplicity

$$u_\alpha := \sum_{q=1}^{n} w_q(t)e_q + \ell \sin\left(\sum_{r=1}^{\nu} \theta_r(t)e_r\right) - y(x) - \lambda(x),$$

$$u_\beta := \sum_{q=1}^{n} w_q(t)e_q - \ell \sin\left(\sum_{r=1}^{\nu} \theta_r(t)e_r\right) - y(x) - \lambda(x),$$

so that (3.23)-(3.24) in this case becomes

$$\begin{cases} M\ddot{w}_k(t) + EI\dfrac{k^4\pi^4}{L^4}w_k(t) = Mg\sqrt{2L}\dfrac{(1-(-1)^k)}{k\pi} - \Big(\kappa(x)[f(u_\alpha)+f(u_\beta)], e_k\Big)_2 \\ \dfrac{M\ell^2}{3}\ddot{\theta}_i(t) + GK\dfrac{i^2\pi^2}{L^2}\theta_i(t) = -\ell\Big(\kappa(x)[f\big(u_\alpha\big) - f\big(u_\beta\big)]\cos\big(\sum\limits_{r=1}^{\nu}\theta_r(t)e_r\big), e_i\Big)_2 \\ \\ w_k(0) = w_k^0 = (w^0, e_k)_2 \qquad \theta_i(0) = \theta_i^0 = (\theta^0, e_i)_2 \\ \dot{w}_k(0) = w_k^1 = (w^1, e_k)_2 \qquad \dot{\theta}_i(0) = \theta_i^1 = (\theta^1, e_i)_2, \end{cases} \tag{4.8}$$

$$\text{for } k = 1, \dots, n \quad i = 1, \dots, \nu.$$

In particular we concentrate most of the energy on the amplitude of a j-th longitudinal mode, assuming all the other initial conditions 10^{-4} smaller, i.e. (3.25) becomes

$$\overline{w}_k^0 = 10^{-4}\cdot\overline{w}_j^0 \quad \forall k \neq j, \qquad \overline{\theta}_i^0 = \overline{w}_k^1 = \overline{\theta}_i^1 = 10^{-4}\cdot\overline{w}_j^0 \quad \forall k, i. \tag{4.9}$$

Since the system is isolated and undamped, we obtain from (4.5)

$$\begin{aligned}\mathcal{E}(t) = \frac{M}{2}\sum_{q=1}^{n}\dot{w}_q^2(t) + \frac{M\ell^2}{6}\sum_{r=1}^{\nu}\dot{\theta}_r^2(t) + \frac{EI\pi^4}{2L^4}\sum_{q=1}^{n}q^4w_q^2(t) + \frac{GK\pi^2}{2L^2}\sum_{r=1}^{\nu}r^2\theta_r^2(t) \\ - \frac{2Mg\sqrt{2L}}{\pi}\sum_{\substack{q=1\\ q \text{ odd}}}^{n}\frac{w_q(t)}{q} + \int_0^L \kappa(x)F\big(u_\alpha\big)dx + \int_0^L \kappa(x)F\big(u_\beta\big)dx = \mathcal{E}(0).\end{aligned}$$

The condition (4.9) implies that

$$\begin{aligned}\mathcal{E}(0) \approx \frac{EI\pi^4 j^4 (w_j^0)^2}{2L^4} - \frac{Mg\sqrt{2L}(1-(-1)^j)w_j^0}{j\pi} \\ + 2\int_0^L \kappa(x)F\big(w_j^0 e_j - y - \lambda\big)dx.\end{aligned} \tag{4.10}$$

From now we deal with the system (4.8) considering only the 2-nd torsional mode, i.e. $i = r = 2$; the reasons of this choice are linked to the observations recorded for the TNB and the surveys of Smith-Vincent [71], see (W3)-(W4)-(W5) in Section 2.3.

Moreover, in [9, 30] a study on the eigenvalue problem $\Delta^2 w = \lambda w$ related to a rectangular plate model, finds a mathematical explanation on why the torsional instability rises with a movement like to the 2-nd torsional mode; the reasons are linked to the nature of the corresponding eigenvalues and to the presence of the sustaining cables which yield a serious constraint. Reinterpreting the statement (W4) in Section 2.3, we want to verify if the 2-nd torsional mode absorbs some energy from the j-th longitudinal mode, producing large oscillations and then torsional instability after some time. To this aim we fix the interval of time $[0, T]$ with $T =$100s and we introduce the maximum amplitude of $\overline{\theta}_2(t)$ and its expansion rate as

$$\Delta = \Delta(T) := \max_{t\in[0,T]} \overline{\theta}_2(t) - \min_{t\in[0,T]} \overline{\theta}_2(t), \qquad \mathcal{E}_r := \frac{\Delta}{2\overline{\theta}_2^0}. \tag{4.11}$$

Let note that Δ is non decreasing and $\mathcal{E}_r$ has sense because in (4.9) we put small initial conditions both on the amplitude and on the velocity. Through $\mathcal{E}_r$ we quantify how much $\theta_2(t)$ grows in time; but, again, how large does $\mathcal{E}_r$ have to be to say that the the j-th longitudinal mode is unstable on $[0, T]$? Recalling Section 3.3.5, we give this

Definition 4.1.2. *We say that the j-th longitudinal mode, solution of (4.8)-*(4.9)*, is **torsionally unstable** if the corresponding component $\overline{\theta}_2(t)$ is such that*

$$\mathcal{E}_r \geq 10. \tag{4.12}$$

In the next sections we will show some numerical results for the system (4.8)-(4.9), considering three kinds of nonlinearity for f. We apply the mechanical constants of the TNB in Table 3.1 assuming the torsional constant $K = 6.44 \cdot 10^{-6}\text{m}^4$; we refer to Section 4.5 for the dependence of the system on these parameters.

Thanks to the information presented in Section 2.3, we include in the simulations the longitudinal modes from 2 to 10, interacting only with the 2-nd torsional mode; we refer to Section 4.2.1 for the motivations on why we neglect the first longitudinal mode. In some cases (not reported here) we have included a larger number of longitudinal modes (until 14), but we have not found substantial differences in terms of torsional stability. It is clear that the precision increases as the number of longitudinal modes grows; however, the computational cost of the numerical experiments for these nonlinearities is relevant. Therefore we consider the previous choice on the number of longitudinal modes a good compromise between limiting computational burden and highlighting the phenomena which we are interested in.

To compare the different nonlinearities we consider $\overline{w}_j^0 = 2$m, slightly wider than the observations prior to the day of the failure, see witness (W2) in 2.3. This choice appears reasonable, considering the witness (W3) and also the videos available on the web [73].

The numerical experiments have been performed with the MATLAB® ODE solver `ode23tb`; for each numerical experiment it was verified the energy conservation, ascertaining a relative error, $|(\max \mathcal{E}(t) - \min \mathcal{E}(t))/\mathcal{E}(0)|$, on the integration time $[0, 100s]$ less than $2 \cdot 10^{-4}$.

4.2 The positive part nonlinearity

A possible choice for the nonlinearity in (4.6) is $f(u) = u^+ = \max\{u, 0\}$, due to McKenna [51]; other authors have adopted this nonlinearity, studying the corresponding problem, see for instance [11,44,53]. In this case the hangers follow the Hooke law if they are in tension (linear behavior, with $\kappa(x) > 0$ as elastic constant), while they slacken if compressed. Recalling (4.1)-(4.3), we can find $\kappa(x)$ from the equilibrium

$$\frac{Mg}{2} = \kappa(x)\big(-y(x) - \lambda(x)\big), \qquad \kappa(x) = -\frac{Mg + 2\kappa_0}{2y(x)}. \tag{4.13}$$

4.2.1 The spread of energy between longitudinal modes

From (W1)-(W3)-(W4) in Section 2.3 we know that the first 10 longitudinal modes are involved in the motion. In general, in the suspension bridges, the 1-st longitudinal

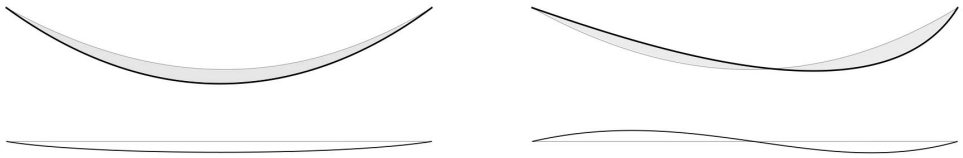

Figure 4.2: *Effects of the 1-st and the 2-nd mode on the cable.*

mode has large deformation energy if compared to the other modes; indeed, the cable undergoes an elongation (or shortening) in each point, while for the other modes only one part of the cable is subjected to elongation, see Figure 4.2. Hence for the 1-st mode case the energy of the cables become dominant; since in our ideal system the cables are fixed and they do not give energetic contributions, we expect that this mode produces unreliable results respect to the others. Indeed, the component $\overline{w}_1(t)$ is linked to the one sign shape function $\sin\left(\frac{\pi}{L}x\right)$ for $x \in (0, L)$ and this fact can give very strange results in the slackening nonlinearities.

In Figures 4.3 and 4.4 we display the solution of system (4.8)-(4.9) with $\overline{w}_5^0 = 2$m in

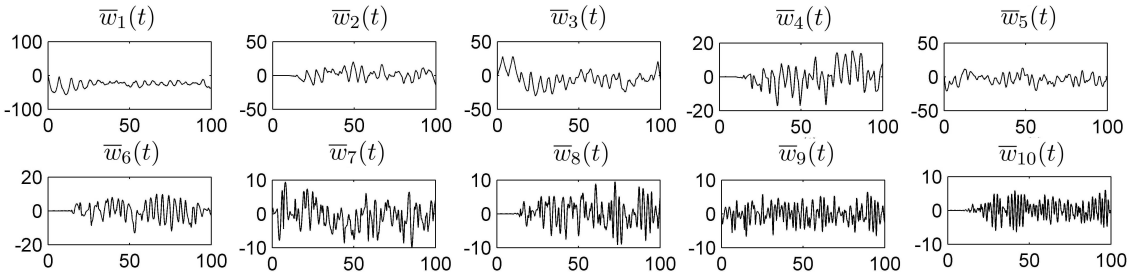

Figure 4.3: *Plots of $\overline{w}_k(t)$ in meters for the problem (4.8)-(4.9) with $f(u) = u^+$, $\theta \equiv 0$, $k = 1, \ldots, 10$ and $\overline{w}_5^0 = 2$m on the time interval $[0, 100s]$.*

the case in which $\theta \equiv 0$; the purpose is to verify how the first mode affects the others and if, during the time simulation, there are exchanges or concentrations of energy in the longitudinal modes.

As we can see in Figure 4.3 the presence of the 1-st mode alters the behavior of the others, catching a lot of energy and generating unrealistic oscillations; $\overline{w}_1(t)$ is almost always negative, so that it does not increase the energy of the system. Indeed, if the negative part of $\overline{w}_1(t)$ grows then the elastic energy does not change; in general, the motion is concentrated where it does not pay in terms of energy for the presence of the positive part function, see Equation (4.10). Since there are no physical systems in which such large displacements do not contribute to the energy, the simulations have only theoretical meaning, see also [32].

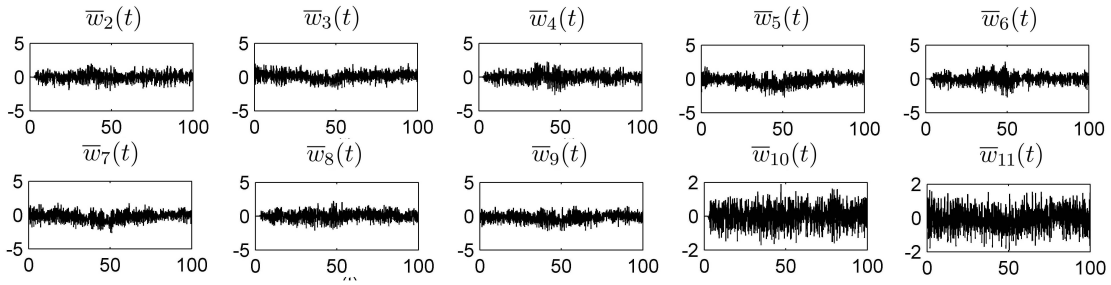

Figure 4.4: *Plots of $\overline{w}_k(t)$ in meters for the problem (4.8)-(4.9) with $f(u) = u^+$, $\theta \equiv 0$, $k = 2, \dots, 11$ and $\overline{w}_5^0 = 2m$ on the time interval $[0, 100s]$.*

If we drop the 1-st mode, the situation becomes more realistic, see Figure 4.4; in particular we observe that, concentrating the initial energy on a single mode, after some time there is a spread of energy on all the others. If the energy is initially concentrated on an odd mode, e.g. in Figure 4.4 on $\overline{w}_5(t)$, an instantaneous exchange of energy with the other odd modes occurs, while the phenomenon is delayed for the even modes. On the other hand if we concentrate the energy on an even mode the spread of energy is instantaneous for all the modes. These facts are confirmed by [32], that demonstrates that for nonlinear beam equations there is a privileged channel of transfer of energy from even to odd modes. In our case we find some similarities and, neglecting the 1-st mode, we observe that after some time all the longitudinal modes oscillate with an amplitude comparable to $\overline{w}_j^0$.

Moreover, we record a tendency in the energy to go towards the lower modes more than towards the higher, giving us a further reason to involve only the first 10 modes in the numerical simulations. We emphasize that the facts mentioned here arise also for the other nonlinearities considered in this chapter.

4.2.2 Numerical results

In this section we present some numerical experiments for the system (4.8)-(4.9) with $f(u) = u^+$, following the approach explained in Section 4.1.3. It was verified that there was slackening during the time, to assure that the system is effectively nonlinear and to have a compatible behavior with respect to the witnesses (W6)-(W7), quoted in Section 2.3.

The typical plot that we have found qualitatively is shown in Figure 4.5. The exchanges of energy pointed out in Section 4.2.1 between longitudinal modes are visible also in this situation. The most interesting result is that, in any case, $\theta_2(t)$ absorbs energy from $w_k(t)$, revealing an unstable behavior during the time. In Figure 4.6 is pro-

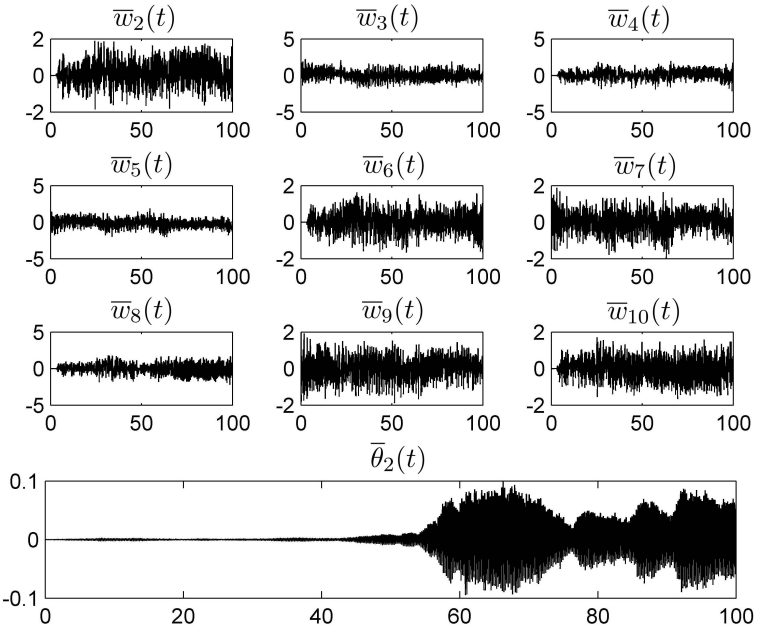

Figure 4.5: *Plots of $\overline{w}_k(t)$ in meters for $k = 2, \ldots, 10$ and $\overline{\theta}_2(t)$ in radians solutions of (4.8)-(4.9) for $f(u) = u^+$, $\overline{w}_9^0 = 2$m on $[0, 100s]$.*

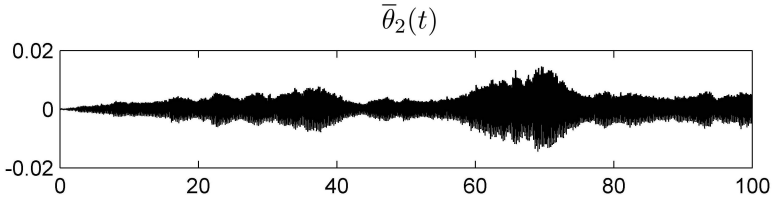

Figure 4.6: *Plot of $\overline{\theta}_2(t)$ in radians solution of (4.8)-(4.9), considering the linearization (3.16) for $f(u) = u^+$, $\overline{w}_9^0 = 2$m on $[0, 100s]$.*

posed the plot of $\overline{\theta}_2(t)$, repeating the same analysis ($\overline{w}_9^0 = 2$m), with the linearization (3.16); comparing it with Figure 4.5 it turns out that the presence of the trigonometric functions in the system generates an instability one order larger and more violent, see (W4) in Section 2.3.

A quantitative comparison between the growths of $\overline{\theta}_2(t)$, exciting different longitudinal modes, is proposed in Table 4.1, with Δ and $\mathcal{E}_r$ as in (4.11). It is evident that exciting the 9-th mode we obtain the largest growth in $\overline{\theta}_2(t)$; despite our model is ideal, it is interesting to note that this result is aligned with the observations recorded by Farquharson, see (W4) in Section 2.3. Moreover, performing the same analysis, changing the initial condition (e.g. $\overline{w}_j^0 = 1$m), we still find that $\theta_2(t)$ absorbs more energy from the 9-th mode, that, in our model, it is the most favored in attaining first the torsional instability threshold.

We do not discuss these results in quantitatively terms, since we are dealing with an ideal system, but we point out that the longitudinal and torsional oscillations lie on a range having physical sense, see Figure 4.5.

From Table 4.1 we also note a strange behavior in the energy linked to the odd

Mode excited	Δ [rad]	$\mathcal{E}_r$	Energy [GJ]
2	0.0756	189	1.67
3	0.1611	403	1.31
4	0.0222	56	1.92
5	0.0032	8	2.36
6	0.0065	16	1.96
7	0.1033	258	1.91
8	0.0163	41	1.97
9	0.1939	485	2.07
10	0.0033	8	2.00

Table 4.1: *Summary of the results on $\overline{\theta}_2(t)$ for (4.8)-(4.9) with $f(u) = u^+$, $\overline{w}_j^0 = 2$m, $\overline{\theta}_2^0 = 2 \cdot 10^{-4}$ on $[0, 100s]$.*

modes; recalling (4.10) we observe that the initial energy (constant in time) is approximately defined by the bending energy, the gravitational energy and the elastic energy of the hangers. We point out that the bending energy linked to the stiffness of the TNB's deck is very small if compared to the other bridges (as a matter of fact it collapsed), see also Section 4.5; then the elastic energy

$$\int_0^L \kappa(x) \left(\left[\overline{w}_j^0 \sin\left(\frac{j\pi}{L}x\right) + \frac{Mg}{2\kappa(x)} \right]^+ \right)^2 dx \tag{4.14}$$

is the prevailing term and it governs the strange trend of the energy which is higher in correspondence of the 5-th mode (for $\overline{w}_j^0 > 0$). Analyzing the integral it turns out that this fact is peculiar of the nonlinearities reproducing slackening and is also due to the presence of $\kappa(x)$. Indeed, the integral $I_j = \int_0^L \left([\sin(\frac{j\pi}{L}x)]^+\right)^2 dx = L(j+1)/4j$ for odd $j \geq 1$, is a decreasing function respect to j and such that $L/4 < I_j \leq L/2$. Now coming back to (4.14), if we neglect $\frac{Mg}{2\kappa(x)}$ which is small, and if we consider that $\kappa(x)$ is always positive and it has a maximum in $x = L/2$ (Figure 4.7), we see why the odd modes for which $\left([\sin(\frac{j\pi}{L}x)]^+\right)^2$ have a maximum in $x = L/2$ (i.e. the 1-st, the 5-th, the 9-th, ...) have greater energy than the other odd (i.e. the 3-rd, the 7-th,...). Obviously the situation is reversed if we consider $\overline{w}_j^0 < 0$, but, in any case, excluding the 1-st mode, the energy is comparable exciting the first 10 modes with the same $\overline{w}_j^0$, see Table 4.1.

Again some words have to be spent for the 1-st mode which, for $\overline{w}_1^0 = 2$m, would introduce in the system an energy equal to 5.64GJ (very large with respect to the others!) and for $\overline{w}_1^0 = -2$m an energy of $7.67 \cdot 10^{-2}$GJ (too small!); it is evident that this fact derives from the structure of (4.14), but physically speaking it has no sense and it clarifies further why we do not consider it in our model.

4.3 A cubic perturbation in the positive part nonlinearity

4.3.1 Motivation for the cubic term

Since we do not know what is the precise analytical expression of the slackening nonlinearity in this section and in the next we propose for (4.6) two variants to the positive part nonlinearity; here, we study $f(u) = (u + \delta u^3)^+$ that represents a cubic perturbation of $f(u) = u^+$. This nonlinearity was introduced in [38], but we give here more emphasis on the physical meaning of this choice, discussing how small has to be δ.

In literature the choice of a cubic perturbation to model the bridge behavior is rather widespread; for instance Plaut and Davis [61] suggest $f(u) = k_1 u + k_2 u^3$ with $k_1, k_2 > 0$. Bartoli and Spinelli [8] also introduce a quadratic perturbation $f(u) = k_1 u + k_2 u^2 + k_3 u^3$ with $k_1, k_2, k_3 > 0$, taking into account the nonlinear behavior of the sustaining cables to which the hangers are connected.

In [32] Garrione and Gazzola compare the nonlinearities $f(u) = u^3$ and $f(u) = (u^3)^+$ for the beam equation, dropping the linear term and highlighting the properties of the corresponding systems.

The case $f(u) = (u + \delta u^3)^+$ can be viewed as an intermediate choice between $f(u) = u^+$ and $f(u) = u^3$, indeed we consider the slackening mechanism, neglecting the contribute of the hangers if compressed and perturbing their linear behavior if stretched.

4.3.2 The choice of $\delta > 0$

Recalling (4.3), we can compute $-\big(y(x) + \lambda(x)\big)$ from the equilibrium

$$\frac{Mg}{2} = \kappa(x)\bigg(-y(x) - \lambda(x) + \delta\big(-y(x) - \lambda(x)\big)^3\bigg) \tag{4.15}$$

$$y(x) + \lambda(x) = -\sqrt[3]{\frac{1}{2\delta}\bigg(\frac{Mg}{2\kappa(x)} + \sqrt{\frac{M^2g^2}{4\kappa^2(x)} + \frac{4}{27\delta}}\bigg)} - \sqrt[3]{\frac{1}{2\delta}\bigg(\frac{Mg}{2\kappa(x)} + \sqrt{\frac{M^2g^2}{4\kappa^2(x)} + \frac{4}{27\delta}}\bigg)}. \tag{4.16}$$

(4.16) is the only real solution of the cubic equation with $\delta \neq 0$; plugging (4.16) into (4.15), recalling (4.1), we obtain $\kappa(x)$

$$\kappa(x) = -\frac{\frac{Mg}{2} + \kappa_0 + \delta\kappa_0\bigg(y^2(x) + \big(y(x) + \lambda(x)\big)^2 + y(x)\big(y(x) + \lambda(x)\big)\bigg)}{y(x) + \delta y^3(x)}. \tag{4.17}$$

In Figure 4.7 are represented the functions $\kappa(x)$ (left) and $-\big(y(x) + \lambda(x)\big)$ (right), for different δ; neglecting for a while the δ unit of measure, we see that for $\delta \gg 1$ there is a discrepancy near to the edges with respect to the case $\delta = 0$, in particular for the function $-\big(y(x) + \lambda(x)\big)$. As expected for $\delta \to 0^+$ we have that $-\big(y(x) + \lambda(x)\big) \to \frac{Mg}{2\kappa(x)}$, then, if we choose $\delta < 1$, we can approximate these functions as in (4.13) making a relative error smaller than $5{\cdot}10^{-6}$ and $5{\cdot}10^{-3}$ respectively for $\kappa(x)$ and $-\big(y(x) + \lambda(x)\big)$. Since we will consider a small δ we will apply this approximation, reducing the computational burden too; but, how small does δ have to be? In literature one finds many suggestions for the coefficients in nonlinearities such as $f(u) = u + ku^3$, generally based on restrictions on the displacement field. For example Plaut and Davis

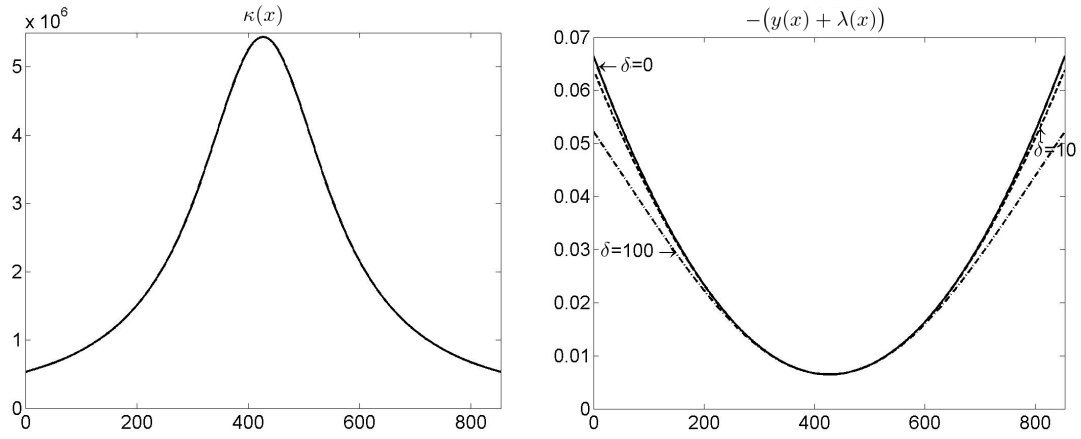

Figure 4.7: *The functions $\kappa(x)$ in N/m^2 and $-\big(y(x)+\lambda(x)\big)$ in meters with respect to x in meters and δ; the changes in $\kappa(x)$ are very small and not visible for such δ.*

[61], studying models with aerodynamic damping, proposed $k = 250$ in case of fixed cable model and $k = 0.0025$ for a deformable cable model.

In our case we have a different nonlinearity, indeed the presence of the slackening avoids problems linked to limitations on the displacements if the hangers are compressed. In $f(u) = (u + \delta u^3)^+$ the parameter δ represents a cubic perturbation of the linear behavior of the hangers if stretched, due to the restoring force applied by the two main cables (fixed in our model). We take δ =0.05m^{-2} because if we have small displacements (u <1m) the presence of the cube does not affect the linear behavior of the hangers ($u + \delta u^3 \approx u$); for u=1m the cubic term increases the displacement of 5%, for u=2m of 20%, for u=3m of 45% and so on, which seems to be reasonable because the restoring action increases with the displacement. Obviously also values of $\delta > 0$ close to 0.05m^{-2} fit with similar arguments.

4.3.3 Numerical results

In this section we show some numerical results for the system (4.8)-(4.9) with the nonlinearity $f(u) = (u + \delta u^3)^+$ with $\delta = 0.05\text{m}^{-2}$ and $\overline{w}_j^0 = 2\text{m}$. We build the Table 4.2 as in Section 4.2.2.

The presence of the cubic term does not increase, in general, the amplitudes of $\theta_2(t)$ more than the positive part nonlinearity; although the increments are smaller, the plots still reveal an unstable behavior of $\theta_2(t)$. In Figure 4.8 is shown a comparison between the solution $\overline{\theta}_2(t)$ with the nonlinearities $f(u) = u^+$ (above) and $f(u) = (u + \delta u^3)^+$, $\delta = 0.05\text{m}^{-2}$ (below) and $\overline{w}_3^0 = 2\text{m}$. It is interesting to observe how the cubic perturbation anticipates the growth of $\overline{\theta}_2(t)$, that starts almost immediately and increases more gradually, in some sense controlled; on the contrary the positive part nonlinearity generates a sudden growth of $\overline{\theta}_2(t)$ that in only about 10s rises of 3 orders of magnitude.

Mode excited	Δ [rad]	$\mathcal{E}_r$	Energy [GJ]
2	0.0079	20	1.79
3	0.3873	968	1.41
4	0.0150	38	2.06
5	0.0040	10	2.54
6	0.0103	26	2.10
7	0.0016	4	2.06
8	0.0017	4	2.12
9	0.0058	15	2.22
10	0.0090	23	2.15

Table 4.2: *Summary of the results on $\overline{\theta}_2(t)$ for (4.8)-(4.9) with $f(u) = (u + \delta u^3)^+$, $\delta = 0.05m^{-2}$, $\overline{w}_j^0 = 2m$, $\overline{\theta}_2^0 = 2 \cdot 10^{-4}$ on $[0, 100s]$.*

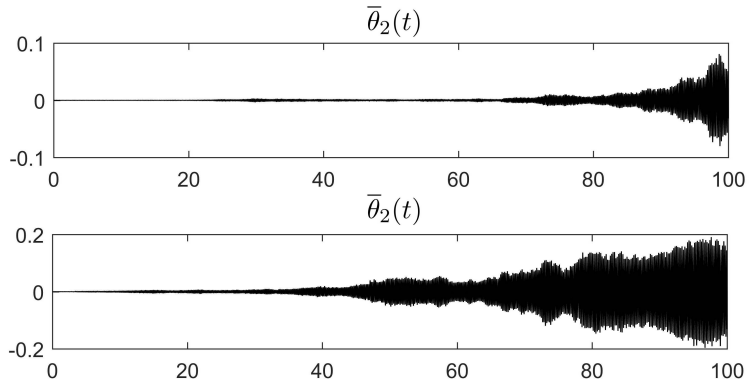

Figure 4.8: *Plots of $\overline{\theta}_2(t)$ in radians on $[0, 100s]$ for (4.8)-(4.9) with $f(u) = u^+$ (above) and $f(u) = (u + \delta u^3)^+$ with $\delta = 0.05m^{-2}$ (below), $\overline{w}_3^0 = 2m$.*

4.4 A smooth nonlinearity

4.4.1 A comparison between nonlinearities

So far, we have considered the slackening mechanisms by adopting positive part functions and consequently by modeling with an instantaneous change the slackening of the hangers. However, Brownjohn [15] claims that *the slackening mechanism is not as simple as an on/off force, as described by the positive part of the elongation.*

Hence, we consider for (4.6) a smooth nonlinearity in which the hangers slacken gradually; a smooth exponential nonlinearity was also considered in [52], clarifying in which range of vertical displacements this makes sense.

In this section we consider the smooth nonlinearity introduced in [49]; we assume

that the elastic force exerted by the hangers is

$$F_h(w \pm \ell \sin\theta) = \kappa(x)\left(w \pm \ell\sin\theta + \sqrt{(w \pm \ell\sin\theta)^2 + \left(\frac{Mg}{2\kappa(x)}\right)^2}\right) \tag{4.18}$$

In Figure 4.9 a comparison between the three considered nonlinearities is shown.

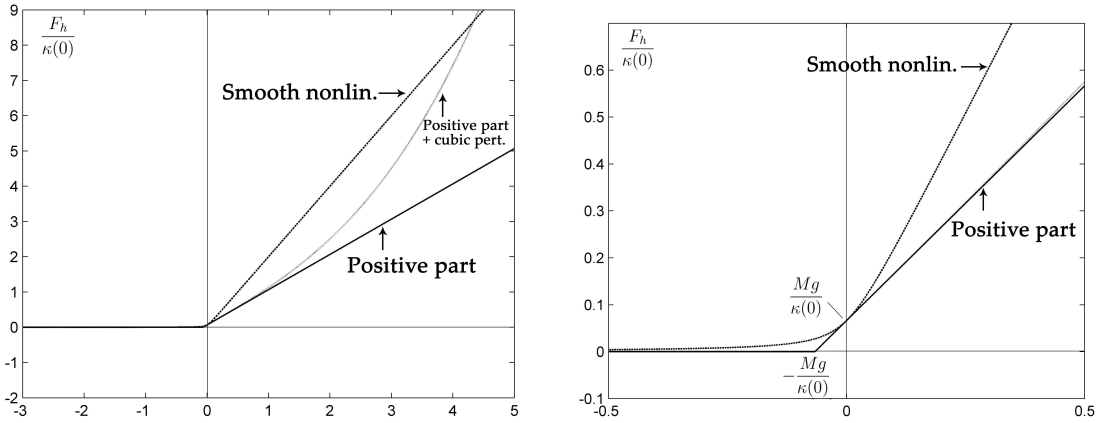

Figure 4.9: *Elastic forces corresponding to the 3 different nonlinearities, normalized with respect to the elastic coefficient $\kappa(x)$ evaluated in $x = 0$, vs vertical displacement. On the right a zoom for small displacements.*

As we can see the nonlinearity in (4.18) has the same behavior as the others at $-\infty$ and the same slope of the positive part function in 0. At $+\infty$ the smooth nonlinearity has a double growth with respect to the positive part; moreover, only after displacements larger than 4m, the cubic perturbation nonlinearity exceeds all the others. In Figure 4.9 on the right is highlighted how the smooth nonlinearity models the slackening mechanism in a gradual way compared with the other two. Introducing $v_\alpha := \sum_{q=2}^{10} w_q(t)e_q + \ell \sin\left(\theta_2(t)e_2\right)$ and $v_\beta := \sum_{q=2}^{10} w_q(t)e_q - \ell \sin\left(\theta_2(t)e_2\right)$ the system (4.8) becomes

$$\begin{cases} M\ddot{w}_k(t) + EI\dfrac{k^4\pi^4}{L^4}w_k(t) = Mg\sqrt{2L}\dfrac{(1-(-1)^k)}{k\pi} \\ \qquad\qquad -\left(\kappa(x)\left[v_\alpha + \sqrt{v_\alpha^2 + \left(\frac{Mg}{2\kappa(x)}\right)^2} + v_\beta + \sqrt{v_\beta^2 + \left(\frac{Mg}{2\kappa(x)}\right)^2}\right], e_k\right)_2 \\ \dfrac{M\ell^2}{3}\ddot{\theta}_2(t) + GK\dfrac{2^2\pi^2}{L^2}\theta_2(t) = -\ell\left(\kappa(x)\left[v_\alpha + \sqrt{v_\alpha^2 + \left(\frac{Mg}{2\kappa(x)}\right)^2}\right]\cos\left(\theta_2(t)e_2\right), e_2\right)_2 \\ \qquad\qquad +\ell\left(\kappa(x)\left[v_\beta + \sqrt{v_\beta^2 + \left(\frac{Mg}{2\kappa(x)}\right)^2}\right]\cos\left(\theta_2(t)e_2\right), e_2\right)_2 \\ w_k(0) = w_k^0 = (w^0, e_k)_2 \qquad \theta_2(0) = \theta_2^0 = (\theta^0, e_2)_2 \\ \dot{w}_k(0) = w_k^1 = (w^1, e_k)_2 \qquad \dot{\theta}_2(0) = \theta_2^1 = (\theta^1, e_2)_2, \end{cases} \tag{4.19}$$

for $k = 2, \ldots, 10$.

4.4.2 Numerical results

In this section we present the numerical results for the system (4.19)-(4.9) with $\overline{w}_j^0 =$ 2m. From the Table 4.3 it turns out that $\theta_2(t)$ absorbs more energy from $w_j(t)$ with

Mode excited	Δ [rad]	$\mathcal{E}_r$	Energy [GJ]
2	0.0887	222	3.25
3	0.1538	385	2.55
4	0.0284	71	3.76
5	0.5279	1320	4.63
6	0.1772	443	3.82
7	0.0011	3	3.74
8	0.4177	1044	3.84
9	0.3121	780	4.03
10	0.3642	911	3.87

Table 4.3: *Summary of the results on $\overline{\theta}_2(t)$ for (4.19)-(4.9) with $\overline{w}_j^0 = 2m$, $\overline{\theta}_2^0 = 2 \cdot 10^{-4}$ on $[0, 100s]$.*

respect to the cases with the other nonlinearities, highlighting an expansion rate in general larger. This fact is due to the initial energy inserted in the system, which, at the same initial conditions, it is here larger; in fact, recalling (4.10), we can compare the initial energies linked to the different nonlinearities, obtaining numerically that

$$\int_0^L \frac{\kappa(x)}{2}\left[\left(\overline{w}_j^0 \sin\left(\frac{j\pi}{L}x\right)\right)^2 + \overline{w}_j^0 \sin\left(\frac{j\pi}{L}x\right)\sqrt{\left(\overline{w}_j^0 \sin\left(\frac{j\pi}{L}x\right)\right)^2 + \left(\frac{Mg}{2\kappa(x)}\right)^2}\right.$$
$$\left. + \left(\frac{Mg}{2\kappa(x)}\right)^2 \log\left(\overline{w}_j^0 \sin(\frac{j\pi}{L}x) + \sqrt{\left(\overline{w}_j^0 \sin\left(\frac{j\pi}{L}x\right)\right)^2 + \left(\frac{Mg}{2\kappa(x)}\right)^2}\right)\right]dx >$$
$$\int_0^L \kappa(x)\frac{[\overline{w}_j^0 \sin\left(\frac{j\pi}{L}x\right) + \frac{Mg}{2\kappa(x)}]^+}{\overline{w}_j^0 \sin\left(\frac{j\pi}{L}x\right) + \frac{Mg}{2\kappa(x)}}\left[\frac{1}{2}\left(\overline{w}_j^0 \sin\left(\frac{j\pi}{L}x\right) + \frac{Mg}{2\kappa(x)}\right)^2 + \frac{\delta}{4}\left(\overline{w}_j^0 \sin\left(\frac{j\pi}{L}x\right) + \frac{Mg}{2\kappa(x)}\right)^4\right]dx$$

for $j \geq 2$ and for a physically reasonable initial condition, e.g. 0.2m$< |\overline{w}_j^0| <$6m.

In Figure 4.10 we show three plots of $\overline{\theta}_2(t)$ corresponding to three different longitudinal modes excited; qualitatively we observe that the instability arises attaining periodically peaks of amplitude that increase with the time.

4.5 Dependence of the stability of the system on the mechanical constants

It is clear that the stability of the system (4.6) strongly depends on the mechanical features of the suspension bridge. Since we have not found substantial differences in terms of torsional instability in the three nonlinearities studied, in this section we consider only the positive part function as slackening nonlinearity.

Among the mechanical parameters involved there are standard values in bridge design, while others highly depending on the designer choice. Typically, when a bridge

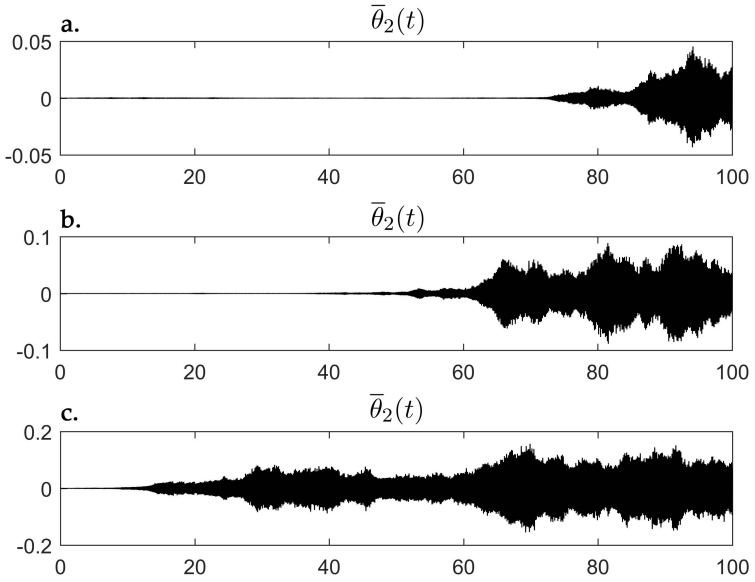

Figure 4.10: *Solutions $\overline{\theta}_2(t)$ in radians for the problem (4.19)-(4.9) with a. $\overline{w}_2^0 = 2m$, b. $\overline{w}_6^0 = 2m$ and c. $\overline{w}_9^0 = 2m$ on $[0, 100s]$.*

is built, the length of the main span L is fixed with respect to the site conditions, and, consequently, the width of the roadway ℓ; in general L also affects the cable geometry, indeed $f = \frac{L}{8} \div \frac{L}{12}$, see (3.4). The usual material employed to build the bearing structure is the steel and then we consider quite reliable E and G, the Young and shear modulus of the deck; on the other hand κ_0, involved in (4.13) and computed through (3.17), depends on the kind of wire ropes, which have a Young modulus E_h varying from 150GPa to 200GPa, see [62, §15.12.2].

An important role on the stability of the system is surely assumed by the moment of inertia I, the torsional constant K and the linear mass M of the deck; we point out that, after the TNB collapse, in the engineering design practice the instability problems of suspension bridges have been solved overbuilding and reinforcing the deck, i.e. increasing I, K, M, see also Section 2.4.2.

To study the sensitivity of the system's stability by the parameters we consider (4.6) in adimensional form. To facilitate this passage we consider, only in this section, approximated solution in form of (3.22), choosing for any $k \geq 1$

$$e_k(x) = \sin\left(\frac{k\pi x}{L}\right);$$

in practice we do not consider the normalizing constant $\sqrt{2/L}$, see (3.21), that, although is a pure number, it could create confusion in this context.

Hence, we introduce the dimension scale μ=1m, τ=1s and the following positive

adimensional constants

$$\begin{aligned} C_1 &:= \frac{EI\tau^2\pi^4}{ML^4}, & C_2 &:= \frac{3GK\tau^2\pi^2}{ML^2\ell^2}, \\ C_3 &:= \frac{3}{L\ell}\left(g + \frac{2\kappa_0}{M}\right)\mu\tau^2, & C_4 &:= \frac{1}{L}\left(g + \frac{2\kappa_0}{M}\right)\tau^2 = \frac{3\mu}{\ell}C_3, \\ C_g &:= \frac{2g\tau^2}{\mu\pi}. \end{aligned} \tag{4.20}$$

With the usual Galerkin procedure, see Section 3.3.3, we pass from (4.6) to a system of ODEs; now, dividing the first equation by μ/τ^2 and the second equation by $1/\tau^2$, we obtain the system in adimensional form

$$\begin{cases} \ddot{w}_k(t) = -C_1k^4w_k(t) + C_g\dfrac{(1-(-1)^k)}{k} - C_4\displaystyle\int_0^L \frac{u_\alpha^+ + u_\beta^+}{-y(x)} \cdot \sin(\tfrac{k\pi}{L}x)\,dx \\ \ddot{\theta}_2(t) = -C_2 2^2\theta_2(t) - C_3\displaystyle\int_0^L \frac{u_\alpha^+ - u_\beta^+}{-y(x)} \cos\left(\theta_2(t)\sin(\tfrac{2\pi}{L}x)\right) \cdot \sin(\tfrac{2\pi}{L}x)\,dx, \\ w_k(0) = w_k^0 = (w^0, e_k)_2 \qquad \theta_2(0) = \theta_2^0 = (\theta^0, e_2)_2 \\ \dot{w}_k(0) = w_k^1 = (w^1, e_k)_2 \qquad \dot{\theta}_2(0) = \theta_2^1 = (\theta^1, e_2)_2, \end{cases} \tag{4.21}$$

for $k = 2, \dots, 10$

in which, $u_\alpha = \sum_{q=2}^{10} w_q(t)\sin(\frac{q\pi}{L}x) + \ell\sin\left(\theta_2(t)\sin(\frac{2\pi}{L}x)\right) - 3gy(x)/(C_3L\ell)$ and $u_\beta = \sum_{q=2}^{10} w_q(t)\sin(\frac{q\pi}{L}x) - \ell\sin\left(\theta_2(t)\sin(\frac{2\pi}{L}x)\right) - 3gy(x)/(C_3L\ell)$. Unlike (4.8) in the system (4.21) all the quantities are meant without unit of measure, even if we do not distinguish them by the previous to not burden the notation. The system is completed by the usual initial conditions

$$\overline{w}_k^0 = 10^{-4}\cdot\overline{w}_j^0 \quad \forall k \neq j, \qquad \overline{\theta}_2^0 = \overline{w}_k^1 = \overline{\theta}_2^1 = 10^{-4}\cdot\overline{w}_j^0 \quad \forall k. \tag{4.22}$$

Since we study the stability of a single torsional mode, we find an estimate on the maximum amplitude of $\theta_2(t)$; we point out that this estimate is very coarse quantitatively, but can give qualitatively some hints on the dependence of the system by parameters.

To this aim we write the energy balance (4.5) in adimensional form for $f(u) = u^+$, $k = 2, \dots, 10$ and $i = r = 2$, i.e.

$$\begin{aligned} &\dot{\theta}_2^2(t) + 4C_2\theta_2^2(t) + \frac{1}{12}\sum_{q=2}^{10}\dot{w}_q^2(t) + \frac{C_1}{12}\sum_{q=2}^{10} q^4w_q^2(t) + \\ &- \frac{C_g}{6}\sum_{q=2}^{10}\frac{(1-(-1)^q)}{q}w_q(t) + \frac{C_3}{6}\int_0^L \frac{\left(u_\alpha^+\right)^2 + \left(u_\beta^+\right)^2}{-y(x)}dx = C_0, \end{aligned} \tag{4.23}$$

in which $C_0 := \dfrac{12\mathcal{E}(0)\tau^2}{ML\ell^2}$. Applying (4.22) as initial conditions, it is possible to prove, through some calculations that we omit, that $C_0 > 0$ for all $w_j^0 \in \mathbb{R}$.

Thanks to Proposition 4.1.1 the existence of critical points of $\theta_2(t)$ is assured when $\dot{\theta}_2(t)$ vanishes. From (4.23) we isolate $\dot{\theta}_2^2(t)$, we put it equal to zero and we obtain some points $\overline{t} \in [0, 100]$ for which $\theta_2(t)$ assumes critical values; denoting by $\overline{\theta}_2 := \theta_2(\overline{t})$ and similarly for $\dot{w}_q(t)$ and $w_q(t)$ we find

$$\begin{aligned}\overline{\theta}_2 = \Bigg\{ \frac{1}{4C_2}\Bigg(C_0 - \frac{1}{12}\sum_{q=2}^{10} \overline{\dot{w}}_q^2 - \frac{C_1}{12}\sum_{q=2}^{10} q^4 \overline{w}_q^2 + \frac{C_g}{6}\sum_{q=2}^{10} \frac{(1-(-1)^q)}{q}\overline{w}_q + \\ - \frac{C_3}{6}\int_0^L \frac{1}{-y(x)}\Bigg(\Bigg[\sum_{q=2}^{10} \overline{w}_q \sin(\frac{q\pi}{L}x) + \ell \sin\left(\overline{\theta}_2 \sin(\frac{2\pi}{L}x)\right) - \frac{3gy(x)}{C_3 L\ell} \Bigg]^+ \Bigg)^2 dx + \\ - \frac{C_3}{6}\int_0^L \frac{1}{-y(x)}\Bigg(\Bigg[\sum_{q=2}^{10} \overline{w}_q \sin(\frac{q\pi}{L}x) - \ell \sin\left(\overline{\theta}_2 \sin(\frac{2\pi}{L}x)\right) - \frac{3gy(x)}{C_3 L\ell} \Bigg]^+ \Bigg)^2 dx \Bigg\}^{1/2}.\end{aligned} \tag{4.24}$$

This equation has sense because $C_0 > 0$ is larger than all the other quantities, due to the conservation of the energy; let note that, except to the gravitational term depending on C_g, all the other quantities are nonnegative. Hence the maximum value (in absolute sense) assumed by $\theta_2(t)$ can be estimated in a very precautionary way as

$$|\overline{\theta}_2| \leq \left\{ \frac{1}{4C_2}\left(C_0 + \frac{C_g}{3}\sum_{\substack{q=3 \\ q \text{ odd}}}^{9} \frac{\max_t |w_q(t)|}{q} \right) \right\}^{1/2}. \tag{4.25}$$

This estimate depends on the initial conditions included in C_0 and on the solution $w_q(t)$ that, we do not know *a priori*, but, from the real observations [73] and the previous numerical analysis we conjecture oscillating around the amplitude of the longitudinal mode excited, in this case w_j^0 =2.

From (4.24) and (4.25) we observe that the maximum oscillations of $\theta_2(t)$ depend inversely by $\sqrt{C_2}$; as C_2 increases lower is $|\overline{\theta}_2|$ and then we gain in terms of torsional stability. Similarly if we raise C_1, by (4.24) we obtain a reduction of $|\overline{\theta}_2|$.

These observations can be inferred also by the structure of (4.21). Let suppose to increase I and K, fixing all the other parameters in Table 3.1, i.e. we multiply C_1 and C_2 by a factor $\alpha > 1$ or, equivalently, we reduce $\ddot{w}_k$, $\ddot{\theta}_i$, C_3 and C_g by α (note that C_4 is linearly dependent on C_3). This operation has some effects on the stability, indeed, to reduce C_3 is equivalent to reduce κ_0, while to reduce $\ddot{w}_k(t)$, $\ddot{\theta}_i(t)$ is equivalent to perform on (4.21) a time scaling by $\frac{1}{\sqrt{\alpha}}$, delaying the torsional instability. This means that

> an increment of the deck stiffness is somehow equivalent to reduce the elastic constant of the hangers and to delay the torsional instability.

If we multiply C_3 by $\alpha > 1$ we obtain equivalently a reduction of C_1, C_2, C_g and the same time scaling as before; hence, we have a delay of torsional instability, but, due to the reduction of the deck stiffness, large torsional oscillations start before as α is larger. In this case

> an increment of the elastic constant of the hangers is somehow equivalent to reduce the deck stiffness.

These facts are confirmed by Figure 4.11 where three plots of $\theta_2(t)$ are shown for the system (4.21)-(4.22) with $f(u) = u^+$ and $w_6^0 = 2$; we considered an amplification

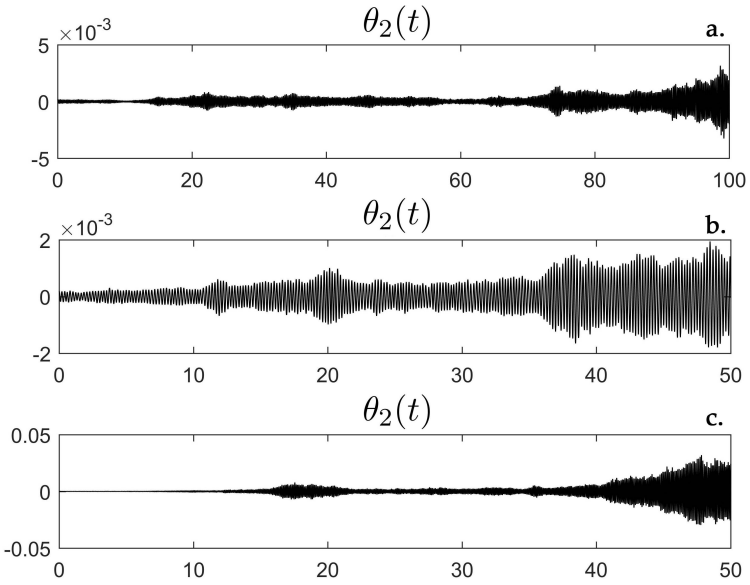

Figure 4.11: *Solutions $\theta_2(t)$ for the problem (4.21)-(4.22) with $f(u) = u^+$, $w_6^0 = 2$, a. $\alpha = 1$, b. $\alpha = 4$ multiplying C_1, C_2 and c. $\alpha = 4$ multiplying C_3.*

factor $\alpha = 4$ and due to the time scaling, we compare the new solutions until $\bar{t} = \frac{t}{2} = 50$. As expected if we amplify C_1, C_2 we obtain torsional oscillations lower (Figure 4.11b), instead, if we amplify C_3 we obtain torsional oscillations larger (Figure 4.11c). Surely a role is played also by C_g, but we do not consider it in this first-hand analysis, since it vanishes for even longitudinal mode and it is not involved in the torsional equation. Moreover, since the integral values in (4.24) depend on the same solutions, is very tricky to give *a priori* previsions on the behavior of $|\overline{\theta}_2|$, overall when we modify parameters like C_3, that appears as multiplier and also in the integrals.
We present now some numerical experiments on (4.21) varying the parameter C_1, C_2 and C_3, exciting the 9-th longitudinal mode with an initial condition equal to $w_9^0 = 2$.

The range of variation of the parameters is not purely numerical, but we point out the correspondence between the numerical values and the physical choice on the corresponding suspension bridge. In [62] many structural features of bridges are discussed and lead to the conclusion that the TNB's deck was structurally undersized and, hence, more prone to develop torsional instability; normalizing the data in [62], we think that a physical meaningful range, in which considering the linear masses for suspension bridges with deck width around 12m, is 6000÷11000 kg/m.
In the first 6 analysis we study the sensitivity of the system with respect to the linear mass M. We consider as reference the TNB cross section ("Ref." in Table 4.4), in which M =7198kg/m, I =0.15m^4, K =6.44·10^{-6}m^4 and κ_0 =4.16·10^{7}N/m, see Table 3.1, and we compute the percentage increase (or decrease) of M considering different linear masses in the range 6000÷11000 kg/m. Since the thickness of the structural elements affects M, but also I and K, in a simplified way we apply to I and K the same percentage related to the corresponding M, such that C_1 and C_2 remain unvaried. In Table 4.4 we summarize these experiments.

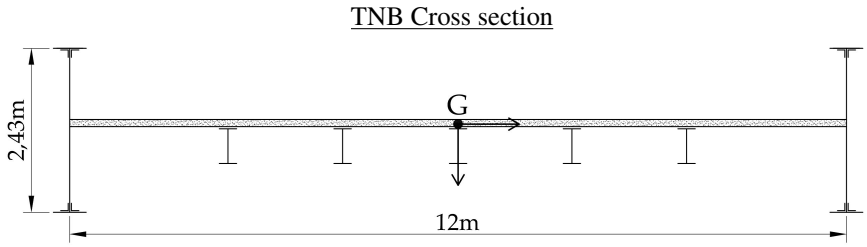

M [kg/m]	%	I [m^4]	K [m^4]	C_3	Δ	$\mathcal{E}_r$
6000	-16.64	0.13	$5.37 \cdot 10^{-6}$	8.12	0.3079	770
7198	Ref.	0.15	$6.44 \cdot 10^{-6}$	6.77	0.1939	485
8000	+11.14	0.17	$7.16 \cdot 10^{-6}$	6.09	0.3729	932
9000	+25.03	0.19	$8.05 \cdot 10^{-6}$	5.42	0.0518	130
10000	+38.93	0.21	$8.95 \cdot 10^{-6}$	4.88	0.1040	260
11000	+52.82	0.23	$9.84 \cdot 10^{-6}$	4.43	0.0926	232

Table 4.4: *Parametric analysis maintaining the TNB's deck geometry. In this case* $C_1 = 8.04 \cdot 10^{-4}$, $C_2 = 8.18 \cdot 10^{-5}$, Δ *and* $\mathcal{E}_r$ *as in (4.11) with* θ_2 *instead of* $\overline{\theta}_2$.

As we can see there is a global trend in the maximum amplitude Δ to decrease as M increases, but this trend is not so clear, because M is involved in all the constants in (4.20) and its role can be ambiguous for its small variations; indeed, to increase M implies to decrease C_1 and C_2 and this fact could reduce the stability. Anyway if we compare the maximum oscillations in the first and latter case in Table 4.4 is evident that a large variation of M gives greater stability to the system, according to the physical sense.

We complete this section with some simulations on other two suspension bridges and on the TNB with modifications on the deck's cross section, to point out the general validity of our model. In this case we also study the influence of the parameter κ_0 on the response of the system, comparing the case E_h=150GPa and E_h=200GPa, see (3.17) and Table 3.1.

In general, the torsional performances of the decks with closed cross sections are better than those with open sections [62]; the TNB had an open cross section, very prone to develop torsional instability. After its failure most long span bridges were built with closed cross section increasing their stiffness (truss-stiffened section); among these we analyze two suspension bridges: the Halsafjorden bridge (Ha), included in the ambitious Norway program to connect the coastal fjords, and the Vincent Thomas bridge (VT), a modest suspension bridge in Los Angeles. In Figure 4.12 we show the Ha's deck [57], composed by two continuous closed elements linked by transverse stiffened steel girders, and the VT's deck [1], having truss-stiffened section. We also include in these analysis the TNB case with the insertion of a continuous steel plate of 20mm under the deck in different positions, see TNB.1 and TNB.2 in Figure 4.12.
The mechanical properties of the bridges are reported in Table 4.5; other meaningful

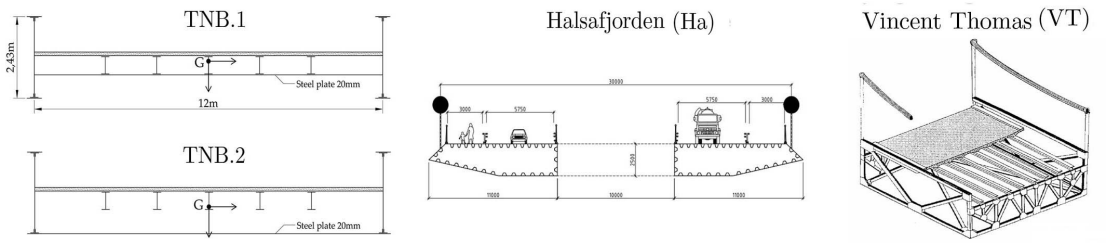

Figure 4.12: *TNB with deck's modifications, Ha's deck [57] and VT's deck [1].*

Bridge	M[kg/m]	L [m]	ℓ [m]	s_0 [m]	f [m]	n_h	ϕ [mm]	l_{int} [m]
TNB.1/2	9068	853.44	6.00	78.36	70.71	4	31.75	15.24
Ha	13250	2050.00	15.00	208.02	205.00	1	100.00	30.00
VT	8120	457.20	9.00	111.33	45.72	1	41.28	9.47

Table 4.5: *Mechanical parameters of TNB.1, TNB.2, Ha and VT bridges.*

parameters are in Table 4.6 with the results of the simulations.

As we can see, the insertion of a steel plate in TNB cross section increases the linear

Case	I [m^4]	K [m^4]	C_1 $\cdot 10^{-3}$	C_2	$E_h = 150$GPa			$E_h = 200$GPa		
					C_3	Δ	$\mathcal{E}_r$	C_3	Δ	$\mathcal{E}_r$
TNB.1	0.19	0.11	0.79	1.07	4.03	0.0444	111	5.38	0.0462	116
TNB.2	0.35	0.71	1.49	7.16	4.03	0.0104	26	5.38	0.0089	22
Ha	93.67	2.08	8.19	0.40	0.58	0.0009	2	0.77	0.0013	3
VT	3.16	0.21	$1.82 \cdot 10^5$	3.73	3.81	0.0004	1	5.08	0.0008	2

Table 4.6: *Parametric analysis on TNB varying deck geometry (TNB.1, TNB.2), on Ha and VT bridges, Δ and $\mathcal{E}_r$ as in (4.11).*

mass, the moment of inertia and, overall, the torsional coefficient of the section; in fact, only closing the cross section, K (and C_2) rises of $5 \div 6$ orders of magnitude and, if the plate is posed in the correct position (TNB.2), the torsional instability is considerably reduced.

In Figure 4.13 there is a comparison between the oscillations of $\theta_2(t)$ for TNB.2, Ha and VT bridges with E_h =150GPa. We point out that our model provides for Ha and VT bridges a situation of stability, also in the sense of the Definition 4.1.2, since $\mathcal{E}_r < 10$. Let us note that in the case of VT we have an oversized bridge with respect to its modest span, that justifies a very large coefficient C_1 in Table 4.6 and oscillations completely stable in Figure 4.13.

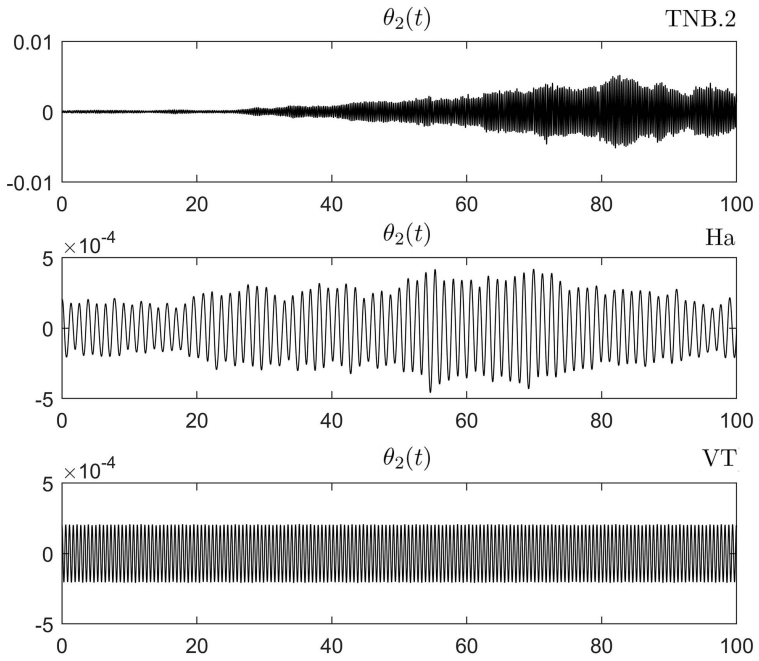

Figure 4.13: *Solutions $\theta_2(t)$ for the problem (4.21)-(4.22) with $f(u) = u^+$, $w_9^0 = 2$, $E_h = 150$GPa for TNB.2, Ha and VT bridges.*

CHAPTER 5

A model for suspension bridges with deformable cables and rigid hangers

In this chapter we present a model that is, in some sense, the counterpart of that considered in Chapter 4. It is inspired by the Melan equation, introduced by the Austrian engineer Josef Melan [55] in 1888; Melan considered the bridge as a combination of a string (the cable) and a beam (the deck) linked through some rigid hangers, considered uniformly distributed along the main span.

The equation can be derived writing the equilibrium of the beam and the string and combining the two equations through the live load, carried in part by the cable and in part by the deck. The result is the following fourth order differential equation

$$\begin{cases} EIw''''(x) - (H + h(w))w''(x) - \frac{q}{H}h(w) = r(x) \quad \forall x \in (0, L) \\ w(0) = w(L) = w''(0) = w''(L) = 0, \end{cases} \tag{5.1}$$

in which $w(x)$ is the vertical displacement of the beam (positive if directed downward), EI is the flexural rigidity of the beam, H is the horizontal tension of the string when subjected to the dead load $-q$, and $h(w)$ is a nonlocal term, representing the additional tension in the cable due to the live load $r(x)$; the beam has a span equal to L and is supposed hinged at the endpoints.

The presence of the nonlocal term makes challenging the study of the equation from both the theoretical as from the numerical point of view, see e.g. [35, 36, 70]; although (5.1) cannot be derived from the variation of the corresponding energy [36], von Kármán-Biot [77] called the Melan equation (5.1) the *fundamental equation of the theory of the suspension bridge.*

This equation is our starting point; in particular, we propose a more reliable model for suspension bridge in which

we consider two deformable cables (the strings) linked to the same deck, through inextensible hangers

as in Figure 3.4. In this way we introduce the torsional rotation of the deck, which cannot be seen in a one-dimensional model. The results presented in this chapter are published in [27].

5.1 The dynamical model

5.1.1 Energy involved in the structure

We refer to Chapter 3 for the general setting of the model, in particular in Figure 3.4 is sketched a generic cross section of the bridge, highlighting the two DOF.

In this section we mainly focus on the energy of the cables, in which is concentrated the nonlinearity of the system. First of all let us introduce the functional $\Gamma : C^1[0, L] \to \mathbb{R}$, representing the variation of the length of the cables

$$\begin{aligned} u \mapsto \Gamma(u) &:= \int_0^L \big(\sqrt{1 + [(u+y)_x]^2} - \sqrt{1 + (y')^2}\big)dx \\ &= \int_0^L \big(\sqrt{1 + [(u+y)_x]^2}\big)dx - L_c, \end{aligned} \tag{5.2}$$

where L_c is the cable length in the initial configuration, see (3.5).

The tension of the cable is composed by two contributes, the tension at rest

$$H(x) = H\xi(x) \tag{5.3}$$

and the additional tension due to the increment of the length $\Gamma(u)$ of each cable

$$\frac{AE_c}{L_c}\Gamma(u) \tag{5.4}$$

in which H is the horizontal tension, A the sectional area, E_c the Young modulus of the cable. To this terms correspond respectively two deformation energies; the amount of energy needed to deform the cable at rest under the tension (5.3) from the original position $y(x)$ to $y(x) + u(x, t)$

$$E_{C1}(u) = H \int_0^L \xi(x)\big(\sqrt{1 + [(u+y)_x]^2} - \xi(x)\big)dx$$

and the energy due to the additional tension (5.4)

$$E_{C2}(u) = \frac{AE_c}{2L_c}\Gamma(u)^2 = \frac{AE_c}{2L_c}\bigg(\int_0^L \big(\sqrt{1 + [(u+y)_x]^2} - \xi(x)\big)dx\bigg)^2.$$

Recalling that the hangers are assumed inextensible, from Figure 3.4 we see that the vertical displacements of the cables are $u(x, t) = w(x, t) \pm \ell \sin\theta(x, t)$ with respect to the cable considered; then, for a cable, we obtain the following energy

$$E_C(w, \theta) = H \int_0^L \xi\big(\sqrt{1 + [(w + \ell\sin\theta + y)_x]^2} - \xi\big)\, dx + \frac{AE_c}{2L_c}\big([\Gamma(w + \ell\sin\theta)]^2. \tag{5.5}$$

By computing the variation of the energy (5.5) with respect to w and integrating by parts, we find for all $\varphi \in C_c^\infty(0,L)$

$$\begin{aligned}\langle dE_C(w,\theta),\varphi\rangle = &-H\int_0^L \left(\frac{(w+\ell\sin\theta+y)_x\xi(x)}{\sqrt{1+[(w+\ell\sin\theta+y)_x]^2}}\right)_x \varphi\,dx\\ &-\frac{AE_c}{L_c}\Gamma(w+\ell\sin\theta)\int_0^L\left(\frac{(w+\ell\sin\theta+y)_x}{\sqrt{1+[(w+\ell\sin\theta+y)_x]^2}}\right)_x\varphi\,dx;\end{aligned}$$

by computing the variation of the energy (5.5) with respect to θ and integrating by parts, we find for all $\psi \in C_c^\infty(0,L)$

$$\begin{aligned}\langle dE_C(w,\theta),\psi\rangle = &-H\ell\int_0^L \cos\theta\left(\frac{(w+\ell\sin\theta+y)_x\xi(x)}{\sqrt{1+[(w+\ell\sin\theta+y)_x]^2}}\right)_x \psi\,dx\\ &-\frac{AE_c\ell}{L_c}\Gamma(w+\ell\sin\theta)\int_0^L\cos\theta\left(\frac{(w+\ell\sin\theta+y)_x}{\sqrt{1+[(w+\ell\sin\theta+y)_x]^2}}\right)_x\psi\,dx;\end{aligned}$$

similar computations can be performed for the second cable. In this model we consider the Vlasov torsional contribute of the deck, so that from (3.18) the total energy of the system is given by

$$\begin{aligned}\mathcal{E}(t) := &\int_0^L\left(\frac{M}{2}w_t^2+\frac{M\ell^2}{6}\theta_t^2+\frac{EI}{2}w_{xx}^2+\frac{EJ}{2}\theta_{xx}^2+\frac{GK}{2}\theta_x^2-Mgw\right)dx\\ &+H\int_0^L(\xi\sqrt{1+[(w+\ell\sin\theta+y)_x]^2}+\xi\sqrt{1+[(w-\ell\sin\theta+y)_x]^2}-2\xi^2)dx\\ &+\frac{AE_c}{2L_c}\big([\Gamma(w+\ell\sin\theta)]^2+[\Gamma(w-\ell\sin\theta)]^2\big),\end{aligned} \tag{5.6}$$

that is conserved in time.

5.1.2 The system of evolution partial differential equations

From the energy balance we derive the following system of equations. The unknowns are $w(x,t)$ and $\theta(x,t)$ for $(x,t)\in(0,L)\times(0,\infty)$

$$\begin{cases} Mw_{tt} = -EIw_{xxxx}+H\left(\frac{(w+\ell\sin\theta+y)_x\xi}{\sqrt{1+[(w+\ell\sin\theta+y)_x]^2}}+\frac{(w-\ell\sin\theta+y)_x\xi}{\sqrt{1+[(w-\ell\sin\theta+y)_x]^2}}\right)_x+Mg\\ \qquad +\frac{AE_c}{L_c}\Gamma(w+\ell\sin\theta)\left(\frac{(w+\ell\sin\theta+y)_x}{\sqrt{1+[(w+\ell\sin\theta+y)_x]^2}}\right)_x\\ \qquad +\frac{AE_c}{L_c}\Gamma(w-\ell\sin\theta)\left(\frac{(w-\ell\sin\theta+y)_x}{\sqrt{1+[(w-\ell\sin\theta+y)_x]^2}}\right)_x\\ \\ \frac{M\ell^2}{3}\theta_{tt} = -EJ\theta_{xxxx}+GK\theta_{xx}+H\ell\cos\theta\left(\frac{(w+\ell\sin\theta+y)_x\xi}{\sqrt{1+[(w+\ell\sin\theta+y)_x]^2}}-\frac{(w-\ell\sin\theta+y)_x\xi}{\sqrt{1+[(w-\ell\sin\theta+y)_x]^2}}\right)_x\\ \qquad +\frac{AE_c\ell}{L_c}\cos\theta\ \ \Gamma(w+\ell\sin\theta)\left(\frac{(w+\ell\sin\theta+y)_x}{\sqrt{(1+[w+\ell\sin\theta+y)_x]^2}}\right)_x\\ \qquad -\frac{AE_c\ell}{L_c}\cos\theta\ \ \Gamma(w-\ell\sin\theta)\left(\frac{(w-\ell\sin\theta+y)_x}{\sqrt{1+[(w-\ell\sin\theta+y)_x]^2}}\right)_x \end{cases} \tag{5.7}$$

where $y(x)$ and $\xi(x)$ depend only on x, as defined respectively in (3.11)-(3.14), and $\Gamma(\cdot)$ is defined in (5.2); the problem is completed by the boundary and initial conditions:

$$\begin{aligned} &w(0,t) = w(L,t) = w_{xx}(0,t) = w_{xx}(L,t) = 0 \qquad \text{for } t \in (0,\infty) \\ &\theta(0,t) = \theta(L,t) = \theta_{xx}(0,t) = \theta_{xx}(L,t) = 0 \qquad \text{for } t \in (0,\infty) \end{aligned} \tag{5.8}$$

$$\begin{aligned} &w(x,0) = w^0(x), \quad \theta(x,0) = \theta^0(x) \qquad \text{for } x \in (0,L) \\ &w_t(x,0) = w^1(x), \quad \theta_t(x,0) = \theta^1(x) \qquad \text{for } x \in (0,L). \end{aligned} \tag{5.9}$$

We want now to find a weak formulation of (5.7); to do this we consider the Hilbert spaces and the scalar products introduced in (3.20). For simplicity we define an application $\boldsymbol{\chi} : C^1[0,L] \to C^0[0,L]$ as

$$u \mapsto \boldsymbol{\chi}(u) := \frac{(u+y)_x}{\sqrt{1+[(u+y)_x]^2}}. \tag{5.10}$$

Computing the derivative of $\boldsymbol{\chi}$ with respect to x, we obtain the cables curvature along the main span. In the initial configuration ($u = 0$), after hooking the deck, the curvature is

$$[\boldsymbol{\chi}(0)]_x = \frac{-8f}{L^2\sqrt{\left(1+\frac{64f^2}{L^4}\left(\frac{L}{2}-x\right)^2\right)^3}} \qquad \forall x \in [0,L].$$

To simplify further the notation we put

$$\begin{aligned} h_\alpha(w,\theta) &:= -\left(H\xi + \frac{AE_c}{L_c}\Gamma(w+\ell\sin\theta)\right)\boldsymbol{\chi}(w+\ell\sin\theta), \\ h_\beta(w,\theta) &:= -\left(H\xi + \frac{AE_c}{L_c}\Gamma(w-\ell\sin\theta)\right)\boldsymbol{\chi}(w-\ell\sin\theta), \end{aligned} \tag{5.11}$$

then (5.7) becomes

$$\begin{cases} Mw_{tt} = -EIw_{xxxx} + Mg - \big[h_\alpha(w,\theta) + h_\beta(w,\theta)\big]_x \\ \dfrac{M\ell^2}{3}\theta_{tt} = -EJ\theta_{xxxx} + GK\theta_{xx} - \ell\cos\theta\big[h_\alpha(w,\theta) - h_\beta(w,\theta)\big]_x. \end{cases} \tag{5.12}$$

with the boundary conditions (5.8) and the initial data (5.9), that we recall here

$$\begin{aligned} &w(x,0) = w^0(x), \quad \theta(x,0) = \theta^0(x) \quad \forall x \in (0,L) \\ &w_t(x,0) = w^1(x), \quad \theta_t(x,0) = \theta^1(x) \quad \forall x \in (0,L) \end{aligned} \tag{5.13}$$

with the regularity

$$w^0, \theta^0 \in H^2 \cap H_0^1(0,L), \qquad w^1, \theta^1 \in L^2(0,L). \tag{5.14}$$

We say that (w,θ) is a weak solution of (5.12) if $(w,\theta) \in X_T^2$, where

$$X_T := C^0\big([0,T]; H^2 \cap H_0^1(0,L)\big) \cap C^1\big([0,T]; L^2(0,L)\big) \cap C^2\big([0,T]; H^*(0,L)\big) \tag{5.15}$$

and if (w,θ) satisfies the following equations

$$\begin{cases} M\langle w_{tt},\varphi\rangle_* + EI(w,\varphi)_{H^2} = \big(Mg,\varphi\big)_2 + \big(h_\alpha(w,\theta) + h_\beta(w,\theta),\varphi_x\big)_2 \\ \dfrac{M\ell^2}{3}\langle\theta_{tt},\psi\rangle_* + EJ(\theta,\psi)_{H^2} + GK(\theta,\psi)_{H^1} = \ell\big(h_\alpha(w,\theta) - h_\beta(w,\theta),(\psi\cos\theta)_x\big)_2 \end{cases} \tag{5.16}$$

for all $\varphi, \psi \in H^2 \cap H_0^1(0, L)$ and $t > 0$. Note that in the space X_T the boundary conditions (5.8) are already included, then from now we will not mention them.

In this framework we are ready to state the result about existence and uniqueness of a weak solution

Theorem 5.1.1. *Let $T > 0$ (including the case $T = \infty$), then for all $w^0, \theta^0, w^1, \theta^1$ satisfying (5.14) there exists a unique (global in time) weak solution $(w, \theta) \in X_T^2$ of (5.12) which satisfies (5.13).*

This result is achieved applying the Galerkin procedure for the existence part and testing the equations with the Green function, applied to the time derivative of the solutions, for the uniqueness part. The presence of the nonlinearities makes challenging the proof that is fully given in Section 5.4.

5.2 Numerical results

In this section we present some numerical experiments on the system (5.7)-(5.8)-(5.9); we follow the procedure given in Section 3.3.3. In this case we seek approximated solutions in the form

$$w(x,t) = \sum_{q=1}^{10} w_q(t)\, e_q, \qquad \theta(x,t) = \sum_{r=1}^{4} \theta_r(t)\, e_r \tag{5.17}$$

where e_k is given in (3.21).

The choice to consider 14 modes is due to the witnesses recorded before and during the collapse of the TNB, that displayed the first 10 longitudinal modes and the second torsional one, see Section 2.3; this is a good compromise between limiting computational burden and focusing on the instability phenomena visible at the TNB. Moreover, we performed the same numerical experiments with a larger number of given modes and we did not find significant changes in the instability thresholds.

Plugging (5.17) into (5.7) and projecting onto the space spanned respectively by the first 10 longitudinal modes and the first 4 torsional modes, we obtain a second order ODEs system of 14 equations as (3.23) with the initial conditions (3.24) and n =10, ν =4. Following Definition 3.3.1, we put $\overline{w}_k^0 := \sqrt{\frac{2}{L}} w_k^0$, $\overline{w}_k^1 := \sqrt{\frac{2}{L}} w_k^1$ and similarly for the θ initial conditions.

As usual we excite one single longitudinal mode (the j-th) at a time, applying an initial condition 10^{-3} smaller on all the other components, i.e. (3.25) becomes

$$\begin{aligned} &\overline{w}_k^0 = 10^{-3} \cdot \overline{w}_j^0, && \forall k \neq j, \\ &\overline{\theta}_i^0 = \overline{w}_k^1 = \overline{\theta}_i^1 = 10^{-3} \cdot \overline{w}_j^0, && \forall k, i. \end{aligned} \tag{5.18}$$

The numerical results are obtained with the software MATLAB® ODE solver `ode23tb` on the integration time $[0, 120s]$, adopting the mechanical constants of the TNB as in Table 3.1 with K =6.07·10^{-6}m^4; we refer to Section 5.3 for an analysis of sensitivity in terms of stability of the system by the mechanical parameters.

In Figures 5.1 and 5.2 we report the results of two analysis on the system, imposing respectively $\overline{w}_9^0$ =0.75m and $\overline{w}_9^0$ =3.87m. As we can see, Figure 5.1 presents a situation of stability, while in Figure 5.2, where we show only the torsional modes for brevity,

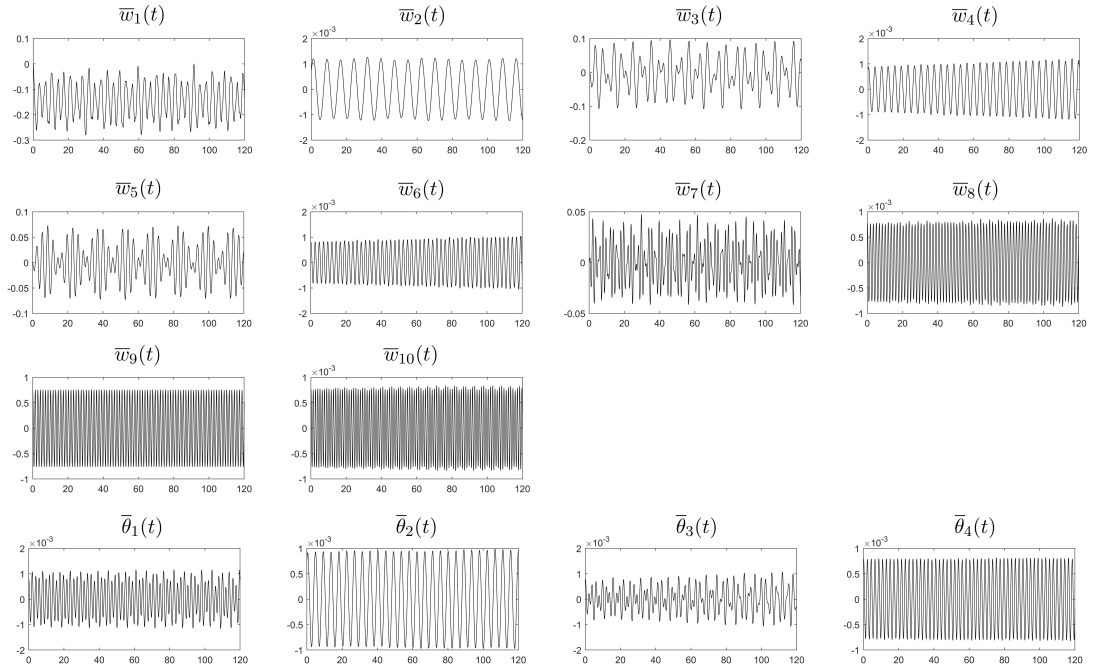

Figure 5.1: *Plots of* $\overline{w}_k(t)$ *(*$k = 1, \ldots, 10$*) in meters and* $\overline{\theta}_i(t)$ *(*$i = 1, \ldots, 4$*) in radians on* $[0, 120s]$ *with* $\overline{w}_9^0 = 0.75m$.

we are close to the torsional instability threshold and the first 3 torsional modes after 80s suddenly begin to grow. These results reveal that there is an exchange of energy

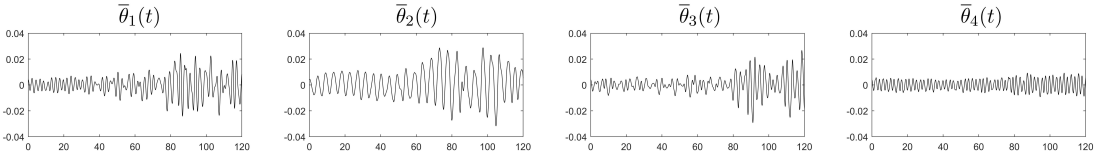

Figure 5.2: *Plots of* $\overline{\theta}_i(t)$ *(*$i = 1, \ldots, 4$*) in radians on* $[0, 120s]$ *with* $\overline{w}_9^0 = 3.87m$.

between longitudinal and torsional modes, due exclusively to the initial amplitude (and then, to the initial energy) of the longitudinal mode excited.

In Table 5.1 we summarize the thresholds of torsional instability of all the longitudinal modes obtained following the definition given in (3.28) for $K = 10^{-3}$. We point out that, exciting higher longitudinal modes, the oscillations of the 2-nd torsional mode increase quantitatively more than the others, confirming the real observations at the TNB, see for instance Figure 5.2. Our results show that, between the highest modes, the 9-th and 10-th longitudinal modes are very prone to develop torsional instability; in these cases we record W_9^0 =3.87m and W_{10}^0 =3.40m much lower with respect, for instance, the thresholds of 7-th and 8-th modes. The only mode having a threshold lower than the 9-th and 10-th modes is the 6-th, but it was not seen the day of the TNB's collapse, see (W3)-(W4)-(W5) in Section 2.3; thus, W_6^0 may be not reliable from a physical point of view.

Mode excited	W_j^0[m]	Energy [J]
1	4.06	$8.01 \cdot 10^7$
2	7.90	$7.65 \cdot 10^7$
3	4.43	$7.39 \cdot 10^7$
4	4.92	$1.35 \cdot 10^8$
5	3.93	$1.56 \cdot 10^8$
6	2.61	$8.43 \cdot 10^7$
7	4.90	$6.83 \cdot 10^8$
8	5.15	$1.12 \cdot 10^9$
9	3.87	$7.42 \cdot 10^8$
10	3.40	$6.94 \cdot 10^8$

Table 5.1: *Thresholds of instability by* (3.28) *and corresponding energy, varying the longitudinal mode excited on* $[0, 120s]$.

5.3 The influence of the mechanical parameters on the stability of the system

The system (5.7) depends on several mechanical constants that characterize the suspension bridge. In this section we study how the torsional instability of this system is affected by these parameters.

In this section we excite only the 9-th longitudinal mode ($\overline{w}_9^0$ =3.87m), applying an initial condition 10^{-3} smaller on all the others components on $[0, 120s]$. We are interested more on the qualitative datum respect to the quantitative; for brevity we do not show the plots of the 10 longitudinal modes.

We denote as "basic situation" the solution of the system with the mechanical properties of the TNB, listed in Table 3.1. Note that the constants L_c and H depend on the previous by the equations (3.5) and (3.10). Hence, in this model the behavior of the suspension bridge is influenced by 11 parameters; among them there are standard values in the bridge design while others highly depend on the designer choice. For the reasons already explained in Section 4.5 we maintain fixed the values L and ℓ, that are given by the site conditions.

The usual material employed to build the bearing structure is the steel and then we consider quite reliable E and G, the Young and shear modulus of the deck; on the other hand, the elastic modulus of the cables has to be reduced with respect to percentage of air void and the kind of ropes used in the assemblage. In [61] E_c =185GPa is considered the conventional value in the design of suspension bridges, moreover, other values of E_c, defined in [62] for every kind of ropes, remain quite close to the previous. For these reasons we do not modify the elastic constants.

The sag-span ratio $\frac{f}{L}$ assumes an important role in the bridge behavior, affecting the horizontal component of the cable force H and the total stiffness of the bridge; in the design practice it holds (3.4) and more the ratio is large more the stresses are

minimized [62]. In the TNB $\frac{f}{L} \approx \frac{1}{12}$, probably due to the requirement to reduce the tower height in order to have an economic safe.

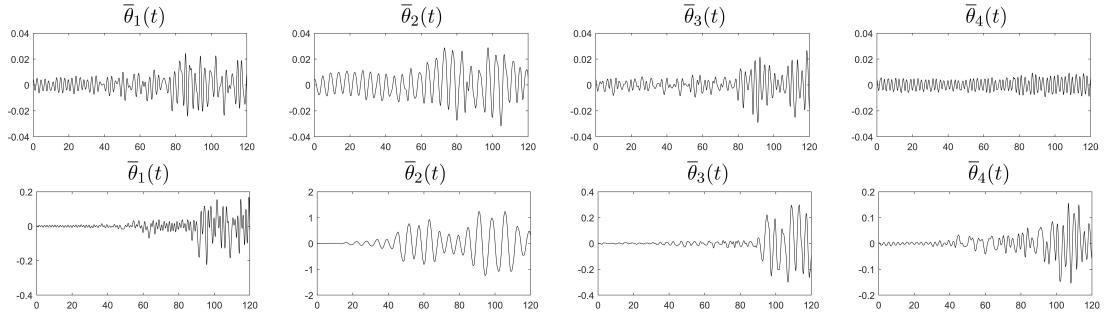

Figure 5.3: *Comparison between the torsional modes in the case $f = 70.71$m, i.e. the basic situation, (above) and $f = 106.71$m (below).*

From (5.7) we observe that the sag-span ratio is highly involved in the system, e.g. in H, L_c, $y'(x)$, $\xi(x)$ and $\Gamma(\cdot)$. In Figure 5.3 we compare the first 4 torsional modes in the cases $f = 70.71$m and $f = 106.71$m, which correspond respectively to a sag-span ratio equal to $\frac{1}{12}$ and $\frac{1}{8}$. It turns out that

> **an increment of the sag f determines a larger torsional instability in the bridge.**

In particular, it is interesting to note that when $f = 106.71$m there is a 30% decrement of H towards a 2% decrement of $\frac{AE_c}{L_c}$. Then we have that the torsional instability of the system is sensitive to the constants H and $\frac{AE_c}{L_c}$ and it grows when H decreases and $\frac{AE_c}{L_c}$ increases.

A further confirmation of it appears if we increase the sectional area of the cable A; note that for static reasons is not possible to reduce too much A and on the other hand for practical reasons (installation and tensioning) to increase overly. In any case a designer should look for reducing the sectional area of the cable not only for the stability aim deriving from our model, but also because, as the cable becomes so heavy, its capability to carry live load decreases, as suggested by [62, §15.9].

The torsional stability of the system can be improved also modifying the geometry of the deck's section. As underlined already in Section 4.5, in general, the torsional performance of closed cross sections is better than that of open sections [69]; the cross section of the TNB was open and this is one of the reasons why it was very prone to develop torsional instability. By Section 2.4.2 we know that after its failure most long span bridges were built with closed cross section increasing their stiffness (truss-stiffened section). In Figure 5.4 are plotted the $\overline{\theta}_i(t)$ $(i = 1, \dots, 4)$ components varying the moment of inertia I (case a.) and the torsional constant of the deck K (case b. and c.). With respect to the basic situation we observe that increasing of 1 order I, e.g. enhancing the thickness of the profiles maintaining an open cross section, we gain in terms of torsional stability. Also acting on the torsional properties of the section can give good results. For instance, comparing Figure 5.4b. and 5.4c. we note that the introduction of a continuous plate of 20mm in the correct position (on the bottom) reduces considerably the torsional instability and produces a relevant growth in the K constant; in fact, only closing the cross section, K rises of 5 orders of magnitude! Then

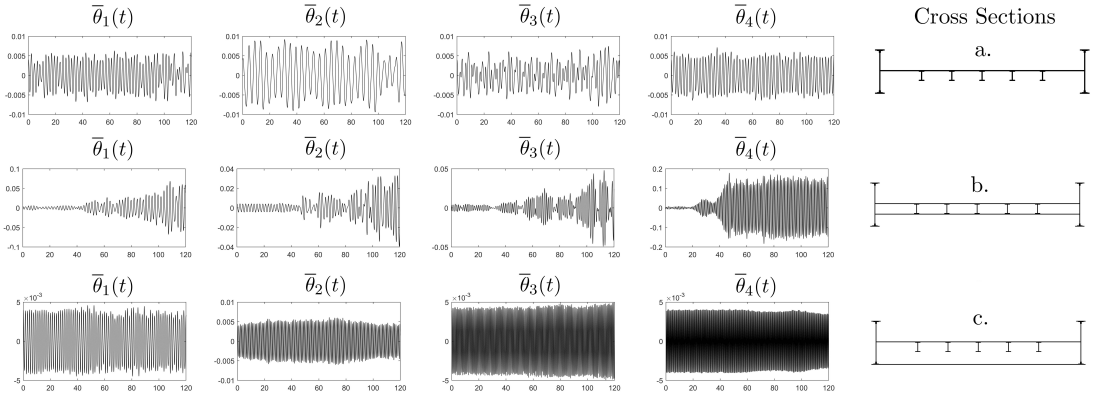

Figure 5.4: *Comparison between the torsional modes in the case a.* $I = 1.54m^4$*, b.* $K = 0.1337m^4$ *and c.* $K = 0.7171m^4$ *with the corresponding cross sections.*

our model shows that

> **a deck with closed cross section is torsionally more stable than the same deck with open section.**

About the warping constant J we record that, modifying the section properties in a physical way, it does not change enough to be considered significant in terms of torsional stability of the bridge.

Last but not least, the linear mass M of the deck is another important parameter to prevent the torsional instability, indeed, an increased mass determines a greater energy-storage capacity of the structure, reducing the oscillation's amplitudes [62]. In (5.7) M is involved in the inertia terms and implicitly in the constant H; to enhance M implies an increment of H and, as discussed before, this fact acts in favor of stability. From a database on suspension bridges published in [62, Tab. 15.13], normalizing the masses to the bridges width, it turns out that TNB had a linear mass approximately equal to $40\% \div 60\%$ the linear mass of the other bridges; even if the others have a span $20\% \div 30\%$ longer, the datum on the TNB mass is surprising and gives a further justification on the torsional oscillations recorded during its collapse. In Figure 5.5

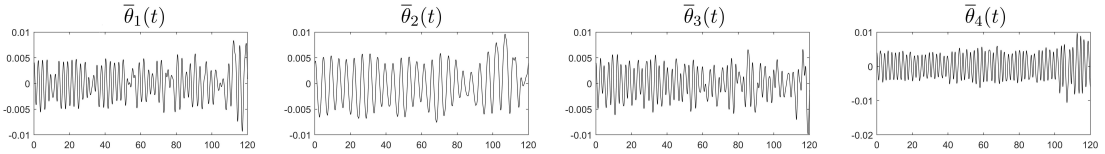

Figure 5.5: *The torsional modes for the TNB with* $M = 10077\frac{kg}{m}$.

we show $\overline{\theta}_i(t)$ $(i = 1, \ldots, 4)$ with the original linear mass of TNB 40% increased; although we are under the average normalized linear mass of the other bridges in [62, Tab. 15.13], the results is meaningful, because we see how

> **an increment in the mass of the deck reduces the torsional instability.**

In this section we have considered separately all the parameters that play a role in suspension bridges stability; we point out that the optimal situation in structural and also in economical sense can be achieved with an accurate combination of all these

parameters. For instance, the increment of M usually implies an increment of I and K, since the cross section is heavier (and thicker), in this way the best solution is not necessarily the most expensive.

5.4 Proof of the Theorem 5.1.1

In this Section we prove the existence and uniqueness of a weak solution of (5.12). The proof uses a Galerkin procedure and is divided in several steps as in classical hyperbolic PDE problems, see for instance [4, 7, 11, 40].

5.4.1 Existence of solutions

First of all we point out that, theoretically, nothing change if we consider the same number of modes for the approximated solutions of w and θ. Hence, we consider (3.22) with $n = \nu$ and the same index $q = r = k$; this choice is applied in order to reduce the notations.

Step 1: Construction of a sequence of solutions in finite dimensional spaces approximating (w, θ)
Recalling e_k in (3.21), for any $n \geq 1$ we introduce the space

$$E_n := \text{span}\{e_1, \dots, e_n\}.$$

We put for any $n \geq 1$

$$w_n^0 := \sum_{k=1}^{n} (w^0, e_k)_2 \, e_k = \frac{L^4}{\pi^4} \sum_{k=1}^{n} \frac{(w^0, e_k)_{H^2}}{k^4} \, e_k,$$

$$\theta_n^0 := \sum_{k=1}^{n} (\theta^0, e_k)_2 \, e_k = \sum_{k=1}^{n} \frac{EJ(\theta^0, e_k)_{H^2} + GK(\theta^0, e_k)_{H^1}}{\left(EJ\frac{k^4\pi^4}{L^4} + GK\frac{k^2\pi^2}{L^2} \right)} \, e_k,$$

$$w_n^1 := \sum_{k=1}^{n} (w^1, e_k)_2 \, e_k, \qquad \theta_n^1 := \sum_{k=1}^{n} (\theta^1, e_k)_2 \, e_k,$$

so that

$$w_n^0 \to w^0 \text{ in } H^2, \quad \theta_n^0 \to \theta^0 \text{ in } H^2, \quad w_n^1 \to w^1 \text{ in } L^2, \quad \theta_n^1 \to \theta^1 \text{ in } L^2 \tag{5.19}$$

as $n \to \infty$. For any $n \geq 1$ we seek (w_n, θ_n) such that

$$w_n(x,t) = \sum_{k=1}^{n} w_n^k(t) \, e_k, \quad \theta_n(x,t) = \sum_{k=1}^{n} \theta_n^k(t) \, e_k$$

and which solves the problem (5.16). Using as test functions $\varphi, \psi \in E_n$, (5.16) becomes

$$\begin{cases} M\big((w_n)_{tt}, e_j\big)_2 + EI\big(w_n, e_j\big)_{H^2} = (Mg, e_j)_2 + \big(h_\alpha(w_n, \theta_n) + h_\beta(w_n, \theta_n), e_j'\big)_2 \\ \dfrac{M\ell^2}{3}\big((\theta_n)_{tt}, e_j\big)_2 + EJ\big(\theta_n, e_j\big)_{H^2} + GK\big(\theta_n, e_j\big)_{H^1} = \ell\big(h_\alpha(w_n, \theta_n) - h_\beta(w_n, \theta_n), (e_j \cos\theta_n)_x\big)_2. \end{cases} \tag{5.20}$$

Testing n times each equation for $j = 1, \dots, n$ we obtain

$$\begin{cases} M\ddot{w}_n^k(t) + EI\dfrac{k^4\pi^4}{L^4}w_n^k(t) = Mg\dfrac{\sqrt{2L}(1-(-1)^k)}{k\pi} + \big(h_\alpha(w_n,\theta_n) + h_\beta(w_n,\theta_n), e_k'\big)_2 \\ \dfrac{M\ell^2}{3}\ddot{\theta}_n^k(t) + \left(EJ\dfrac{k^4\pi^4}{L^4} + GK\dfrac{k^2\pi^2}{L^2}\right)\theta_n^k(t) = \ell\big(h_\alpha(w_n,\theta_n) - h_\beta(w_n,\theta_n), (e_k\cos\theta_n)_x\big)_2 \end{cases} \tag{5.21}$$

$$\forall k = 1,\dots,n.$$

Since $h_\alpha(w_n,\theta_n)$ and $h_\beta(w_n,\theta_n)$ are continuous, from the theory of ODEs this finite-dimensional system with the initial conditions

$$w_n^k(0) = (w^0,e_k)_2, \qquad \theta_n^k(0) = (\theta^0,e_k)_2 \qquad \dot{w}_n^k(0) = (w^1,e_k)_2, \qquad \dot{\theta}_n^k(0) = (\theta^1,e_k)_2$$

admits a local solution defined on some $[0,t_n)$ with $t_n \in (0,T]$.

Step 2: Uniform bounds for the sequence $\{(w_n,\theta_n)\}$
We omit for the moment the spatial dependence of the approximated solutions. We test the first equation in (5.20) by $\dot{w}_n$, the second by $\dot{\theta}_n$, we integrate in x on $(0,L)$ and we sum the two equations; then we find

$$\begin{aligned} &\frac{M}{2}\frac{d}{dt}||\dot{w}_n||_2^2 + \frac{EI}{2}\frac{d}{dt}||w_n||_{H^2}^2 + \frac{M\ell^2}{6}\frac{d}{dt}||\dot{\theta}_n||_2^2 + \frac{EJ}{2}\frac{d}{dt}||\theta_n||_{H^2}^2 + \frac{GK}{2}\frac{d}{dt}||\theta_n||_{H^1}^2 = \\ &- H\int_0^L \xi\frac{(w_n+\ell\sin\theta_n+y)_x}{\sqrt{1+[(w_n+\ell\sin\theta_n+y)_x]^2}}(\dot{w}_n+\ell\dot{\theta}_n\cos\theta_n)_x dx \\ &- H\int_0^L \xi\frac{(w_n-\ell\sin\theta_n+y)_x}{\sqrt{1+[(w_n-\ell\sin\theta_n+y)_x]^2}}(\dot{w}_n-\ell\dot{\theta}_n\cos\theta_n)_x dx \\ &- \frac{AE_c}{L_c}\int_0^L \Gamma(w_n+\ell\sin\theta_n)\frac{(w_n+\ell\sin\theta_n+y)_x}{\sqrt{1+[(w_n+\ell\sin\theta_n+y)_x]^2}}(\dot{w}_n+\ell\dot{\theta}_n\cos\theta_n)_x dx \\ &- \frac{AE_c}{L_c}\int_0^L \Gamma(w_n-\ell\sin\theta_n)\frac{(w_n-\ell\sin\theta_n+y)_x}{\sqrt{1+[(w_n-\ell\sin\theta_n+y)_x]^2}}(\dot{w}_n-\ell\dot{\theta}_n\cos\theta_n)_x dx \\ &+ \int_0^L Mg\dot{w}_n dx \end{aligned} \tag{5.22}$$

Recalling the energy (5.6), we write (5.22) as

$$\begin{aligned} &\frac{d}{dt}\Bigg[\frac{M}{2}||\dot{w}_n||_2^2 + \frac{EI}{2}||w_n||_{H^2}^2 + \frac{M\ell^2}{6}||\dot{\theta}_n||_2^2 + \frac{EJ}{2}||\theta_n||_{H^2}^2 + \frac{GK}{2}||\theta_n||_{H^1}^2 - Mg\int_0^L w_n dx \\ &+ H\int_0^L (\xi\sqrt{1+[(w_n+\ell\sin\theta_n+y)_x]^2} + \xi\sqrt{1+[(w_n-\ell\sin\theta_n+y)_x]^2})dx \\ &+ \frac{AE_c}{2L_c}\big([\Gamma(w_n+\ell\sin\theta_n)]^2 + [\Gamma(w_n-\ell\sin\theta_n)]^2\big)\Bigg] = 0. \end{aligned} \tag{5.23}$$

We denote by

$$\begin{aligned}\mathcal{E}_n(t) := &\int_0^L \left(\frac{M}{2}\dot{w}_n^2 + \frac{M\ell^2}{6}\dot{\theta}_n^2 + \frac{EI}{2}[(w_n)_{xx}]^2 + \frac{EJ}{2}[(\theta_n)_{xx}]^2 + \frac{GK}{2}[(\theta_n)_x]^2\right)dx \\ &+ H\int_0^L (\xi\sqrt{1+[(w_n+\ell\sin\theta_n+y)_x]^2} + \xi\sqrt{1+[(w_n-\ell\sin\theta_n+y)_x]^2})dx \\ &+ \frac{AE_c}{2L_c}\big([\Gamma(w_n+\ell\sin\theta_n)]^2 + [\Gamma(w_n-\ell\sin\theta_n)]^2\big) - Mg\int_0^L w_n\,dx,\end{aligned} \tag{5.24}$$

the energy $\mathcal{E}(t)$ of the approximated solution (w_n, θ_n), introduced in (5.6) up to an additive constant. Integrating (5.23) in s on $(0,t)$ for $t \in (0,T)$ we find

$$\mathcal{E}_n(t) = c_n \tag{5.25}$$

where

$$\begin{aligned}c_n := &\frac{M}{2}||w_n^1||_2^2 + \frac{EI}{2}||w_n^0||_{H^2}^2 + \frac{M\ell^2}{6}||\theta_n^1||_2^2 + \frac{EJ}{2}||\theta_n^0||_{H^2}^2 + \frac{GK}{2}||\theta_n^0||_{H^1}^2 - Mg\int_0^L w_n^0 dx + \\ &+ H\int_0^L (\xi\sqrt{1+[(w_n^0+\ell\sin\theta_n^0+y)']^2} + \xi\sqrt{1+[(w_n^0-\ell\sin\theta_n^0+y)']^2})dx + \frac{AE_c}{2L_c}\cdot \\ &\cdot\left\{\left(\int_0^L [\sqrt{1+[(w_n^0+\ell\sin\theta_n^0+y)']^2} - \xi]dx\right)^2 + \left(\int_0^L [\sqrt{1+[(w_n^0-\ell\sin\theta_n^0+y)']^2} - \xi]dx\right)^2\right\}.\end{aligned}$$

We recall the Poincaré inequality $\|w\|_2 \le \Lambda\|w\|_{H^2}$ for every $w \in H^2 \cap H_0^1$ ($\Lambda > 0$) and we observe that in $\mathcal{E}_n(t)$ only the gravitational term has undefined sign. In order to estimate this term we notice that for all $\varepsilon \in (0, \frac{1}{4}]$ we have

$$-\int_0^L w_n dx \ge -\int_0^L (1+\varepsilon w_n^2)dx = -(L+\varepsilon\|w_n\|_2^2) \ge -(L+\varepsilon\Lambda^2\|w_n\|_{H^2}^2).$$

Choosing a sufficiently small $\varepsilon \in (0, \frac{1}{4}]$, we find $\eta > 0$ such that

$$\begin{aligned}\mathcal{E}_n(t) &\ge \frac{M}{2}\|\dot{w}_n\|_2^2 + \left(\frac{EI}{2} - Mg\Lambda\varepsilon\right)\|w_n\|_{H^2}^2 + \frac{M\ell^2}{6}\|\dot{\theta}_n\|_2^2 + \frac{EJ}{2}\|\theta_n\|_{H^2}^2 + \frac{GK}{2}\|\theta_n\|_{H^1}^2 \\ &\quad + H\int_0^L (\xi\sqrt{1+[(w_n+\ell\sin\theta_n+y)_x]^2} + \xi\sqrt{1+[(w_n-\ell\sin\theta_n+y)_x]^2})dx \\ &\quad + \frac{AE}{2L_c}\big([\Gamma(w_n+\ell\sin\theta_n)]^2 + [\Gamma(w_n-\ell\sin\theta_n)]^2\big) - MgL \\ &\ge \eta(\|\dot{w}_n\|_2^2 + \|w_n\|_{H^2}^2 + \|\dot{\theta}_n\|_2^2 + \|\theta_n\|_{H^2}^2 + \|\theta_n\|_{H^1}^2) - MgL.\end{aligned}$$

Then (5.25) becomes

$$\eta(||\dot{w}_n||_2^2 + ||w_n||_{H^2}^2 + ||\dot{\theta}_n||_2^2 + ||\theta_n||_{H^2}^2 + ||\theta_n||_{H^1}^2) \le C_0 + MgL.$$

where the constant $C_0 := \sup_n(|c_n|) < \infty$ is independent on n and finite thanks to (5.14). Then, we have the bound on (w_n, θ_n)

$$||\dot{w}_n||_2^2 + ||w_n||_{H^2}^2 + ||\dot{\theta}_n||_2^2 + ||\theta_n||_{H^2}^2 + ||\theta_n||_{H^1}^2 \le C_1 \qquad \forall t \in [0,T]. \tag{5.26}$$

Since $C_1 > 0$ does not depend on n and t, the global existence of (w_n, θ_n) on $[0,T]$ is ensured.

Step 3: A strongly convergent subsequence for $\{(w_n, \theta_n)\}$
To simplify the notation we denote by $L^p(V)$ the space $L^p((0,T);V(0,L))$ for $1 \leq p \leq \infty$ and by $Q = (0,T) \times (0,L)$. From the estimate (5.26) we see that

$$\begin{aligned} &\{w_n\}, \{\theta_n\} && \text{are bounded in} && L^\infty(H^2), \\ &\{\dot{w}_n\}, \{\dot{\theta}_n\} && \text{are bounded in} && L^\infty(L^2). \end{aligned}$$

Then, it is possible to extract a subsequence, still denoted by n, such that

$$\begin{aligned} &w_n \overset{*}{\rightharpoonup} w, \quad \theta_n \overset{*}{\rightharpoonup} \theta && \text{in} && L^\infty(H^2), \\ &\dot{w}_n \overset{*}{\rightharpoonup} z, \quad \dot{\theta}_n \overset{*}{\rightharpoonup} \alpha && \text{in} && L^\infty(L^2), \end{aligned}$$

in which the symbol $\overset{*}{\rightharpoonup}$ indicates the weak* convergence in L^∞; from the definition of weak* convergence and distributional derivative we obtain that $\dot{w} = z$ and $\dot{\theta} = \alpha$.
In particular from the boundedness of $\{w_n\}, \{\theta_n\}$ and $\{\dot{w}_n\}, \{\dot{\theta}_n\}$ we also have weak converge respectively in $L^2(H^2)$ and $L^2(Q)$; then, due to the compact embedding $H^1(Q) \subset L^2(Q)$, we obtain the strong convergence

$$w_n \to w, \quad \theta_n \to \theta \qquad \text{in} \qquad L^2(Q),$$

from which $\sin\theta_n \to \sin\theta$ in $L^2(Q)$, since $||\sin\theta_n - \sin\theta||_{L^2(Q)} \leq ||\theta_n - \theta||_{L^2(Q)} \to 0$ as $n \to \infty$, (similarly $\cos\theta_n \to \cos\theta$).

About the nonlocal term Γ, defined in (5.2), we see that

$$\Gamma(w_n \pm \ell\sin\theta_n) = \int_0^L \big(\sqrt{1+[(w_n \pm \ell\sin\theta_n + y)_x]^2} - \sqrt{1+[y']^2}\big)dx \to \Gamma(w \pm \ell\sin\theta),$$

thanks to the Lebesgue's dominated convergence Theorem.

Let now consider the functional $\boldsymbol{\chi}$, defined in (5.10) and let note that $|\boldsymbol{\chi}(u)| < 1$ for all $u \in C^1[0,L]$; then we have that $\boldsymbol{\chi}^2(w_n \pm \ell\sin\theta_n) < 1$ and

$$||\boldsymbol{\chi}(w_n \pm \ell\sin\theta_n)||^2_{L^2(Q)} = \int_0^T \int_0^L \frac{[(w_n \pm \ell\sin\theta_n + y)_x]^2}{1+[(w_n \pm \ell\sin\theta_n + y)_x]^2} dxdt < LT.$$

Hence $\boldsymbol{\chi}(w_n \pm \ell\sin\theta_n)$ converges weakly, up to a subsequence, to $\boldsymbol{\chi}(w \pm \ell\sin\theta)$ in $L^2(Q)$ and it is possible to pass to the limit the first equation in (5.20).

To do the same for second equation in (5.20) we consider that there exists $C_2 > 0$ such that

$$||\boldsymbol{\chi}(w_n \pm \ell\sin\theta_n)\cos\theta_n||^2_{L^2(Q)} < LT \qquad ||\boldsymbol{\chi}(w_n \pm \ell\sin\theta_n)\theta_{nx}\sin\theta_n||^2_{L^2(Q)} \leq C_2||\theta_n||^2_{L^\infty(H^1)},$$

which implies the weak convergence of these terms in $L^2(Q)$. Next, recalling the convergence of the initial conditions (5.19), we find that (w,θ) is a weak solution of (5.12)-(5.13), such that $w, \theta \in L^\infty((0,T); H^2 \cap H_0^1(0,L))$ and $\dot{w}, \dot{\theta} \in L^\infty((0,T); L^2(0,L))$. Thanks to Lemma 3.2 [74, p.69] we infer that the components $w, \theta \in C^0([0,T]; L^2(0,L))$ and $\dot{w}, \dot{\theta} \in C^0([0,T]; H^*(0,L))$. Hence, exploiting this fact and the boundedness of $w(t)$ and $\theta(t)$ in H^2 (resp. $\dot{w}(t)$ and $\dot{\theta}(t)$ in L^2), we deduce the weak continuity of the solution with respect to time.

The strong continuity can be inferred integrating the energy equality (5.23) satisfied by (w,θ), from $(0,t_n)$ and from $(0,t_0)$, subtracting the two results and passing to the

limit for all $t_n \to t_0$.
Adding from (5.12) the regularity $w \in C^2([0,T]; H^*(0,L))$, we have proved the existence of a weak solution $(w,\theta) \in X_T^2$ of (5.12) over the interval $(0,T)$, satisfying (5.13).

We know that the total energy of (5.7) is conserved in time, then the solution cannot blow up in finite time and the global existence is obtained for an arbitrary $T > 0$. □

5.4.2 Uniqueness of the solution

For contradiction, consider two solutions (w_1,θ_1), $(w_2,\theta_2) \in X_T^2$ satisfying the same initial conditions (5.13). By subtracting the two systems satisfied by (w_j,θ_j) with $j = 1,2$ and denoting by $w = w_1 - w_2$ and $\theta = \theta_1 - \theta_2$, we see that (w,θ) is a solution of

$$\begin{cases} M\langle w_{tt},\varphi\rangle_* + EI(w,\varphi)_{H^2} = \big(h_\alpha(w_1,\theta_1) - h_\alpha(w_2,\theta_2),\varphi_x\big)_2 + \big(h_\beta(w_1,\theta_1) - h_\beta(w_2,\theta_2),\varphi_x\big)_2 \\ \dfrac{M\ell^2}{3}\langle\theta_{tt},\psi\rangle_* + EJ(\theta,\psi)_{H^2} + GK(\theta,\psi)_{H^1} = \ell\big(h_\alpha(w_1,\theta_1),(\psi\cos\theta_1)_x\big)_2 \\ -\ell\big(h_\alpha(w_2,\theta_2),(\psi\cos\theta_2)_x\big)_2 - \ell\big(h_\beta(w_1,\theta_1),(\psi\cos\theta_1)_x\big)_2 + \ell\big(h_\beta(w_2,\theta_2),(\psi\cos\theta_2)_x\big)_2 \end{cases} \tag{5.27}$$

for all $\varphi,\psi \in H^2 \cap H_0^1(0,L)$ with homogeneous initial conditions and $t > 0$.

Let us introduce the Green operator $\mathcal{G} : H^{-1}(0,L) \to H_0^1(0,L)$ relative to $-\frac{d^2}{dx^2}$; then the scalar product of $u,v \in H^{-1}(0,L)$ can be computed as $(\mathcal{G}^{1/2}u,\mathcal{G}^{1/2}v)_2$ for all $u,v \in H^{-1}(0,L)$.
We omit at the moment the spatial dependence of the solutions; testing the two equations in (5.27) respectively by $\varphi = \mathcal{G}\dot w$ and $\psi = \mathcal{G}\dot\theta$ we obtain

$$\begin{cases} \dfrac{M}{2}\dfrac{d}{dt}||\dot w||^2_{H^{-1}} + \dfrac{EI}{2}\dfrac{d}{dt}||w||^2_{H^1} = \big(h_\alpha(w_1,\theta_1) - h_\alpha(w_2,\theta_2),\mathcal{G}^{1/2}\dot w\big)_2 \\ +\big(h_\beta(w_1,\theta_1) - h_\beta(w_2,\theta_2),\mathcal{G}^{1/2}\dot w\big)_2 \\ \\ \dfrac{M\ell^2}{6}\dfrac{d}{dt}||\dot\theta||^2_{H^{-1}} + \dfrac{EJ}{2}\dfrac{d}{dt}||\theta||^2_{H^1} + \dfrac{GK}{2}\dfrac{d}{dt}||\theta||^2_2 = \ell\big(h_\alpha(w_1,\theta_1),(\mathcal{G}\dot\theta\cos\theta_1)_x\big)_2 + \\ -\ell\big(h_\alpha(w_2,\theta_2),(\mathcal{G}\dot\theta\cos\theta_2)_x\big)_2 - \ell\big(h_\beta(w_1,\theta_1),(\mathcal{G}\dot\theta\cos\theta_1)_x\big)_2 + \ell\big(h_\beta(w_2,\theta_2),(\mathcal{G}\dot\theta\cos\theta_2)_x\big)_2 \end{cases} \tag{5.28}$$

Now our aim is to find an upper bound for the right hand sides terms of (5.28). We observe that the nonlinearities h_α, h_β, as defined in (5.11), depend only on functions globally Lipschitzian. Indeed, introducing the integrand $\gamma(u) := \sqrt{1+[(u+y)_x]^2}$ of $\Gamma(u)$ and considering $\boldsymbol{\chi}(u)$, respectively as in (5.2) and (5.10), we have that for all $(x,t) \in (0,L)\times(0,\infty)$ $\exists \varrho := \varrho(x,t) \in \big((w_1+\ell\sin\theta_1)_x,(w_2+\ell\sin\theta_2)_x\big)$ such that

$$|\gamma(w_1+\ell\sin\theta_1) - \gamma(w_2+\ell\sin\theta_2)| = \left|\frac{(\varrho+y_x)\big(w_1-w_2+\ell(\sin\theta_1-\sin\theta_2)\big)_x}{\sqrt{1+[\varrho+y_x]^2}}\right| \le |w_x| + \ell|\theta_x| + \ell|\theta_{2x}\theta|,$$

$$\big|\boldsymbol{\chi}(w_1+\ell\sin\theta_1) - \boldsymbol{\chi}(w_2+\ell\sin\theta_2)\big| = \frac{\big|\big(w_1-w_2+\ell(\sin\theta_1-\sin\theta_2)\big)_x\big|}{(1+[\varrho+y_x]^2)^{\frac{3}{2}}} \le |w_x| + \ell|\theta_x| + \ell|\theta_{2x}\theta|.$$

Then, recalling h_α as in (5.11), we obtain

$$
\begin{aligned}
&|h_\alpha(w_1,\theta_1)-h_\alpha(w_2,\theta_2)| \leq \big|H\xi\big\{\boldsymbol{\chi}(w_1+\ell\sin\theta_1)-\boldsymbol{\chi}(w_2+\ell\sin\theta_2)\big\}\\
&+\frac{AE_c}{L_c}\big\{\Gamma(w_1+\ell\sin\theta_1)\boldsymbol{\chi}(w_1+\ell\sin\theta_1)-\Gamma(w_2+\ell\sin\theta_2)\boldsymbol{\chi}(w_2+\ell\sin\theta_2)\big\}\big| \leq\\
&\leq H\xi(|w_x|+\ell|\theta_x|+\ell|\theta_{2x}\theta|)+\frac{AE_c}{L_c}\big|\Gamma(w_1+\ell\sin\theta_1)\big[\boldsymbol{\chi}(w_1+\ell\sin\theta_1)-\boldsymbol{\chi}(w_2+\ell\sin\theta_2)\big]\\
&+\boldsymbol{\chi}(w_2+\ell\sin\theta_2)\big[\Gamma(w_1+\ell\sin\theta_1)-\Gamma(w_2+\ell\sin\theta_2)\big]\big| \leq\\
&\leq \left(H\xi_M+\frac{AE_c}{L_c}\overline{C}\right)(|w_x|+\ell|\theta_x|+\ell|\theta_{2x}\theta|)+\frac{AE_c}{L_c}\int_0^L(|w_x|+\ell|\theta_x|+\ell|\theta_{2x}\theta|)dx,
\end{aligned}
\tag{5.29}
$$

in which $\xi_M \geq \xi(x)$, see (3.14), and we have used again that $|\boldsymbol{\chi}|<1$ and $|\Gamma(u)| = \overline{C} > 0$. Now considering (5.29), applying the Schwartz and Young inequalities, it is possible to estimate the right hand side term of the first equation in (5.28)

$$
\big|\big(h_\alpha(w_1,\theta_1)-h_\alpha(w_2,\theta_2),\mathcal{G}^{1/2}\dot{w}\big)_2\big| \leq K_1\big(||\dot{w}||^2_{H^{-1}}+||w||^2_{H^1}+||\dot{\theta}||^2_{H^{-1}}+||\theta||^2_{H^1}+||\theta||^2_2\big), \tag{5.30}
$$

with $K_1 > 0$. To obtain a similar result for the right hand side term of the second equation in (5.28) we need the following inequality ($K_2 > 0$)

$$
\begin{aligned}
&\int_0^L|[\mathcal{G}\dot{\theta}(\cos\theta_1-\cos\theta_2)]_x|dx \leq \int_0^L\big(|\mathcal{G}^{1/2}\dot{\theta}(\cos\theta_1-\cos\theta_2)|+|\mathcal{G}\dot{\theta}\ (\theta_{1x}\sin\theta_1-\theta_{2x}\sin\theta_2)|\big)dx \leq\\
&\leq ||\dot{\theta}||_{H^{-1}}||\cos\theta_1-\cos\theta_2||_2+||\dot{\theta}||_{H^*}||\theta||_{H^1}+||\dot{\theta}||_{H^*}||\theta_{2x}(\sin\theta_1-\sin\theta_2)||_2 \leq\\
&\leq K_2||\dot{\theta}||_{H^{-1}}\big(||\theta||_{H^1}+||\theta||_2\big),
\end{aligned}
$$

derived thanks to the Schwartz inequality, the embedding $H^{-1} \subset H^*$ and the Lipschitz property of the sine and cosine functions. Then the terms in the second equation of (5.28) are bounded ($K_3 > 0$)

$$
\begin{aligned}
&\big|\big(h_\alpha(w_1,\theta_1),(\mathcal{G}\dot{\theta}\cos\theta_1)_x\big)_2-\big(h_\alpha(w_2,\theta_2),(\mathcal{G}\dot{\theta}\cos\theta_2)_x\big)_2\big| =\\
&\big|\big(h_\alpha(w_1,\theta_1)-h_\alpha(w_2,\theta_2),(\mathcal{G}\dot{\theta}\cos\theta_1)_x\big)_2+\big(h_\alpha(w_2,\theta_2),[\mathcal{G}\dot{\theta}(\cos\theta_1-\cos\theta_2)]_x\big)_2\big| \leq\\
&\leq K_3\big(||\dot{w}||^2_{H^{-1}}+||w||^2_{H^1}+||\dot{\theta}||^2_{H^{-1}}+||\theta||^2_{H^1}+||\theta||^2_2\big).
\end{aligned}
\tag{5.31}
$$

Next, integrating (5.28) in s on $(0,t)$, adding the two left hand sides terms, we obtain a constant $\eta > 0$ such that

$$
\begin{aligned}
M||\dot{w}||^2_{H^{-1}}+EI||w||^2_{H^1}+\frac{M\ell^2}{3}||\dot{\theta}||^2_{H^{-1}}+EJ||\theta||^2_{H^1}+GK||\theta||^2_2 \geq\\
\geq \eta\big(||\dot{w}||^2_{H^{-1}}+||w||^2_{H^1}+||\dot{\theta}||^2_{H^{-1}}+||\theta||^2_{H^1}+||\theta||^2_2\big).
\end{aligned}
$$

Hence, from (5.30)-(5.31) and similar bounds for the terms in (5.28) involving the functional h_β, we obtain $C > 0$ such that

$$
\begin{aligned}
&||\dot{w}||^2_{H^{-1}}+||w||^2_{H^1}+||\dot{\theta}||^2_{H^{-1}}+||\theta||^2_{H^1}+||\theta||^2_2 \leq\\
&\leq C\int_0^t\big(||\dot{w}||^2_{H^{-1}}+||w||^2_{H^1}+||\dot{\theta}||^2_{H^{-1}}+||\theta||^2_{H^1}+||\theta||^2_2\big)ds.
\end{aligned}
$$

Thanks to the Gronwall Lemma we have

$$||\dot{w}(t)||^2_{H^{-1}} + ||w(t)||^2_{H^1} + ||\dot{\theta}(t)||^2_{H^{-1}} + ||\theta(t)||^2_{H^1} + ||\theta(t)||^2_2 \leq$$
$$\leq \big(||\dot{w}(0)||^2_{H^{-1}} + ||w(0)||^2_{H^1} + ||\dot{\theta}(0)||^2_{H^{-1}} + ||\theta(0)||^2_{H^1} + ||\theta(0)||^2_2\big)e^{Ct},$$

and this fact ensures

$$||\dot{w}||^2_{H^{-1}} + ||w||^2_{H^1} + ||\dot{\theta}||^2_{H^{-1}} + ||\theta||^2_{H^1} + ||\theta||^2_2 = 0 \quad \forall t \in [0,T].$$

In this way the uniqueness of the weak solution $(w,\theta) \in Z_T^2$, where

$$Z_T := C^0\big([0,T]; H_0^1(0,L)\big) \cap C^1\big([0,T]; H^{-1}(0,L)\big),$$

is obtained. Thanks to the regularity of (w,θ) and the fact that $X_T \subset Z_T$ we have a unique weak solution $(w,\theta) \in X_T^2$, satisfying the initial conditions (5.13). This fact completes the proof of Theorem 5.1.1. □

CHAPTER 6

A model for suspension bridges involving the convexification of the cables

THIS chapter can be considered as the conclusion of a multi step process involving the modeling of suspension bridges as isolated systems. The models presented in Chapter 4 and 5 represent intermediate steps aimed to give the necessary results to deal with a realistic model in which both hangers and cables are deformable.

The motivations to introduce this new model comes directly from the limits of the previous ones; it is clear that the assumption on fixed cables is very unrealistic (Chapter 4), so that the most part of the engineering literature proposes models with deformable cables and rigid hangers (Chapter 5), see e.g. [46]; in these cases the hangers are considered as rigid bars so that the deck and the cables undergo the same movement. Nevertheless also this assumption is unreasonable since the hangers resist to traction but not to compression and slackening of the hangers was observed, see (W6)-(W7) in Section 2.3.

In the simplified model considered in Chapter 5, the cable displayed shapes similar to those depicted in Figure 6.1. These pictures reproduce the shape every 10s on $[0, L]$ (with L =853.44m as for the TNB). The nonconvex shape becomes more and more evident if the energy in the system (the amplitude of oscillation) is increased. For the plots in Figure 6.1 the oscillating mode of the deck is the 9th and the initial amplitude is 3.87m, which lies in a physical range. Therefore, the assumption of rigid hangers leads to unrealistic shapes: in real bridges, the cables never take this shape due to their mass and because, instead of the cables losing convexity, the slackening of the hangers occurs. Moreover, a nonconvex configuration would increase the energy and the tension of the cable, against the variational principle of minimization of the energy. For these reasons, as in [37] we assume here that the actual shape of the cables coincides

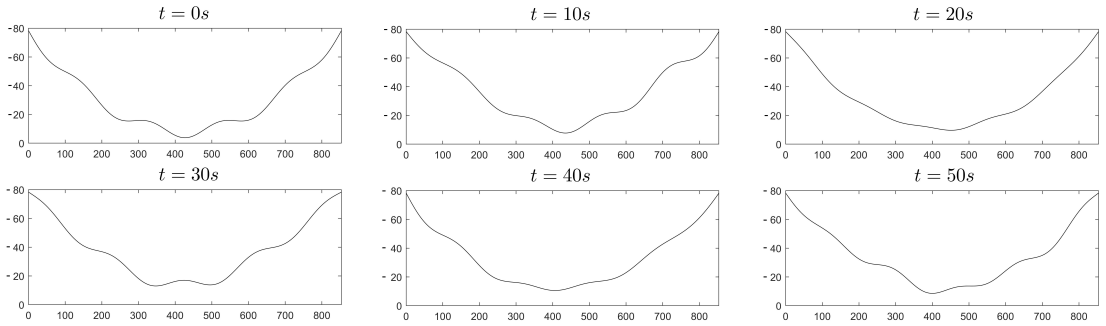

Figure 6.1: *In case of rigid hangers, cable shape with the deck oscillating on the 9th longitudinal mode of initial amplitude* $3.87m$*, see [27].*

with its *convexified shape*, namely the shape minimizing its length at the same loading condition. Acting only on this geometric feature, we are able to propose a model with only two DOF in which the slackening of the hangers is considered indirectly. The great advantage is that we do not need to find a nonlinearity simulating the slackening mechanisms.

The drawback is that the convexity constraint leads to some technical mathematical difficulties, see [16, 18]. This is why Section 6.1 is fully devoted to state some general results related to the convexification of one dimensional functions. The results of this chapter comes from [25].

6.1 The convexification of one-dimensional smooth functions

6.1.1 A possible procedure to find f^{**}

Let $\mathcal{I} = (a, b) \subset \mathbb{R}$ be an open bounded interval. Since we are interested in the specific application of a *real physical* cable, whose shape is described by a function in $H^2(\mathcal{I}) \subset C^1(\overline{\mathcal{I}})$, we consider functions

$$f \in C^1(\overline{\mathcal{I}}) \tag{6.1}$$

avoiding more general assumptions on f. Thanks to (6.1) the existence of a tangent line for all $x \in \overline{\mathcal{I}}$ is ensured.

The convexification of a function can be defined in several different equivalent ways, see [26]. Here we start with the following.

Definition 6.1.1. *Given f satisfying (6.1), its convexification $f^{**}(x)$ is the largest convex function everywhere less than or equal to $f(x)$. Hence,*

$$f^{**}(x) \leq f(x), \quad f^{**}(x) \geq f^{**}(\overline{x}) + f^{**\prime}(\overline{x})(x - \overline{x}) \qquad \forall x, \overline{x} \in \overline{\mathcal{I}}, \tag{6.2}$$

and $f^{**}(x)$ is the largest convex function satisfying (6.2).

If f is globally convex, then $f = f^{**}$ in $\overline{\mathcal{I}}$, and the graph of f lies above the tangent line in each point $\big(\overline{x}, f(\overline{x})\big)$, namely

$$f(x) \geq f(\overline{x}) + f'(\overline{x})(x - \overline{x}) \qquad \forall x, \overline{x} \in \mathcal{I}. \tag{6.3}$$

If $f \neq f^{**}$, inequality (6.3) suggests a simple way to obtain its convexification. Denote by N the set of the points $\overline{x} \in \mathcal{I}$ such that (6.3) is not verified for some $x \in \mathcal{I}$. Due to

the continuity of f and f', see (6.1), the set N is open and is composed by a number of disjoint open maximal nonempty intervals, that we denote by I^i with i varying in some possibly infinite set of integers $J := \{1, 2, \dots\}$:

$$N = \{\overline{x} \in \mathcal{I} : \exists x \in \mathcal{I} \ \ s.t. \ \ f(x) < f(\overline{x}) + f'(\overline{x})(x - \overline{x})\} = \bigcup_{i \in J} I^i.$$

All these intervals are nonempty and delimited by two points that we denote by a^i and b^i:

$$I^i := (a^i, b^i) \subset \mathcal{I} \qquad \forall i \in J.$$

In order to find f^{**}, we replace f on these intervals with linear functions whose graphs link the endpoints $\big(a^i, f(a^i)\big)$ and $\big(b^i, f(b^i)\big)$ for all $i \in J$, namely

$$f^{**}(x) = \begin{cases} f(a^i) + \dfrac{f(b^i) - f(a^i)}{b^i - a^i}(x - a^i) & x \in I^i, \ i \in J, \\ f(x) & x \in \overline{\mathcal{I}} \setminus \bigcup\limits_{i \in J} I^i. \end{cases} \tag{6.4}$$

Note that if $a^i \neq a$ and $b^i \neq b$ for some $i \in J$, see Figure 6.2 on the left, the graph of

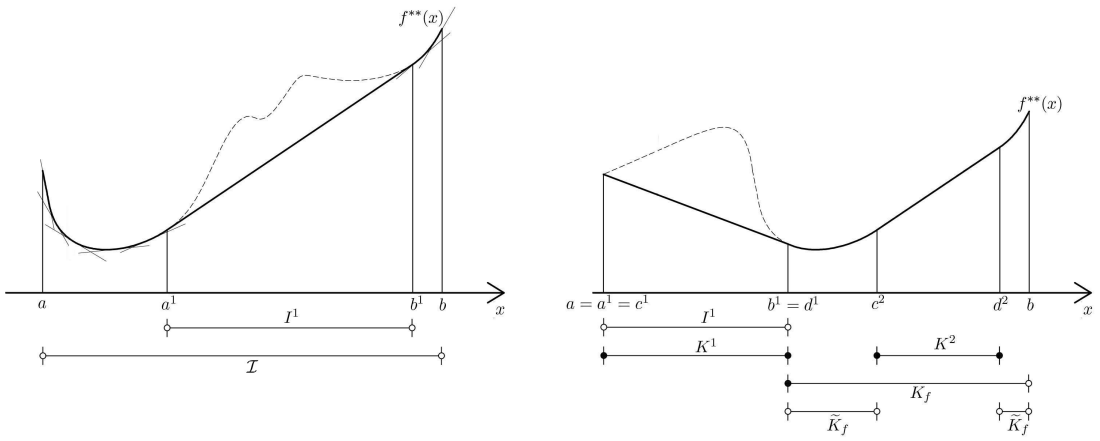

Figure 6.2: *Examples of convexification of f.*

the linear function coincides with the tangent lines to f at the endpoints of this interval, that is,

$$\frac{f(b^i) - f(a^i)}{b^i - a^i} = f'(a^i) = f'(b^i). \tag{6.5}$$

If $a^i = a$ or $b^i = b$ for some $i \in J$, then (6.5) holds except at the boundary points, see Figure 6.2 on the right. In any case, we obtain that $f^{**} \in C^1(\overline{\mathcal{I}})$.

In the sequel a major role will be played by the maximal intervals where f^{**} is affine. We denote by $K^i = [c^i, d^i]$, $i \in J_C$, the (possibly countable) family of all these intervals. Let $K_f := \mathcal{I} \setminus N$ be the contact set of f, i.e.

$$K_f := \{x \in \mathcal{I} : \ f(x) = f^{**}(x)\}$$

and note that $c^i, d^i \in K_f \cup \{a, b\}$. We also use the notation

$$\widetilde{K}_f := K_f \setminus \bigcup_{i \in J_C} K^i.$$

Around points $x \in \widetilde{K}_f$ the function f is strictly convex, meaning that

$$f^{**}(x) > f(x_0) + f'(x_0)\,(x - x_0), \qquad \forall x \in [a, b],\ x \neq x_0.$$

More precisely, the set $\{(x, f^{**}(x)) : x \in \widetilde{K}_f \cup \{a, b\}\}$ coincides with the set $\operatorname{expo}\operatorname{epi} f^{**}$ of exposed points of the epigraph of f^{**}, see Section 6.5 for the precise definitions and Figure 6.2 on the right.

6.1.2 The variation of functionals of convexified functions

In order to study the behavior of the cables, we need to compute the variation of energies depending on the convexification of a function. We deal with functionals such as $u \mapsto \int_{\mathcal{I}} [\Lambda(u)]^{**} dx$ with $\Lambda \in C^1(\mathbb{R})$ and we need to compute the Gateaux derivative of such functionals. As we shall see, in general these functionals are not Gateaux differentiable at every point. To illustrate this phenomenon, let us consider first the particular case $\Lambda(u) = u$.

Proposition 6.1.2. *Let $f \in C^1(\overline{\mathcal{I}})$ and let f^{**}, $K^i = [c^i, d^i]$ ($i \in J_C$) and $\widetilde{K}_f$ be as in Section 6.1.1. Let $\varphi \in C_c^\infty(\mathcal{I})$, and, for every $i \in J_C$, let us define the extended real-valued functions*

$$\varphi_i^{\pm} \colon K^i \to \overline{\mathbb{R}}, \qquad \varphi_i^{\pm}(x) := \begin{cases} \varphi(x) & x \in K^i \cap (K_f \cup \{a, b\}), \\ \pm\infty & x \in K^i \setminus (K_f \cup \{a, b\}). \end{cases} \tag{6.6}$$

Then we have

$$\lim_{s \to 0^{\pm}} \int_{\mathcal{I}} \frac{(f + s\varphi)^{**} - f^{**}}{s}\, dx = \int_{\mathcal{I}} \mathcal{J}_{\pm}^{\varphi}\, dx, \tag{6.7}$$

where

$$\mathcal{J}_{\pm}^{\varphi}(x) := \begin{cases} \pm(\pm\varphi_i^{\pm})^{**}(x) & x \in K^i,\ i \in J_C, \\ \varphi(x) & x \in \widetilde{K}_f. \end{cases} \tag{6.8}$$

The proof of Proposition 6.1.2 is given in Section 6.5. As a straightforward consequence of Proposition 6.1.2, we have

Corollary 6.1.3. *Under the same assumptions of Proposition 6.1.2, the functional $f \mapsto \int_{\mathcal{I}} f^{**}$ is Gateaux–differentiable at f if and only if*

$$\overline{K_f} = \overline{\widetilde{K}_f}, \quad \textit{i.e., } f > f^{**} \textit{ on any open interval where } f^{**} \textit{ is affine}. \tag{6.9}$$

In this case, for every $\varphi \in C_c^\infty(\mathcal{I})$ it holds that $\mathcal{J}_+^{\varphi} = \mathcal{J}_-^{\varphi} =: \mathcal{J}^{\varphi}$, with

$$\mathcal{J}^{\varphi}(x) := \begin{cases} \varphi(a^i) + \dfrac{\varphi(b^i) - \varphi(a^i)}{b^i - a^i}(x - a^i) & x \in I^i,\ i \in J, \\ \varphi(x) & x \in K_f. \end{cases} \tag{6.10}$$

Remark 6.1.4. When condition (6.9) is satisfied, the intervals I^i coincide with the interior of the intervals K^i, i.e. one has that $a^i = c^i$ and $b^i = d^i$ for every $i \in J$, see Figure 6.2 on the right.

Remark 6.1.5. Note that if $f \in C^1(\overline{\mathcal{I}})$ and $\varphi \in C_c^\infty(\mathcal{I})$ then $\mathcal{J}_\pm^\varphi, \mathcal{J}^\varphi \in W^{1,1}(0, L)$.

Proposition 6.1.2 states that the shape of the test function φ may not be preserved whenever the variation involving a convexification is concerned, see Figure 6.3b). Clearly, in the case where f is globally convex the shape of φ is maintained, and we are back to the classical Gateaux derivative. This possible change of φ makes the problem mathematically very challenging and this is the price to pay in order to have a physically reliable modeling of the cables.

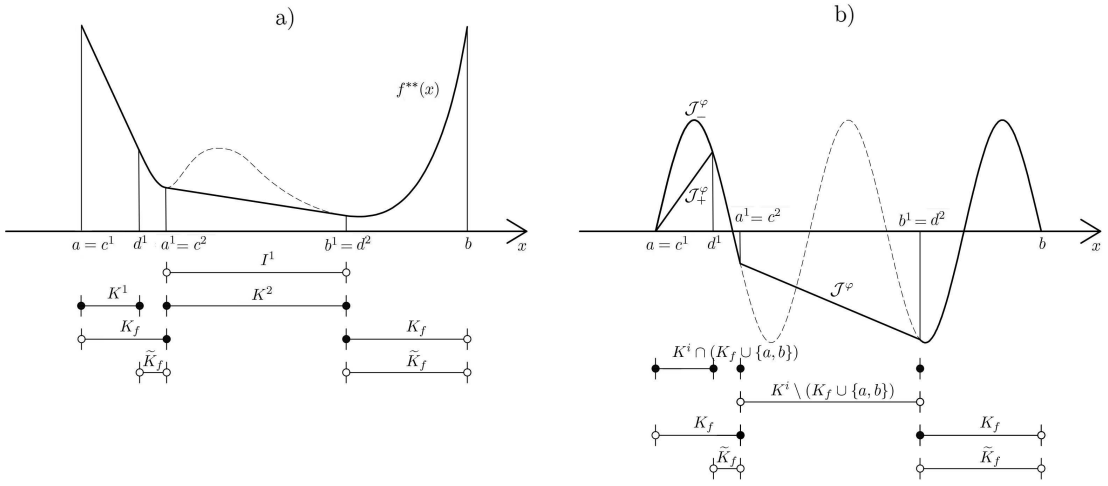

Figure 6.3: *a) Convexification of a function f and b) the corresponding $\mathcal{J}_\pm^\varphi(x)$, $\mathcal{J}^\varphi(x)$ introduced, respectively, in (6.8) and (6.10).*

In the following example we explain why assumption (6.9) is necessary in order to have the Gateaux–differentiability of the functional.

Example 6.1.6. For some $\mu, \upsilon \in \mathbb{R}$, take $f(x) = \mu x + \upsilon$ on $\mathcal{I} = (-2, 2)$ and take $\varphi \in C_c^\infty(\mathcal{I})$ defined by

$$\varphi(x) = \begin{cases} e^{\frac{1}{x^2-1}} & x \in (-1, 1), \\ 0 & x \in \overline{\mathcal{I}} \setminus (-1, 1). \end{cases}$$

Computing the limits (6.7) we obtain

$$\lim_{s \to 0\pm} \int_{\mathcal{I}} \frac{(s\varphi)^{**}}{s}\, dx = \int_{\mathcal{I}} \pm(\pm\varphi)^{**} dx, \tag{6.11}$$

that depend on the sign of s. Indeed, if $s > 0$ we have $(s\varphi)^{**} \equiv 0$ so that (6.11) vanishes, on the other hand, if $s < 0$, we have that $(s\varphi)^{**} = s[-(-\varphi)^{**}]$, and we obtain the point $\zeta \approx 0.25$, such that

$$-(-\varphi)^{**}(x) = \begin{cases} \varphi(x) & |x| \in [0, \zeta], \\ \dfrac{e^{\frac{1}{\zeta^2-1}}}{\zeta - 2}(|x| - 2) & |x| \in (\zeta, 2), \end{cases}$$

see Figure 6.4. It is readily seen that the right and left limits of (6.11) are different,

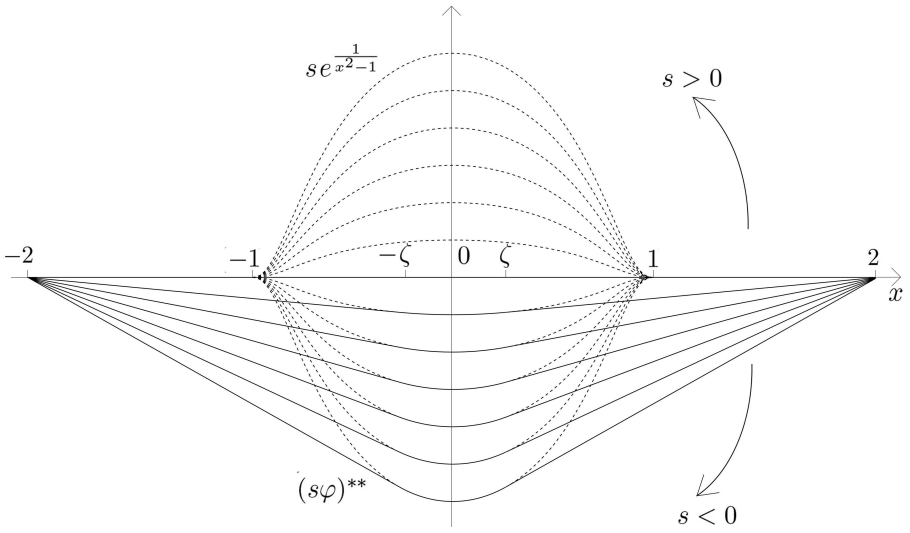

Figure 6.4: *Plot of $(s\varphi)^{**}$ and $s\varphi$ (dashed), for some values of the parameter s.*

implying the non-existence of the Gateaux derivative. □

Let us show in a simple case how the functions $\varphi_i^{\pm}$, defined at (6.6), appear in the computation of $\mathcal{J}_{\pm}^{\varphi}$.

Example 6.1.7. Let $\mathcal{I} = (0, 4\pi)$ and let $f\colon \overline{\mathcal{I}} \to \mathbb{R}$ be the function $f(x) = 1 - \cos x$. Hence, $f \in C^1(\overline{\mathcal{I}})$, $f^{**} \equiv 0$, $K_f = \{2\pi\}$, so that there is only one maximal interval $K^1 := [0, 4\pi]$ where f^{**} is affine. Given $\varphi \in C_c^\infty(\mathcal{I})$, we have that

$$\varphi_1^+(x) = \begin{cases} \varphi(x) & x \in \{0, 2\pi, 4\pi\}, \\ +\infty & \text{otherwise.} \end{cases}$$

Hence $(\varphi_1^+)^{**}$ is the continuous function, affine in $[0, 2\pi]$ and $[2\pi, 4\pi]$, such that $(\varphi_1^+)^{**}(2k\pi) = \varphi(2k\pi)$ for $k = 0, 1, 2$, and $\mathcal{J}_+^{\varphi} = (\varphi_1^+)^{**}$. The function $\mathcal{J}_-^{\varphi}$ can be computed in a similar way. □

The next statement generalizes Proposition 6.1.2 and provides the main result of this section.

Theorem 6.1.8. *Consider $u \in C^1(\overline{\mathcal{I}}, \mathbb{R})$, $\Lambda \in C^1(\mathbb{R})$ and let Λ' be its derivative. Let $f := \Lambda \circ u : \overline{\mathcal{I}} \to \mathbb{R}$ and let f^{**}, I^i $(i \in J)$, K^i $(i \in J_C)$ and $\widetilde{K}_f$ be as in Section 6.1.1. Furthemore, let f satisfy assumption* (6.9)*. Then, for all $\varphi \in C_c^\infty(\mathcal{I})$, we have*

$$\lim_{s\to 0} \int_{\mathcal{I}} \frac{[\Lambda(u + s\varphi)]^{**} - [\Lambda(u)]^{**}}{s}\, dx = \int_{\mathcal{I}} \mathcal{G}^{u,\varphi}\, dx,$$

where

$$\mathcal{G}^{u,\varphi}(x) := \begin{cases} \varphi(a^i)\Lambda'\big(u(a^i)\big) + \dfrac{\varphi(b^i)\Lambda'\big(u(b^i)\big) - \varphi(a^i)\Lambda'\big(u(a^i)\big)}{b^i - a^i}(x - a^i) & x \in I^i, \\ \varphi(x)\Lambda'\big(u(x)\big) & x \in \overline{\mathcal{I}} \setminus \bigcup\limits_{i\in J} I^i. \end{cases}$$

Also the proof of Theorem 6.1.8 is given in Section 6.5. Here we give an instructive application of Theorem 6.1.8.

Example 6.1.9. Take $\theta \in C^1(\overline{\mathcal{I}})$, $\Lambda(\theta) = \sin\theta$ and $\psi \in C_c^\infty(\mathcal{I})$, then Theorem 6.1.8 yields

$$\lim_{s\to 0} \int_{\mathcal{I}} \frac{[\sin(\theta + s\psi)]^{**} - [\sin\theta]^{**}}{s}\, dx = \int_{\mathcal{I}} \mathcal{G}^{\theta,\psi}\, dx,$$

with

$$\mathcal{G}^{\theta,\psi}(x) := \begin{cases} \psi(a^i)\cos\big(\theta(a^i)\big) + \dfrac{\psi(b^i)\cos\big(\theta(b^i)\big) - \psi(a^i)\cos\big(\theta(a^i)\big)}{b^i - a^i}(x - a^i) & x \in I^i, \\ \psi(x)\cos\big(\theta(x)\big) & x \in \overline{\mathcal{I}} \setminus \bigcup\limits_{i\in J} I^i. \end{cases} \tag{6.12}$$

6.1.3 Properties of the projection on the cone of convex functions

In this section we give some properties of convexified functions that we will use in the sequel to obtain a priori estimates. In the sequel we denote by $\|\cdot\|_p$ the norm related to the Lebesgue space $L^p(a,b)$ with $1 \le p \le \infty$. All the proofs are given in Section 6.5.

Proposition 6.1.10. *Let $T\colon C^0([a,b]) \to C^0([a,b])$ be the operator defined by*

$$Tf := (F^{**})', \qquad \text{where } F(x) := \int_a^x f(y)\, dy, \quad y \in [a,b]. \tag{6.13}$$

Then

$$\int_a^b |Tf - Tg| \le \int_a^b |f - g| \qquad \forall f, g \in C^0([a,b]). \tag{6.14}$$

Proposition 6.1.10 is essential to show that the map T is Lipschitzian from L^1 to L^1.

Proposition 6.1.11. *Let $T\colon L^1(a,b) \to L^1(a,b)$ be the operator defined by* (6.13). *Then*

$$\|Tf - Tg\|_1 \le \|f - g\|_1 \qquad \forall f, g \in L^1(a,b). \tag{6.15}$$

In turn, Proposition 6.1.11 enables us to prove that the convexification is a Lipschitzian transformation from $W_0^{1,1}$ to $W_0^{1,1}$.

Corollary 6.1.12. *The operator $P\colon W_0^{1,1}(a,b) \to W_0^{1,1}(a,b)$, defined by $P[F] := F^{**}$, is Lipschitz continuous. More precisely,*

$$\|F^{**} - G^{**}\|_{W^{1,1}} \le \left(\frac{b-a}{2} + 1\right) \|F' - G'\|_1 \qquad \forall F, G \in W_0^{1,1}(a,b).$$

In the sequel we use Tg and G in analogy to Tf and F as defined in (6.13); moreover, we denote by $\mathcal{J}_F^\varphi$, $\mathcal{G}^{F,\psi}$ and $\mathcal{J}_G^\varphi$, $\mathcal{G}^{G,\psi}$ the corresponding functions associated respectively to F and G as in (6.10) and (6.12). About the regularity of $\mathcal{J}_F^\varphi$ and $\mathcal{J}_G^\varphi$ we refer to Remark 6.1.5 and similarly for $\mathcal{G}^{F,\psi}$ and $\mathcal{G}^{G,\psi}$.

The next statement will be crucial to prove the existence and uniqueness result in Section 6.3.2.

Proposition 6.1.13. *Let $T\colon L^1(a,b) \to L^1(a,b)$ be the operator defined by* (6.13)*. Then*

$$\left| \int_a^b [Tf\ (\mathcal{J}_F^\varphi)' - Tg\ (\mathcal{J}_G^\varphi)']dx \right| \leq \|\varphi'\|_\infty \|f-g\|_1 \qquad \forall f,g \in L^1(a,b),\ \forall \varphi \in C_c^\infty(\mathcal{I}).$$

Similarly, it is possible to state the following more general result.

Proposition 6.1.14. *Let Λ and $\mathcal{G}^{\theta,\psi}$ be as in Example 6.1.9, $\mathcal{H} \in \mathrm{Lip}(\mathbb{R})$ with Lipschitz constant $\mathcal{L} > 0$. Then:*

i) $\left| \int_a^b [\mathcal{H}(Tf)\ (\mathcal{J}_F^\varphi)' - \mathcal{H}(Tg)\ (\mathcal{J}_G^\varphi)']dx \right| \leq \mathcal{L}\|\varphi'\|_\infty \|f-g\|_1 \quad \forall f,g \in L^1(a,b),\ \forall \varphi \in C_c^\infty(\mathcal{I});$

ii) $\exists C > 0$ *such that*
$\left| \int_a^b [\mathcal{H}(Tf)\ (\mathcal{G}^{F,\psi})' - \mathcal{H}(Tg)\ (\mathcal{G}^{G,\psi})']dx \right| \leq C\|F-G\|_{W^{1,1}} \quad \forall f,g \in L^1(a,b),\ \forall \psi \in C_c^\infty(\mathcal{I}).$

We conclude this section with a statement on the continuous dependence of $(\mathcal{J}^\varphi)'$ with respect to f.

Proposition 6.1.15. *Let $f, f_n \in C^1(\overline{\mathcal{I}})$, $n \in \mathbb{N}$, satisfy assumption* (6.9)*, assume that the sequence $\{f_n\}$ converges uniformly to f, and let $\varphi \in C_c^\infty(\mathcal{I})$. Denote by $\mathcal{J}^\varphi$ the function related to f defined in* (6.10) *and by $\mathcal{J}_n^\varphi$ the corresponding function related to f_n. Then*

$$\|\mathcal{J}_n^\varphi - \mathcal{J}^\varphi\|_1 \to 0, \qquad \|(\mathcal{J}_n^\varphi)' - (\mathcal{J}^\varphi)'\|_1 \to 0.$$

6.2 Energy balance in the suspension bridge

6.2.1 The deformation energy of the cables

We refer to Chapter 3 for the general setting of the model, in particular in Figure 6.5 we sketch a cross section of the bridge useful to derive the energy of the two cables.

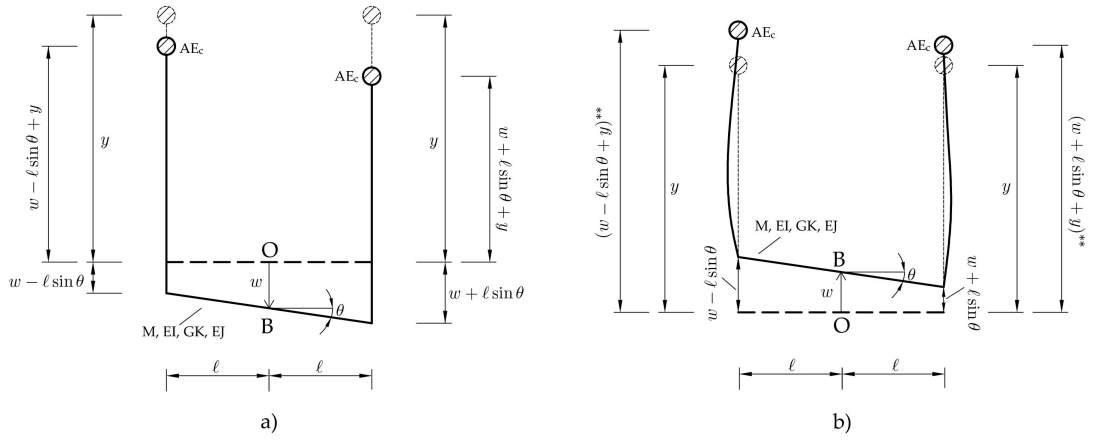

Figure 6.5: *Mutual positions of the cross section of the bridge and of the cables.*

First of all we recall that at rest the cables assume the parabolic shape $y(x)$ for $x \in [0, L]$ as in (3.11) and the function $\xi(x)$, in which $y'(x)$ is involved (3.14), assumes values close to 1, see (3.15). We refer to Section 3.2.2 about the engineering tendency to approximate $\xi(x)$ with 1. Moreover, we underline that $\xi(x)$ remains closer to its mean value $\overline{\xi}$ over the interval $[0, L]$; for these reasons, in this models, we shall use the approximation

$$\xi(x) \approx \overline{\xi} := \frac{\int_0^L \xi(x)dx}{L}. \tag{6.16}$$

We point out that for the TNB, $\xi_M = 1.05$ and $\overline{\xi} = 1.02$ so that, by assuming (6.16), the maximum error is less than 2.86%. We refer to Section 6.3.3 for some issues related to the presence of the non approximated $\xi(x)$ in our system and to the consequences that this function produces on the system in terms of existence and uniqueness of a solution.

To obtain the energy of the cables we need to find their convexified shapes. Let us clarify how we apply the procedure explained in Section 6.1.1. In Figure 6.5a) is shown the situation with tensioned hangers, in which the edges of the deck have moved downwards of $w \pm \ell \sin\theta$. In this case, the cables maintain their convex shape and the hangers behave like inextensible elements so that the cables have the same displacement of the deck and their positions are equal to $(w \pm \ell \sin\theta + y)$. In Figure 6.5b) we represent the innovative part of our model. If the endpoints of the cross section of the deck move upwards, above the position $(w \pm \ell \sin\theta + y) = 0$, then the slackening of the hangers may occur, producing a vertical displacement in the cables equal to $(w \pm \ell \sin\theta + y)^{**}$. The shape of the cables is then given by the convexification of the function $(w \pm \ell \sin\theta + y)$, that depends not only on x, but also on t.

To determine the deformation energy of a cable we proceed similarly to Section5.1.1; hence, we need to compute its variation of length with respect to its initial length L_c, see (3.5). To this end, we introduce the functional $\Gamma : C^1[0, L] \to \mathbb{R}$ as

$$\begin{aligned} \Gamma(u) :&= \int_0^L \left(\sqrt{1 + \{[(u+y)^{**}]_x\}^2} - \sqrt{1 + (y')^2}\right) dx \\ &= \int_0^L \left(\sqrt{1 + \{[(u+y)^{**}]_x\}^2}\right) dx - L_c. \end{aligned} \tag{6.17}$$

$\Gamma(u)$ is well-defined, since the convexification preserves the C^1-regularity of u.

The deformation energy E_C of the cables is composed by two contributions. The first is related to the tension at rest and the second to the additional tension due to the increment of the length $\Gamma(w \pm \ell \sin\theta)$ of each cable. Hence if $\overline{\xi}$ is as in (6.16), we have

$$\begin{aligned} E_C = &H\overline{\xi} \int_0^L \left(\sqrt{1 + \{[(w + \ell\sin\theta + y)^{**}]_x\}^2} - \sqrt{1 + (y')^2}\right) dx \\ &+ H\overline{\xi} \int_0^L \left(\sqrt{1 + \{[(w - \ell\sin\theta + y)^{**}]_x\}^2} - \sqrt{1 + (y')^2}\right) dx \\ &+ \frac{AE_c}{2L_c}\left([\Gamma(w + \ell\sin\theta)]^2 + [\Gamma(w - \ell\sin\theta)]^2\right), \end{aligned} \tag{6.18}$$

in which H is the horizontal tension, A the sectional area and E_c the Young modulus of the cable, see Section 3.2.3.

6.2.2 Functional spaces and total energy of the system

Let us recall the Hilbert spaces introduced in Section 3.3.2 endowed with the scalar products (3.20). The solutions of the equations are required to satisfy $(w,\theta) \in X_T^2$, where

$$X_T := C^0\big([0,T];H^2\cap H_0^1(0,L)\big)\cap C^1\big([0,T];L^2(0,L)\big)\cap C^2\big([0,T];H^*(0,L)\big). \tag{6.19}$$

Then, by adding all the energetic contributions of the system, for every $(w,\theta)\in X_T^2$ we find the functional

$$\begin{aligned}\mathcal{E}(w,\theta) :=& \int_0^L \left(\frac{M}{2}w_t^2 + \frac{M\ell^2}{6}\theta_t^2 + \frac{EI}{2}w_{xx}^2 + \frac{EJ}{2}\theta_{xx}^2 + \frac{GK}{2}\theta_x^2 - Mgw\right)dx\\ &+ H\overline{\xi}\int_0^L \big(\sqrt{1+\{[(w+\ell\sin\theta+y)^{**}]_x\}^2}-\xi\big)dx\\ &+ H\overline{\xi}\int_0^L \big(\sqrt{1+\{[(w-\ell\sin\theta+y)^{**}]_x\}^2}-\xi\big)dx\\ &+ \frac{AE_c}{2L_c}\big([\Gamma(w+\ell\sin\theta)]^2+[\Gamma(w-\ell\sin\theta)]^2\big),\end{aligned} \tag{6.20}$$

that is well-defined and represents the energy of the system. Note the difference with respect to (5.6); in both the cases we consider the Vlasov torsional contribute of the deck, here we apply the approximation (6.16) and the cables' shapes are convexified.

Proposition 6.2.1. *The functional $\mathcal{E}: X_T^2\to\mathbb{R}$ is locally Lipschitz continuous.*

Proof. The Proposition holds if, for every bounded subset $X\subset X_T^2$ there exists $\mathcal{L}>0$ such that, given (w_1,θ_1) and $(w_2,\theta_2)\in X$ we have

$$|\mathcal{E}(w_1,\theta_1)-\mathcal{E}(w_2,\theta_2)|\le\mathcal{L}\big(||(w_1-w_2)_t||_1+||(\theta_1-\theta_2)_t||_1+||w_1-w_2||_{W^{2,1}}+||\theta_1-\theta_2||_{W^{2,1}}\big). \tag{6.21}$$

By (6.20) we observe that the most tricky terms are those including $\Gamma(\cdot)$ and $\overline{\xi}$, while for the others (6.21) is easily proved. Let us recall the inequality

$$|\sqrt{1+(u_1+v)^2}-\sqrt{1+(u_2+v)^2}|\le|(u_1+v)-(u_2+v)|=|u_1-u_2|\quad\forall u_1,u_2,v\in\mathbb{R},$$

that gives

$$\begin{aligned}&\big|\sqrt{1+\{[(w_1\pm\ell\sin\theta_1+y)^{**}]_x\}^2}-\sqrt{1+\{[(w_2\pm\ell\sin\theta_2+y)^{**}]_x\}^2}\big|\\ &\le\big|[(w_1\pm\ell\sin\theta_1+y)^{**}-(w_2\pm\ell\sin\theta_2+y)^{**}]_x\big|.\end{aligned}$$

Hence, it is possible to apply Proposition 6.1.11 so that there exists $L_1>0$ such that

$$\begin{aligned}&H\overline{\xi}\int_0^L\big|\sqrt{1+\{[(w_1\pm\ell\sin\theta_1+y)^{**}]_x\}^2}-\sqrt{1+\{[(w_2\pm\ell\sin\theta_2+y)^{**}]_x\}^2}\big|dx\\ &\le H\overline{\xi}\big(||(w_1-w_2)_x||_1+\ell||(\sin\theta_1-\sin\theta_2)_x||_1\big)\\ &\le L_1\big(||(w_1-w_2)_x||_1+||\theta_1-\theta_2||_{W^{1,1}}\big).\end{aligned}$$

The same argument can be applied to the terms $[\Gamma(w\pm\ell\sin\theta)]^2$, see (6.17). □

This result enables us to use the notion of Clarke subdifferential [23] and to compute the variation of (6.20) in the general framework of the differential inclusions.

6.3 Suspension bridges with convexified cables

6.3.1 The variation of the deformation energy of the cables

The presence of the convexified functions within the functional $\mathcal{E}(w,\theta)$ in (6.20) introduces some difficulties in computing its variation; from Proposition 6.1.2 the unilateral Gateaux derivative exists and is always bounded, while the Gateaux derivative may not exist in some special cases.

Let us focus on one cable, the other being similar. We introduce

$$D^- := \big[H\overline{\xi} + \frac{AE_c}{L_c}\Gamma(w+\ell\sin\theta)\big]\int_0^L \frac{[(w+\ell\sin\theta+y)^{**}]_x(\mathcal{J}_-^\varphi)'}{\sqrt{1+\{[(w+\ell\sin\theta+y)^{**}]_x\}^2}}\,dx$$

$$D^+ := \big[H\overline{\xi} + \frac{AE_c}{L_c}\Gamma(w+\ell\sin\theta)\big]\int_0^L \frac{[(w+\ell\sin\theta+y)^{**}]_x(\mathcal{J}_+^\varphi)'}{\sqrt{1+\{[(w+\ell\sin\theta+y)^{**}]_x\}^2}}\,dx,$$

where $\mathcal{J}_\pm^\varphi(x)$ are defined in (6.8) with $f=(w+\ell\sin\theta+y)$. By applying Proposition 6.1.2, we find the following inclusion related to the variation of the energy (6.18) with respect to w

$$\langle dE_C(w,\theta),\varphi\rangle \in \big[\min\{D^-,D^+\},\max\{D^-,D^+\}\big].$$

To avoid this heavy notation, in the sequel we always write

$$\langle dE_C(w,\theta),\varphi\rangle \in \big[H\overline{\xi} + \frac{AE_c}{L_c}\Gamma(w+\ell\sin\theta)\big]\int_0^L \frac{[(w+\ell\sin\theta+y)^{**}]_x(\mathcal{J}_\pm^\varphi)'}{\sqrt{1+\{[(w+\ell\sin\theta+y)^{**}]_x\}^2}}\,dx \quad \forall\varphi\in C_c^\infty(\mathcal{I}).$$

By applying Theorem 6.1.8 with $\Lambda(\theta)=\sin\theta$ we obtain the inclusion related to the variation of the energy (6.18) with respect to θ

$$\langle dE_C(w,\theta),\psi\rangle \in \big[H\overline{\xi} + \frac{AE_c}{L_c}\Gamma(w+\ell\sin\theta)\big]\ell\int_0^L \frac{[(w+\ell\sin\theta+y)^{**}]_x(\mathcal{G}_\pm^{\theta,\psi})_x}{\sqrt{1+\{[(w+\ell\sin\theta+y)^{**}]_x\}^2}}\,dx \quad \forall\psi\in C_c^\infty(\mathcal{I}),$$

where $\mathcal{G}_\pm^{\theta,\psi}(x)$ is defined for every $t\geq 0$ fixed, in analogy with $\mathcal{J}_\pm^\varphi(x)$ as

$$\mathcal{G}_\pm^{\theta,\psi}(x) := \begin{cases} \pm(\pm g_i^\pm)^{**}(x) & x\in K^i,\ i\in J_C,\\ \psi(x)\cos\big(\theta(x)\big) & x\in \widetilde{K}_f, \end{cases} \tag{6.22}$$

with

$$g_i^\pm\colon K^i\to\overline{\mathbb{R}},\qquad g_i^\pm(x) := \begin{cases} \psi(x)\cos\big(\theta(x)\big) & x\in K^i\cap(K_f\cup\{a,b\}),\\ \pm\infty & x\in K^i\setminus(K_f\cup\{a,b\}). \end{cases}$$

Note that the functions $\mathcal{J}_\pm^\varphi$ and $\mathcal{G}_\pm^{\theta,\psi}$ are spatially continuous with a finite number of angular points, so that $(\mathcal{J}_\pm^\varphi)'$ and $(\mathcal{G}_\pm^{\theta,\psi})_x$ are bounded on the interval $[0,L]$ and continuous almost everywhere in $[0,L]$, see Remark 6.1.5.

In the simple cases in which the cable is strictly convex (or concave!) we gain the differentiability of (6.20) and the inclusions become equalities. In the first case, because $\widetilde{K}_f=\mathcal{I}$ so that $\mathcal{J}_\pm^\varphi$ and $\mathcal{G}_\pm^{\theta,\psi}$ coincide respectively with φ and $\psi\cos\theta$. In the second case, $K^1=\overline{I}^1=\overline{\mathcal{I}}$ so that $\mathcal{I}^\varphi=\mathcal{G}^{\theta,\psi}=0$ and $(w+\ell\sin\theta+y)^{**}=-y_0$ for

all $x \in [0, L]$; this situation corresponds to a zero variation in the cable energy since the slackening of all the hangers occurs, implying the total disconnection between the cable and the deck. We point out that in the case where the cable is perfectly horizontal we obtain the same physical result, due to $(w+\ell\sin\theta+y)_x = [(w+\ell\sin\theta+y)^{**}]_x = 0$ for all $x \in [0, L]$, while $\mathcal{I}^{\varphi}_{\pm}$ and $\mathcal{G}^{\theta,\psi}_{\pm}$ maintain their oscillatory nature.

6.3.2 The system of partial differential inclusions

In this section we state the problem in the general framework of partial differential inclusions, resulting from the variation of (6.20). To this aim we introduce the subscripts α and β to denote the terms corresponding respectively to the cable with shape $(w + \ell\sin\theta + y)^{**}$ and $(w - \ell\sin\theta + y)^{**}$; in this way we have $\mathcal{J}^{\varphi}_{\alpha\pm}(x)$, $\mathcal{G}^{\theta,\psi}_{\alpha\pm}(x)$ and $\mathcal{J}^{\varphi}_{\beta\pm}(x)$, $\mathcal{G}^{\theta,\psi}_{\beta\pm}(x)$ that correspond to $\mathcal{J}^{\varphi}_{\pm}(x)$, $\mathcal{G}^{\theta,\psi}_{\pm}(x)$ related respectively to $f_\alpha = (w + \ell\sin\theta + y)$ and $f_\beta = (w - \ell\sin\theta + y)$, as defined in (6.8) and (6.22).

As for the action, one has to take the difference between kinetic energy and potential energy and integrate over an interval of time $[0, T]$:

$$\begin{aligned}\mathcal{A}(w,\theta) := \int_0^T \Bigg[\int_0^L \left(\frac{M}{2}w_t^2 + \frac{M\ell^2}{6}\theta_t^2\right) dx - \int_0^L \left(\frac{EI}{2}w_{xx}^2 + \frac{EJ}{2}\theta_{xx}^2 + \frac{GK}{2}\theta_x^2 - Mgw\right)dx \\ - H\bar{\xi}\Bigg\{ \int_0^L \big(\sqrt{1+\{[(w+\ell\sin\theta+y)^{**}]_x\}^2} + \sqrt{1+\{[(w-\ell\sin\theta+y)^{**}]_x\}^2}\big)dx - 2L_c\Bigg\} \\ - \frac{AE_c}{2L_c}\big([\Gamma(w+\ell\sin\theta)]^2 + [\Gamma(w-\ell\sin\theta)]^2\big)\Bigg] dt.\end{aligned}$$

The differential inclusion describing the motion of the bridge is obtained by considering the critical points of the functional $\mathcal{A}$, which leads to the following

Definition 6.3.1. *We say that $(w, \theta) \in X^2_T$, see* (6.19)*, is a weak solution of the differential inclusion, resulting from critical points of the action $\mathcal{A}$, if (w, θ) satisfies*

$$\begin{cases} M\langle w_{tt},\varphi\rangle_* + EI(w,\varphi)_{H^2} - \big(Mg,\varphi\big)_2 \in \\ \qquad -\big[H\bar{\xi} + \frac{AE_c}{L_c}\Gamma(w+\ell\sin\theta)\big]\left(\dfrac{[(w+\ell\sin\theta+y)^{**}]_x}{\sqrt{1+\{[(w+\ell\sin\theta+y)^{**}]_x\}^2}}, (\mathcal{J}^{\varphi}_{\alpha\pm})'\right)_2 \\ \qquad -\big[H\bar{\xi} + \frac{AE_c}{L_c}\Gamma(w-\ell\sin\theta)\big]\left(\dfrac{[(w-\ell\sin\theta+y)^{**}]_x}{\sqrt{1+\{[(w-\ell\sin\theta+y)^{**}]_x\}^2}}, (\mathcal{J}^{\varphi}_{\beta\pm})'\right)_2 \\ \dfrac{M\ell}{3}\langle\theta_{tt},\psi\rangle_* + \dfrac{EJ}{\ell}(\theta,\psi)_{H^2} + \dfrac{GK}{\ell}(\theta,\psi)_{H^1} \in \\ \qquad -\big[H\bar{\xi} + \frac{AE_c}{L_c}\Gamma(w+\ell\sin\theta)\big]\left(\dfrac{[(w+\ell\sin\theta+y)^{**}]_x}{\sqrt{1+\{[(w+\ell\sin\theta+y)^{**}]_x\}^2}}, (\mathcal{G}^{\theta,\psi}_{\alpha\pm})_x\right)_2 \\ \qquad +\big[H\bar{\xi} + \frac{AE_c}{L_c}\Gamma(w-\ell\sin\theta)\big]\left(\dfrac{[(w-\ell\sin\theta+y)^{**}]_x}{\sqrt{1+\{[(w-\ell\sin\theta+y)^{**}]_x\}^2}}, (\mathcal{G}^{\theta,\psi}_{\beta\pm})_x\right)_2 \end{cases} \tag{6.23}$$

for all $\varphi, \psi \in H^2 \cap H^1_0(0, L)$ and $t > 0$.

The system (6.23) is complemented with the initial conditions:

$$\begin{aligned} &w(x,0) = w^0(x), \quad \theta(x,0) = \theta^0(x) && \text{for } x \in (0,L) \\ &w_t(x,0) = w^1(x), \quad \theta_t(x,0) = \theta^1(x) && \text{for } x \in (0,L), \end{aligned} \tag{6.24}$$

having the following regularity

$$w^0, \theta^0 \in H^2 \cap H_0^1(0,L), \qquad w^1, \theta^1 \in L^2(0,L). \tag{6.25}$$

From [6, 21, 23] we learn that to prove existence results for a differential inclusion can be a difficult task, requiring some regularity assumptions on the right hand side terms, e.g. the continuity. For our purposes to approach problem (6.23)-(6.24) in fully generality is not really necessary: since we are dealing with the modeling of a civil structure, it is possible to perform some simplifications. In Section 3.3.3 we underline that civil structures typically oscillate on low modes. Hence, we apply the Galerkin approximation (3.22); in this model, since the notation is quite heavy, we avoid to distinguish the indexes related to the approximation of w and θ, i.e. we put

$$w_n(x,t) = \sum_{k=1}^{n} w_n^k(t)\, e_k(x), \qquad \theta_n(x,t) = \sum_{k=1}^{n} \theta_n^k(t)\, e_k(x),$$

in which e_k is given in (3.21). Thanks to the Galerkin procedure we obtain a finite system of ordinary differential inclusions. In fact, in this finite dimensional setting, the inclusions become equalities, since for every fixed $n \in \mathbb{N}$, all the intervals of affinity (if any) of $(w_n \pm \ell \sin\theta_n + y)^{**}$ are such that

$$(w_n \pm \ell \sin\theta_n + y) > (w_n \pm \ell \sin\theta_n + y)^{**}.$$

Then Corollary 6.1.3 applies and the Gateaux derivative exists, leading to a finite system of ordinary differential equations

$$\begin{cases} M\big((w_n)_{tt}, e_r\big)_2 + EI\big(w_n, e_r\big)_{H^2} - (Mg, e_r)_2 = \\ \qquad -\big[H\bar{\xi} + \frac{AE_c}{L_c}\Gamma(w_n + \ell\sin\theta_n)\big]\left(\dfrac{[(w_n + \ell\sin\theta_n + y)^{**}]_x}{\sqrt{1+\{[(w_n + \ell\sin\theta_n + y)^{**}]_x\}^2}}, [\mathcal{J}_\alpha^{e_r}]'\right)_2 \\ \qquad -\big[H\bar{\xi} + \frac{AE_c}{L_c}\Gamma(w_n - \ell\sin\theta_n)\big]\left(\dfrac{[(w_n - \ell\sin\theta_n + y)^{**}]_x}{\sqrt{1+\{[(w_n - \ell\sin\theta_n + y)^{**}]_x\}^2}}, [\mathcal{J}_\beta^{e_r}]'\right)_2 \\ \dfrac{M\ell}{3}\big((\theta_n)_{tt}, e_r\big)_2 + \dfrac{EJ}{\ell}\big(\theta_n, e_r\big)_{H^2} + \dfrac{GK}{\ell}\big(\theta_n, e_r\big)_{H^1} = \\ \qquad -\big[H\bar{\xi} + \frac{AE_c}{L_c}\Gamma(w_n + \ell\sin\theta_n)\big]\left(\dfrac{[(w_n + \ell\sin\theta_n + y)^{**}]_x}{\sqrt{1+\{[(w_n + \ell\sin\theta_n + y)^{**}]_x\}^2}}, [\mathcal{G}_\alpha^{\theta_n, e_r}]_x\right)_2 \\ \qquad +\big[H\bar{\xi} + \frac{AE_c}{L_c}\Gamma(w_n - \ell\sin\theta_n)\big]\left(\dfrac{[(w_n - \ell\sin\theta_n + y)^{**}]_x}{\sqrt{1+\{[(w_n - \ell\sin\theta_n + y)^{**}]_x\}^2}}, [\mathcal{G}_\beta^{\theta_n, e_r}]_x\right)_2, \end{cases} \tag{6.26}$$

for $r = 1, \dots, n$, with the initial conditions

$$\begin{aligned} w_n^k(0) &= (w^0, e_k)_2, \qquad & \theta_n^k(0) &= (\theta^0, e_k)_2 \\ \dot{w}_n^k(0) &= (w^1, e_k)_2, \qquad & \dot{\theta}_n^k(0) &= (\theta^1, e_k)_2. \end{aligned} \tag{6.27}$$

In Section 6.6 we prove

Theorem 6.3.2. *Let $n \geq 1$ an integer and $T > 0$ (including the case $T = \infty$), then for all $w^0, \theta^0, w^1, \theta^1$ satisfying (6.25) there exists a unique solution $(w_n, \theta_n) \in X_T^2$ of (6.26) which satisfies (6.27).*

This justifies the following

Definition 6.3.3. *For all $n \in \mathbb{N}$, we say that the solution (w_n, θ_n) of (6.26)-(6.27) is an **approximate solution** of (6.23)-(6.24).*

Among the solutions of (6.23)-(6.24) we are interested in those being approximable, according to

Definition 6.3.4. *We say that $(w, \theta) \in X_T^2$ is an **approximable solution** of (6.23)-(6.24) if there exists a sequence of approximate solutions of (6.23)-(6.24), converging to it as $n \to \infty$, up to a subsequence.*

We state now the main result of this section.

Theorem 6.3.5. *Let $T > 0$ (including the case $T = \infty$), then for all $w^0, \theta^0, w^1, \theta^1$ satisfying (6.25) there exists an approximable solution of (6.23) which satisfies (6.24) on $[0, T]$.*

The proof of Theorem 6.3.5 is given in Section 6.6.

Remark 6.3.6. The results obtained in this section on the approximate solution (w_n, θ_n) can be achieved in the same way considering a different number of modes for w and θ, i.e. taking (w_n, θ_ν) with $n \neq \nu$.

6.3.3 A remark on the approximation (6.16)

Let us write (6.26) more simply, including all the nonlinearities of the system into the functionals

$$h_\alpha(w_n, \theta_n) := -\left(H\overline{\xi} + \frac{AE_c}{L_c}\Gamma(w_n + \ell \sin\theta_n)\right) \frac{[(w_n + \ell\sin\theta_n + y)^{**}]_x}{\sqrt{1 + \{[(w_n + \ell\sin\theta_n + y)^{**}]_x\}^2}}$$
$$h_\beta(w_n, \theta_n) := -\left(H\overline{\xi} + \frac{AE_c}{L_c}\Gamma(w_n - \ell \sin\theta_n)\right) \frac{[(w_n - \ell\sin\theta_n + y)^{**}]_x}{\sqrt{1 + \{[(w_n - \ell\sin\theta_n + y)^{**}]_x\}^2}}.$$

Testing n times the equations (6.26) for $r = 1, \dots, n$ and $t \geq 0$ we obtain a system of ordinary differential equations for all $k = 1, \dots, n$

$$\begin{cases} M\ddot{w}_n^k(t) + EI\dfrac{k^4\pi^4}{L^4} w_n^k(t) = Mg\dfrac{\sqrt{2L}(1-(-1)^k)}{k\pi} \\ \qquad\qquad + \big(h_\alpha(w_n, \theta_n), [\mathcal{J}_\alpha^{e_k}]'\big)_2 + \big(h_\beta(w_n, \theta_n), [\mathcal{J}_\beta^{e_k}]'\big)_2 \\ \dfrac{M\ell}{3}\ddot{\theta}_n^k(t) + \left(EJ\dfrac{k^4\pi^4}{L^4\ell} + GK\dfrac{k^2\pi^2}{L^2\ell}\right)\theta_n^k(t) = \\ \qquad\qquad \big(h_\alpha(w_n, \theta_n), [\mathcal{G}_\alpha^{\theta_n, e_k}]_x\big)_2 - \big(h_\beta(w_n, \theta_n), [\mathcal{G}_\beta^{\theta_n, e_k}]_x\big)_2 \end{cases} \tag{6.28}$$

with the initial conditions (6.27).

In Section 6.2.1 we have approximated the function $\xi(x)$ with its mean value $\overline{\xi}$ assumed on $[0, L]$. In this section we present some observations related to system (6.28) without assuming (6.16). Even if $\xi(x)$ does not depend on the solution and is a smooth and bounded function on $[0, L]$, see (3.14), its presence generates some problems related to the existence and uniqueness of (w_n^k, θ_n^k).

In this case it is possible to apply for the existence result a fixed point argument; in particular, we introduce the vectors $Z(t) = [z_n^1(t), \dots, z_n^n(t)] \in C^1(\mathbb{R})$, $\Pi(t) =$

$[\Pi_n^1(t),\dots,\Pi_n^n(t)] \in C^1(\mathbb{R})$ and $e(x) = [e_1(x),\dots,e_n(x)] \in C^\infty([0,L])$ and we plug them into the right hand side terms of (6.28). Hence, we obtain

$$F_k(t) := \int_0^L \left[H\xi(x) + \frac{AE_c}{L_c}\Gamma\big(Z\cdot e + \ell\sin(\Pi\cdot e)\right]\chi\left([Z\cdot e + \ell\sin(\Pi\cdot e) + y]^{**}\right)\,(\mathcal{J}_\alpha^{e_k})'dx;$$

note that Proposition 6.1.14 does not hold, since the fundamental identity (6.45) (see Section 6.5) is not verified and the locally Lipschitz continuity is not assured (similarly for $G_k(t)$). Proposition 6.1.15 guarantees that $F_k(t)$ and $G_k(t)$ are time continuous for all $k = 1,\dots,n$, indeed, taking $t_j \to t$, and following the scheme of the proof of Theorem 6.3.2, we have $K > 0$ such that

$$|F_k(t_j) - F_k(t)| \le K(\|Z(t_j)\cdot e - Z(t)\cdot e\|_1 + \|\Pi(t_j)\cdot e - \Pi(t)\cdot e\|_{W^{1,1}} + \|(\mathcal{J}_\alpha^{e_k}(t_j) - \mathcal{J}_\alpha^{e_k}(t))'\|_1) \to 0,$$

for all $k = 1,\dots,n$.

Thanks to the classical ODEs theory there exists a solution $(\Phi w_n^k(t), \Psi\theta_n^k(t)) \in C^2[0,t_n) \times C^2[0,t_n)$ for all $k = 1,\dots,n$ and for $t_n \in (0,T]$ of the linear problem

$$\begin{cases} M\ddot{\Phi}w_n^k(t) + EI\dfrac{k^4\pi^4}{L^4}\Phi w_n^k(t) = Mg\dfrac{\sqrt{2L}(1-(-1)^k)}{k\pi} \\ \qquad\qquad +\big(h_\alpha(Z\cdot e,\Pi\cdot e),[\mathcal{J}_\alpha^{e_k}]'\big)_2 + \big(h_\beta(Z\cdot e,\Pi\cdot e),[\mathcal{J}_\beta^{e_k}]'\big)_2 \\ \dfrac{M\ell}{3}\ddot{\Psi}\theta_n^k(t) + \left(EJ\dfrac{k^4\pi^4}{L^4\ell} + GK\dfrac{k^2\pi^2}{L^2\ell}\right)\Psi\theta_n^k(t) = \\ \qquad\qquad \big(h_\alpha(Z\cdot e,\Pi\cdot e),[\mathcal{G}_\alpha^{\Pi\cdot e,e_k}]_x\big)_2 - \big(h_\beta(Z\cdot e,\Pi\cdot e),[\mathcal{G}_\beta^{\Pi\cdot e,e_k}]_x\big)_2 \end{cases}$$

with the initial conditions

$$\begin{aligned} \Phi w_n^k(0) &= (w^0,e_k)_2, & \Psi\theta_n^k(0) &= (\theta^0,e_k)_2 \\ \dot{\Phi}w_n^k(0) &= (w^1,e_k)_2, & \dot{\Psi}\theta_n^k(0) &= (\theta^1,e_k)_2. \end{aligned}$$

Now we choose $\Phi w_n^k(t)$ and $\Psi\theta_n^k(t)$ as the components of the vectors $Z(t)$ and $\Pi(t)$ and we plug them into (6.28). In this way we obtain two operators $\Phi : C^1([0,t_n)) \to C^1([0,t_n))$, $\Psi : C^1([0,t_n)) \to C^1([0,t_n))$ that are compact due to the compact embedding $C^2 \subset C^1$, so that there exists a fixed point $\Phi w_n^k = w_n^k$ and $\Psi\theta_n^k = \theta_n^k$ for all $k = 1,\dots,n$, thanks to the Schauder fixed point theorem; this implies the existence of a solution on some $[0,t_n)$ for $t_n \in (0,T]$, while the global existence on $[0,T]$ can be deduced as in the proof of Theorem 6.3.2.

6.4 Numerical results

In this section we present some numerical experiments on the system (6.26)-(6.27), following the procedure given in Section 3.3.3. For the same reasons explained in Section 5.2, we consider the first 10 longitudinal modes interacting with the first 4 torsional modes and we adopt the mechanical constants of the TNB as in Table 3.1 with K =6.07·10^{-6}m^4.

Hence, due to the boundary conditions, we seek solutions of (6.26) in the form

$$w(x,t) = \sum_{k=1}^{10} w_k(t)\,e_k, \qquad \theta(x,t) = \sum_{k=1}^{4}\theta_k(t)\,e_k \tag{6.29}$$

where e_k is given in (3.21). In this way we obtain a system of 14 ODEs as (6.28) with the initial conditions

$$w_k(0) = w_k^0 = (w^0, e_k)_2, \qquad \dot{w}_k(0) = w_k^1 = (w^1, e_k)_2, \qquad \forall k = 1, \dots, 10$$
$$\theta_k(0) = \theta_k^0 = (\theta^0, e_k)_2, \qquad \dot{\theta}_k(0) = \theta_k^1 = (\theta^1, e_k)_2 \qquad \forall k = 1, \dots, 4.$$

We follow as usual the Definition 3.3.1, denoting by $\overline{\theta}_k$, instead of $\overline{\theta}_i$, the k-th torsional mode. We excite one single longitudinal mode (the j-th) at a time, applying an initial condition 10^{-3} smaller on all the other components, i.e. (3.25) becomes

$$\overline{w}_k^0 = 10^{-3} \cdot \overline{w}_j^0 \quad \forall k \neq j, \qquad \overline{\theta}_k^0 = \overline{w}_k^1 = \overline{\theta}_k^1 = 10^{-3} \cdot \overline{w}_j^0 \quad \forall k.$$

Based on the procedure described in Section 6.1.1, we approximate convexifications numerically. The verification of the tangency condition (6.3) should take place continuously for all $x \in \mathcal{I}$, which is impossible from a numerical point of view. Hence, we evaluate (6.3) in a finite number of points, obtained by the discretization of $\mathcal{I} = (0, L)$ with a certain step Δx (in our case $\Delta x = L/2000$). Following this scheme we obtain an algorithm converging to (6.4) as $\Delta x \to 0$, thanks to the boundedness of $\mathcal{I}$. More precisely we solve (6.28) passing properly to a system of first order ODEs, so that we apply an implicit ODEs algorithm, e.g. Crank-Nicolson or Runge-Kutta; the numerical work-flow of each temporal iteration is organized as follows: we compute in the order the affinity intervals of convexification of the two cables, we compute the spatial integrals by discretizing $[0, L]$, see the right hand side terms of (6.28), and we use these values to run the ODEs algorithm.

As explained in Section 6.2.1, through the procedure of convexification, we are able to simulate the slackening of the hangers. To have an idea of the slackening quantity occurring in our numerical experiments, we identify the two cables by the subscripts α and β as in Section 6.3.2, and we recall that, in the numerical discretization, $[0, T]$ is equally divided in m time step; hence, we compute for each time step Δt_h ($h = 1, \dots, m$) a measure of the percentage of hangers slackened as the ratio between the measure of the union of the intervals of linearity for each cable and the length of the deck L, i.e.

$$\mathcal{M}_h^\alpha := \frac{1}{L} \left| \bigcup_{i \in J_\alpha} I_\alpha^i \right| \qquad \mathcal{M}_h^\beta := \frac{1}{L} \left| \bigcup_{j \in J_\beta} I_\beta^j \right| \qquad \forall h = 1, \dots, m.$$

Since the angle of rotation is small, the two cables behave quite similarly and, therefore, we define a mean value of the **measure of slackening** as

$$\mathcal{M} = \frac{1}{2m} \left[\sum_{h=1}^{m} \mathcal{M}_h^\alpha + \sum_{h=1}^{m} \mathcal{M}_h^\beta \right]. \tag{6.30}$$

Our purpose is to compare the instability thresholds of the model with convexification to those of the same model without convexification, see [27], i.e. we study how the slackening of the hangers affects the system. In Table 6.1 we have this comparison in terms of initial energy and amplitude threshold of instability of the j-th longitudinal mode excited, computed following (3.28) with k instead of i in the θ subscript. For

each numerical experiment we verified the energy conservation, ascertaining a relative error, $|(\max \mathcal{E}(t) - \min \mathcal{E}(t))/\mathcal{E}(0)|$, on the integration time $[0, 120s]$, less than $4 \cdot 10^{-3}$. Let us observe that the thresholds related to the non convexified model are not significantly different from the thresholds in Table 5.1; the small differences are due to the approximation (6.16) not performed in Chapter 5.

	Convexification (Slackening)			**No convexification** (Rigid hangers)	
Mode	W_j^0[m]	$\mathcal{E}(0)$[J]	$\mathcal{M}$[%]	W_j^0[m]	$\mathcal{E}(0)$[J]
1	4.09	$7.96{\cdot}10^7$	1.92	4.09	$7.96{\cdot}10^7$
2	8.37	$8.74{\cdot}10^7$	2.94	8.22	$8.37{\cdot}10^7$
3	4.89	$8.58{\cdot}10^7$	2.40	4.82	$8.23{\cdot}10^7$
4	5.35	$1.63{\cdot}10^8$	41.79	4.92	$1.35{\cdot}10^8$
5	4.25	$1.77{\cdot}10^8$	39.40	3.93	$1.52{\cdot}10^8$
6	3.64	$1.64{\cdot}10^8$	43.46	2.64	$8.72{\cdot}10^7$
7	3.65	$2.38{\cdot}10^8$	51.72	5.25	$8.29{\cdot}10^8$
8	3.28	$2.27{\cdot}10^8$	50.05	5.15	$1.12{\cdot}10^9$
9	2.31	$1.54{\cdot}10^8$	42.55	3.87	$7.40{\cdot}10^8$
10	2.65	$2.34{\cdot}10^8$	52.73	3.41	$6.97{\cdot}10^8$

Table 6.1: *Thresholds of instability as in (3.28), corresponding energy and measure of slackening as in (6.30), varying the longitudinal mode excited on* $[0, 120s]$.

From the data in Table 6.1 we notice different tendencies depending on the mode excited. The first 3 longitudinal modes give substantially the same thresholds of instability in the case with convexification and without, due to the very low percentage of slackening, see $\mathcal{M}$. This fact is not surprising, since a longitudinal motion of the deck like a $\sin(\frac{\pi}{L}x)$ modifies the convexity of the cable only for very large displacements, requiring a so large amount of energy that the threshold of instability is achieved before the appearance of slackening.

Quite different is the behavior of the modes from the 4-th onward, since in these cases we appreciate differences between two models, due to the strong percentage of slackening in the convexified case. We distinguish two tendencies respectively for the intermediate modes (4-th, 5-th and 6-th) and the higher modes. The thresholds of the intermediate modes reveal that the instability arises earlier for the model with inextensible hangers, so that the latter can be adopted in favor of safety. We point out that the 4-th, 5-th and 6-th modes were not seen the day of the collapse of the TNB; the witnesses recorded that, before the rise of the torsional instability, the bridge manifested longitudinal oscillations with 9 or 10 waves, involving the motion of higher longitudinal modes. For these modes the presence of the slackening puts down the thresholds of instability so that the assumption of rigid hangers is not in favor of safety. We underline that in these cases we see more instability despite the injection of energy is smaller; this behavior is peculiar of the hangers slackening that favors a greater transfer of energy

between modes with respect to the case with inextensible hangers, see also [28]. The results in Table 6.1 highlight furthermore that the 9-th and 10-th longitudinal modes present the lowest torsional instability threshold in the case with slackening, confirming the real observations at the TNB collapse.

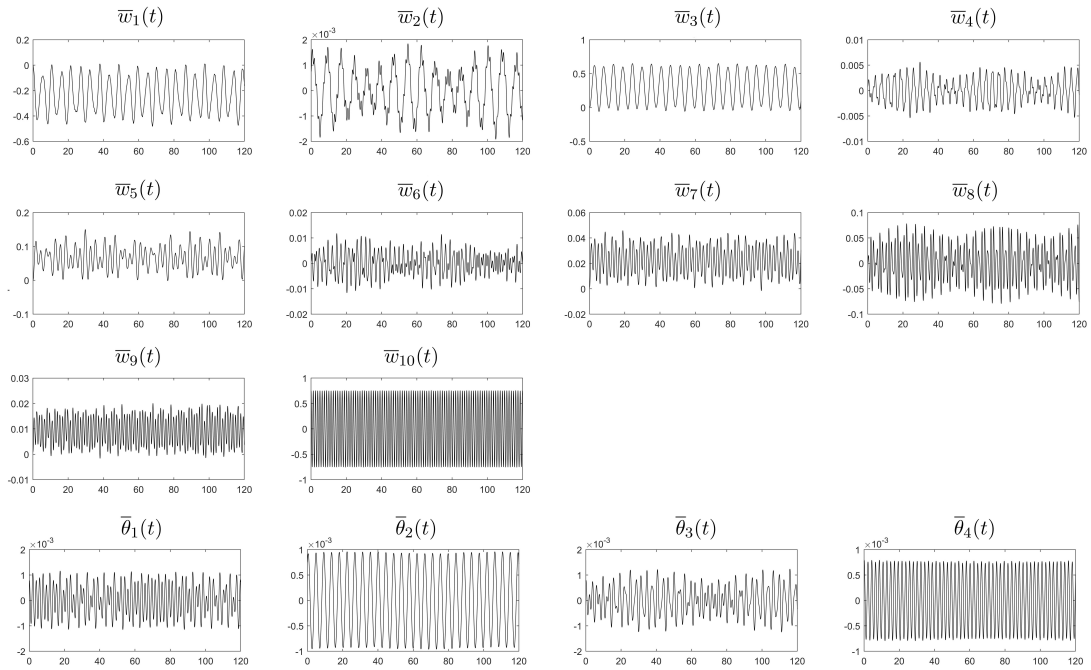

Figure 6.6: *Plots of $\overline{w}_k(t)$ ($k = 1, \dots, 10$) in meters and $\overline{\theta}_k(t)$ ($k = 1, \dots, 4$) in radians on $[0, 120s]$ with $\overline{w}_{10}^0$=0.75m.*

In Figure 6.6 we exhibit an example of stability obtained on the system with convexification, imposing $\overline{w}_{10}^0$ =0.75m; we record a very little exchange of energy between modes and, in general, the torsional modes oscillate around their initial amplitude, revealing a stable behavior. In this case some slack is present ($\mathcal{M} = 13.50\%$), while reducing further the initial amplitude would produce, as one can imagine, the total absence of slackening and a clear stable situation, see [27]; this happens for instance if $\overline{w}_9^0 \leq$0.60m and $\overline{w}_{10}^0 \leq$0.55m.

For brevity in Figure 6.7 we present only the torsional modes related to the instability thresholds of the 9-th and 10-th longitudinal modes, obtained respectively applying $\overline{w}_9^0$ =2.31m and $\overline{w}_{10}^0$ =2.65m. In general, when (3.28) is verified all the torsional modes begin to grow, but Figure 6.7 confirms that the 9-th and 10-th longitudinal modes are more prone to develop instability on the 2-nd torsional mode, since it attains the largest grow on $[0, 120s]$.

From Table 6.1 we also observe that the mean measure of the slackening $\mathcal{M}$ is increasing with respect to the energy introduced in the system, as physically one can expect. We now introduce a *mean measure of the hangers slackening* of each cable with respect to their position on $[0, L]$. We define it for the cable having vertical displacement

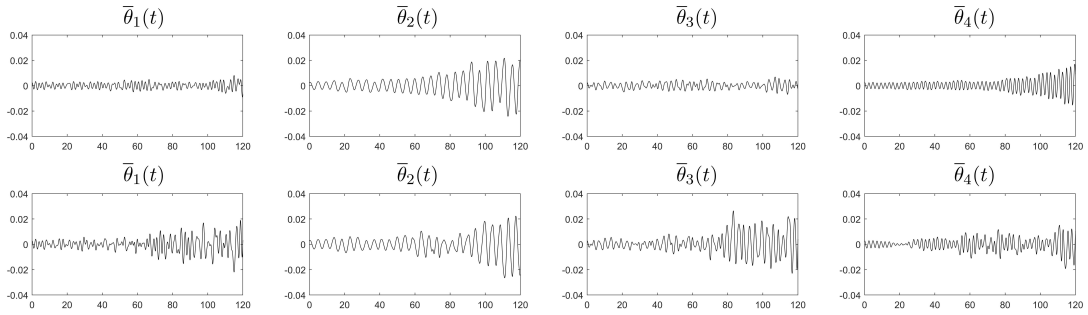

Figure 6.7: *Plots of $\overline{\theta}_k(t)$ ($k = 1, \dots, 4$) in radians on $[0, 120s]$ with $\overline{w}_9^0$=2.31m (above) and $\overline{w}_{10}^0$=2.65m (below).*

$(w + \ell \sin\theta + y)^{**}$ as

$$\mathcal{S}^\alpha(x) := \frac{1}{m}\sum_{h=1}^{m} \chi_h^\alpha(x) \qquad \chi_h^\alpha(x) := \begin{cases} 1 & x \in \bigcup\limits_{i \in J_\alpha} K_\alpha^i, \\ 0 & x \in \overline{\mathcal{I}} \setminus \bigcup\limits_{i \in J_\alpha} K_\alpha^i, \end{cases} \tag{6.31}$$

in which $\chi_h^\alpha(x)$ is computed for every time step Δt_h; a similar relationship can be found for the other cable.

In Figure 6.8 we plot the function $\mathcal{S}^\alpha(x)$, defined in (6.31), representing the mean measure of the hangers slackening with respect to their position on $[0, L]$. As we can see in the stable situation ($\overline{w}_{10}^0$=0.75m, on the left) there is a clear trend of maximum slackening for the hangers corresponding to the points $x = \frac{L}{20} + \frac{L}{10}k$ with $k = 0, \dots, 9$, i.e. the peaks of the function $\sin(\frac{10\pi}{L}x)$; indeed, in this case, the deck's motion follows sharply the 10-th longitudinal mode, excited through the initial conditions, see Figure 6.6. In Figure 6.8 we also show $\mathcal{S}^\alpha(x)$ for two unstable situations corresponding to $\overline{w}_9^0$=2.31m and $\overline{w}_{10}^0$=2.65m; we distinguish some peaks distinctive of the longitudinal modes excited, but, due to the transfer of energy to the other modes, $\mathcal{S}^\alpha(x)$ assumes shapes less clear. Similar plots can be found for the hangers related to the other main cable.

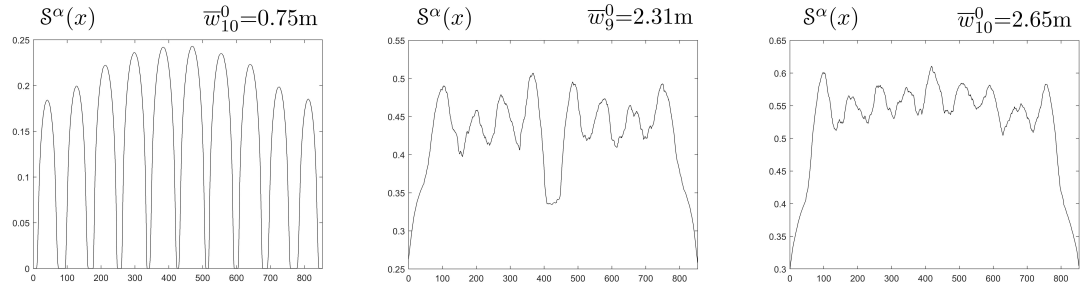

Figure 6.8: *Plots of $\mathcal{S}^\alpha(x)$ on $[0, L]$, from the left in the cases $\overline{w}_{10}^0$=0.75m, $\overline{w}_9^0$=2.31m and $\overline{w}_{10}^0$=2.65m.*

Our numerical results show that structures displaying only low modes of vibration may be treated assuming inextensible hangers; this simplification reduces the computational costs and gives safe instability thresholds. On the other hand, if the structure vibrates on higher modes, this assumption could give overestimated thresholds to the

detriment of safety; in this case the slackening of the hangers plays an important role. This fact should be a warning for the designers of bridges that are able to exhibit, in realistic situations, large vibration frequencies.

6.5 Proofs of the results on the convexification

The proofs of the results of Sections 6.1.2 and 6.1.3 require some basic tools of convex analysis (see e.g. [26, 66]).

Given a closed convex set $E \subset \mathbb{R}^n$, a point $p \in \partial E$ is an extreme point of E if it is not contained in any open segment $]r, q[$ with $r, q \in \partial E$, whereas it is an exposed point of E if there exists a support hyperplane H to E with $H \cap E = \{p\}$. We denote by $\operatorname{extr} E$ and $\operatorname{expo} E$, respectively, the sets of extremal and exposed points of E, see Figure 6.9.

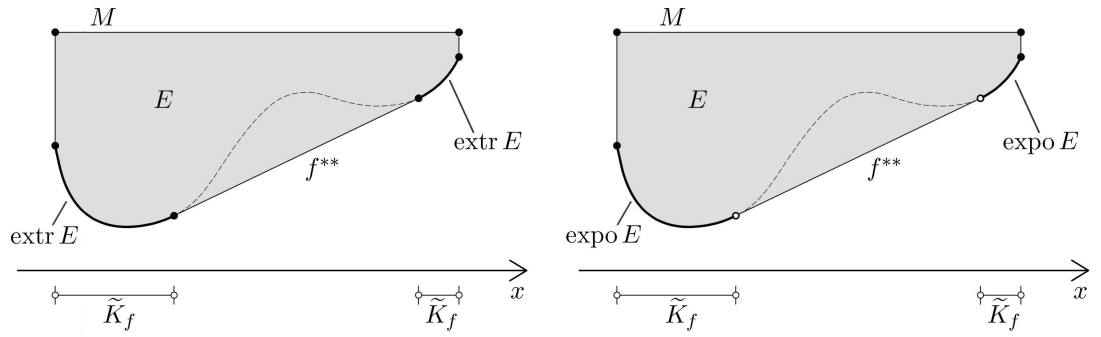

Figure 6.9: *An example of $f^{**}(x)$ in which $\operatorname{extr} E$ and $\operatorname{expo} E$ are in evidence.*

Clearly, $\operatorname{expo} E \subseteq \operatorname{extr} E$, but the inclusion may be strict even in dimension $n = 2$. If E is a compact convex set, then the Straszewicz's Theorem states that $\operatorname{extr} E \subseteq \overline{\operatorname{expo} E}$. Moreover, in dimension $n = 2$, the set $\operatorname{extr} E$ is closed (since every point $p \in \partial E \setminus \operatorname{extr} E$ is contained in a relatively open segment of ∂E).

Let us prove the following preliminary

Lemma 6.5.1. *Let $f \in C^1(\overline{\mathcal{I}})$, and let $(f_n) \subset C^1(\overline{\mathcal{I}})$ be a sequence converging uniformly to f. Then it holds:*

(a) If $x_0 \in \widetilde{K}_f$ and, for every $n \in \mathbb{N}$, $[a_n, b_n] \subset \overline{\mathcal{I}}$, $\lambda_n \in [0, 1]$ satisfy

$$x_0 = (1 - \lambda_n)a_n + \lambda_n b_n, \qquad f_n^{**}(x_0) = (1 - \lambda_n)f_n(a_n) + \lambda_n f_n(b_n),$$

then $a_n, b_n \to x_0$.

(b) If, in addition, f satisfies assumption (6.9)*, i.e. $\overline{K_f} = \overline{\widetilde{K}_f}$, and (a_0, b_0) is one of the maximal intervals I^i where f^{**} is affine, then for every $n \in \mathbb{N}$ there exists a maximal interval (a_n, b_n) where f_n^{**} is affine such that $a_n \to a_0$, $b_n \to b_0$.*

Proof. (a) Since x_0 is an exposed point of the epigraph of f^{**}, it holds

$$f(x) \geq f^{**}(x) > f(x_0) + f'(x_0)(x - x_0) \qquad \forall x \neq x_0.$$

Assume by contradiction that at least one of the sequences (a_n), (b_n) does not converge to x_0. Then there exists a subsequence (n_j) such that $a_{n_j} \to \overline{a}$, $b_{n_j} \to \overline{b}$, with $\overline{a} \le x_0 \le \overline{b}$ and $\overline{a} < \overline{b}$. Moreover, we clearly have $\lambda_{n_j} \to \lambda := (x_0 - \overline{a})/(\overline{b} - \overline{a})$. Hence,

$$f^{**}(x_0) = \lim_j f_{n_j}^{**}(x_0) = \lim_j (1-\lambda_{n_j}) f_{n_j}(a_{n_j}) + \lambda_{n_j} f_{n_j}(b_{n_j}) = (1-\lambda) f(\overline{a}) + \lambda f(\overline{b}) > f^{**}(x_0),$$

a contradiction.

(b) In view of (a), it is enough to prove that, if $x_0 \in (a_0, b_0)$, then $x_0 \notin K_{f_n}$ for n large enough.

Assume by contradiction that there exists a subsequence (n_j) such that $x_0 \in K_{f_{n_j}}$ for every j, i.e., $f_{n_j}(x_0) = f_{n_j}^{**}(x_0)$ for every j. Since, by assumption, $f > f^{**}$ on (a_0, b_0), one has

$$f(x_0) > f^{**}(x_0) = \lim_j f_{n_j}^{**}(x_0) = \lim_j f_{n_j}(x_0) = f(x_0),$$

a contradiction. □

Proof of Proposition 6.1.2. Let $M > \max_{[a,b]} f$, so that $E := \operatorname{epi} f^{**} \cap \{y \le M\}$ is a compact convex subset of $\mathbb{R}^2$. Moreover, we have that

$$\{(x, f(x)) : \ x \in \widetilde{K}_f \cup \{a, b\}\} = \operatorname{expo} E \cap \{y < M\},$$

i.e., the set at left-hand side coincides with the set of exposed points of $\operatorname{epi} f^{**}$.

We introduce the notation

$$f_s := f + s\,\varphi, \quad f_s^{**} := (f_s)^{**}, \qquad s \in \mathbb{R}.$$

By the Dominated Convergence Theorem, Proposition 6.1.2 will be a consequence of the following pointwise convergences:

$$\lim_{s\to 0} \frac{f_s^{**}(x_0) - f^{**}(x_0)}{s} = \varphi(x_0) \qquad \text{if} \quad x_0 \in \widetilde{K}_f, \tag{6.32}$$

$$\lim_{s\to 0^\pm} \frac{f_s^{**}(x_0) - f^{**}(x_0)}{s} = \pm(\varphi_i^\pm)^{**}(x_0) \qquad \text{if} \quad x_0 \in K^i,\ i \in J_C. \tag{6.33}$$

STEP 1. Proof of (6.32).

We have already observed that, if $x_0 \in \widetilde{K}_f$, then $f^{**}(x_0) = f(x_0)$ and $(x_0, f(x_0)) \in \operatorname{expo} E$.

Since $f \in C^1$, by definition of exposed point we have that

$$f(x) \ge f^{**}(x) > f(x_0) + f'(x_0)\,(x - x_0) =: h(x), \qquad \forall x \in [a, b],\ x \ne x_0.$$

For every $s \in \mathbb{R}$ let $a_s \in [a, x_0]$, $b_s \in [x_0, b]$, and $\lambda_s \in [0, 1]$ be such that

$$x_0 = (1 - \lambda_s) a_s + \lambda_s\, b_s, \qquad f_s^{**}(x_0) = (1 - \lambda_s) f_s(a_s) + \lambda_s\, f_s(b_s)\,. \tag{6.34}$$

Let us first prove that

$$\lim_{s\to 0^+} \frac{f_s^{**}(x_0) - f^{**}(x_0)}{s} = \varphi(x_0)\,. \tag{6.35}$$

Since

$$\frac{f_s^{**}(x_0) - f^{**}(x_0)}{s} \leq \frac{f_s(x_0) - f(x_0)}{s} = \varphi(x_0), \qquad \forall s > 0,$$

it follows that

$$\limsup_{s \to 0^+} \frac{f_s^{**}(x_0) - f^{**}(x_0)}{s} \leq \varphi(x_0),$$

hence it remains to prove that

$$l := \liminf_{s \to 0^+} \frac{f_s^{**}(x_0) - f^{**}(x_0)}{s} \geq \varphi(x_0).$$

Let $s_n \searrow 0$ be a sequence such that

$$l = \lim_{n \to +\infty} \frac{f_{s_n}^{**}(x_0) - f^{**}(x_0)}{s_n}.$$

Using (6.34) it holds

$$\begin{aligned} \frac{f_{s_n}^{**}(x_0) - f^{**}(x_0)}{s_n} &= \frac{(1-\lambda_{s_n}) f_{s_n}(a_{s_n}) + \lambda_{s_n} f_{s_n}(b_{s_n}) - f(x_0)}{s_n} \\ &= \frac{(1-\lambda_{s_n}) f(a_{s_n}) + \lambda_{s_n} f(b_{s_n}) - f(x_0)}{s_n} + (1-\lambda_{s_n})\varphi(a_{s_n}) + \lambda_{s_n}\varphi(b_{s_n}). \end{aligned} \tag{6.36}$$

Since the sequence $\{f_{s_n}\}$ converges uniformly to f, by Lemma 6.5.1(i) it follows that $a_{s_n}, b_{s_n} \to x_0$, hence the right-hand side of (6.36) converges to a quantity greater than or equal to $\varphi(x_0)$, so that $l \geq \varphi(x_0)$ and (6.35) follows.

The computation of the limit (6.35) for $s \to 0^-$ can be done similarly, observing that the same inequalities as above hold with reversed signs. Hence, we conclude that (6.32) holds.

STEP 2. Proof of (6.33).

We shall prove (6.33) only for $s \to 0^+$, being the proof for $s \to 0^-$ entirely similar. Let $i \in J_C$ and let us denote

$$B := K^i \cap (K_f \cup \{a, b\}), \qquad A := K^i \setminus B.$$

Clearly, the set B is closed and contains both the endpoints of the interval K^i.

It is not restrictive to assume that $f^{**}(x) = 0$ for every $x \in K^i$, so that

$$f(x) = 0 \quad \forall x \in B, \qquad f(x) > 0 \quad \forall x \in A. \tag{6.37}$$

Let us extend the function φ_i^+ to $+\infty$ outside K^i. Since $\varphi \leq \varphi_i^+$ and $(f + s\,\varphi_i^+)(x) = s\,\varphi_i^+(x)$ for every $x \in K^i$, we have that

$$f_s^{**}(x) = (f + s\,\varphi)^{**}(x) \leq (f + s\,\varphi_i^+)^{**}(x) = s\,(\varphi_i^+)^{**}(x), \qquad \forall x \in K^i,$$

hence

$$\limsup_{s \to 0^+} \frac{f_s^{**}(x_0) - f^{**}(x_0)}{s} \leq (\varphi_i^+)^{**}(x_0), \qquad \forall x_0 \in K^i.$$

Let $s_n \searrow 0$ be a sequence such that

$$l := \liminf_{s\to 0^+} \frac{f_s^{**}(x_0) - f^{**}(x_0)}{s} = \lim_{n\to+\infty} \frac{f_{s_n}^{**}(x_0) - f^{**}(x_0)}{s_n},$$

and let $E_n := \operatorname{epi} f_{s_n}^{**} \cap \{y \le M\}$, $n \in \mathbb{N}$. By (6.37), for every $\varepsilon > 0$, there exists $N_\varepsilon \in \mathbb{N}$ such that, for $n \ge N_\varepsilon$, the extreme points of E_n are contained in $B + B_\varepsilon$, so that

$$K_{f_{s_n}} \cap K^i \subset B + B_\varepsilon \qquad \forall n \ge N_\varepsilon. \tag{6.38}$$

Let

$$\varphi_\epsilon(x) := \begin{cases} \varphi(x) & x \in B + B_\varepsilon, \\ +\infty & \text{otherwise}, \end{cases}$$

so that $\varphi_\epsilon(x) = \varphi_i^+(x)$ for every $x \in B$ and $\varphi_\epsilon \to \varphi_i^+$ pointwise in K_i. From the inclusion (6.38) it holds

$$f_{s_n}^{**}(x) = (f + s_n\,\varphi_\epsilon)^{**}(x), \qquad \forall x \in K^i,\ \forall n \ge N_\varepsilon,$$

so that

$$l = \lim_{n\to+\infty} \frac{f_{s_n}^{**}(x_0) - f^{**}(x_0)}{s_n} \ge \liminf_{n\to+\infty} \frac{(f + s_n\,\varphi_\epsilon)^{**}(x_0) - f^{**}(x_0)}{s_n} \ge \varphi_\varepsilon^{**}(x_0).$$

Finally, letting $\varepsilon \to 0$, we conclude that $l \ge (\varphi_i^+)^{**}(x_0)$, concluding the proof. □

Proof of Theorem 6.1.8. Since f satisfies assumption (6.9), we can use the same arguments of Step 1 in Proposition 6.1.2. We omit the details. □

Proof of Proposition 6.1.10. If $f \in C^0([a,b])$, it is easily seen that $Tf \in C^0([a,b])$, the functions F and F^{**} are in $C^1([a,b])$, and $F(a) = F^{**}(a) = 0$, $F(b) = F^{**}(b)$. As a consequence,

$$\int_a^b Tf(y)\,dy = \int_a^b f(y)\,dy \qquad \forall f \in C^0([a,b]). \tag{6.39}$$

In the following, we shall denote by K_F the contact set of F, defined by

$$K_F := \{x \in (a,b) :\ F(x) = F^{**}(x)\}.$$

We remark that $f = Tf$ on K_F. Moreover, we have the following characterization of K_F:

$$\begin{aligned} K_F &= \{x \in (a,b) :\ F(y) - F(x) - (y-x)F'(x) \ge 0,\ \forall y \in [a,b]\} \\ &= \left\{x \in (a,b) :\ \int_x^y [f(s) - f(x)]\,ds \ge 0,\ \forall y \in [a,b]\right\}. \end{aligned} \tag{6.40}$$

Let $f, g \in C^0([a,b])$ and let $F(x) := \int_a^x f(y)\,dy$, $G(x) := \int_a^x g(y)\,dy$, $x \in [a,b]$. We claim that

$$f, g \in C^0([a,b]),\ f \le g \qquad \Longrightarrow \qquad Tf \le Tg. \tag{6.41}$$

Before proving this claim, let us observe that, from (6.39), (6.41) and Proposition 1 in [24], we can conclude that (6.14) holds.

It remains to prove that (6.41) holds. It will be convenient to perform a couple of reductions.

Reduction 1: it is not restrictive to assume that

$$f(a) = Tf(a), \quad f(b) = Tf(b), \qquad g(a) = Tg(a), \quad g(b) = Tg(b). \tag{6.42}$$

Namely, since

$$Tf(a) = \inf_{x\in(a,b]} \frac{F(x) - F(a)}{x - a} = \inf_{x\in(a,b]} \frac{1}{x - a} \int_a^x f(s)\, ds,$$

it is clear that $Tf(a) \le f(a)$. If $Tf(a) < f(a)$, then there exists $\beta \in (a, b]$ such that (a, β) is a connected component of $(a, b) \setminus K_F$. Given $\varepsilon > 0$, let $c_\varepsilon := (1 + 1/\sqrt{2})\varepsilon$, and define the function

$$\varphi_\varepsilon(t) := \begin{cases} -1 + t/\varepsilon & \text{if } t \in [0, c_\varepsilon], \\ -1 + (2c_\varepsilon - t)/\varepsilon & \text{if } t \in [c_\varepsilon, 2c_\varepsilon - \varepsilon], \\ 0 & \text{otherwise,} \end{cases}$$

so that $\varphi_\varepsilon(0) = -1$ and $\int_0^{2c_\varepsilon-\varepsilon} \varphi_\varepsilon = 0$.

It is not difficult to show that, for $\varepsilon > 0$ small enough, the function $f_\varepsilon(x) := f(x) + [f(a) - Tf(a)]\, \varphi_\varepsilon(x - a)$ satisfies $Tf_\varepsilon = Tf$ and $Tf_\varepsilon(a) = f_\varepsilon(a)$. Moreover, we have $\|f_\varepsilon - f\|_1 \to 0$ as $\varepsilon \to 0$.

Similarly, we can modify f near b and the same can be done for the function g.

Reduction 2: it is not restrictive to assume that

$$f < g \qquad \text{in } [a, b]. \tag{6.43}$$

Namely, it is enough to check that $T(g + \varepsilon) = Tg + \varepsilon$.

So, let $f, g \in C([a, b])$ satisfy (6.42) and (6.43), and define

$$x_0 := \max\{x \in [a, b] :\ Tf(y) \le Tg(y)\ \forall y \in [a, x]\}.$$

Since $F \le G$, we have that $F^{**} \le G^{**}$ and hence $Tf(a) \le Tg(a)$. Moreover, by (6.42) and (6.43), we clearly have $x_0 > a$.

Assume by contradiction that $x_0 < b$, so that $Tf(x_0) = Tg(x_0)$, and let us consider the following cases.

Case 1: $x_0 \in K_F \cap K_G$. Hence,

$$Tf(x_0) = f(x_0) < g(x_0) = Tg(x_0),$$

in contradiction with $Tf(x_0) = Tg(x_0)$.

Case 2: $x_0 \in K_F$, $x_0 \notin K_G$. Let (α, β) be the maximal connected component of $(a, b) \setminus K_G$ containing x_0, so that Tg is constant on $[\alpha, \beta]$ and $g(\alpha) = Tg(\alpha)$, $g(\beta) = Tg(\beta)$. Here it is worth to remark that these equalities hold also in the case $\alpha = a$ or $\beta = b$ thanks to (6.42).

By the characterization (6.40) we have that:

$$x_0 \in K_F \quad \Longrightarrow \quad \int_{x_0}^{\beta} [f(s) - f(x_0)]\, ds \geq 0,$$

$$\beta \in K_G \text{ or } \beta = b \quad \Longrightarrow \quad \int_{x_0}^{\beta} [g(\beta) - g(s)]\, ds \geq 0,$$

so that

$$\int_{x_0}^{\beta} [g(\beta) - g(s) + f(s) - f(x_0)]\, ds \geq 0. \tag{6.44}$$

On the other hand $g(\beta) = Tg(\beta) = Tg(x_0)$ and $f(x_0) = Tf(x_0)$. Since $Tf(x_0) = Tg(x_0)$, we conclude that $g(\beta) = f(x_0)$, hence from (6.44) it holds

$$\int_{x_0}^{\beta} [f(s) - g(s)]\, ds \geq 0,$$

contradicting the assumption $f < g$.

Case 3: $x_0 \notin K_F$, $x_0 \in K_G$. We can reason as in the previous case, considering the connected component (α, β) of $(a, b) \setminus K_f$ containing x_0, and obtaining the inequality

$$\int_{\alpha}^{x_0} [g(x_0) - g(s) + f(s) - f(\alpha)]\, ds \geq 0.$$

Since, in this case, $g(x_0) = f(\alpha)$, we get again a contradiction with the assumption $f < g$.

Case 4: $x_0 \notin K_F$, $x_0 \notin K_G$. In this case Tf and Tg are locally constant in a neighborhood of x_0, again in contradiction with the definition of x_0. □

Proof of Proposition 6.1.11. We divide the proof into two steps.

STEP 1. If $f \in L^1(a, b)$, and $(f_n) \subset C^0([a, b])$ is a sequence converging to f in L^1, then

$$Tf_n \to Tf \quad \text{a.e.,} \quad \text{and} \quad \|Tf_n - Tf\|_1 \to 0.$$

Let $F(x) := \int_a^x f$, $F_n(x) := \int_a^x f_n$. We have that $F_n \to F$ uniformly in $[a, b]$, hence also $F_n^{**} \to F^{**}$ uniformly in $[a, b]$. (Proof: use the characterization $F^{**}(x) = \min\{(1 - \lambda)F(x_0) + \lambda F(x_1) : \lambda \in [0, 1],\ (1 - \lambda)x_0 + \lambda x_1 = x\}$.) By Theorem 24.5 in [66] we deduce that $(F_n^{**})' \to (F^{**})'$ at every point of differentiability of F^{**}, i.e. almost everywhere in $[a, b]$. By definition of T, it follows that $Tf_n \to Tf$ almost everywhere in $[a, b]$.

The L^1 convergence of (Tf_n) to Tf follows from Proposition 6.1.10. Namely, from (6.14) we have that $\|Tf_n - Tf_m\|_1 \leq \|f_n - f_m\|_1$, hence (Tf_n) is a Cauchy sequence in L^1 (and so it converges to its pointwise limit).

STEP 2. Completion of the proof.

Given $f, g \in L^1(a, b)$, let $(f_n), (g_n) \subset C^0([a, b])$ sequences converging in L^1 respectively to f and g. By Proposition 6.1.10, we have that $\|Tf_n - Tg_n\|_1 \leq \|f_n - g_n\|_1$ for every n. Hence, by Step 1, passing to the limit as $n \to +\infty$ we obtain (6.15). □

Proof of Proposition 6.1.13. By (6.4) and (6.10) we have that

$$Tf = \begin{cases} \dfrac{F(b^i) - F(a^i)}{b^i - a^i} & x \in I^i,\ i \in J, \\ F'(x) & x \in K_F. \end{cases} \qquad (\mathcal{J}_F^\varphi)' = \begin{cases} \dfrac{\varphi(b^i) - \varphi(a^i)}{b^i - a^i} = \dfrac{\int_{a^i}^{b^i} \varphi' dx}{b^i - a^i} & x \in I^i,\ i \in J, \\ \varphi'(x) & x \in K_F, \end{cases}$$

and similarly for Tg and $(\mathcal{J}_G^\varphi)'$. Then we have the fundamental integral equivalence

$$\int_a^b [Tf\ (\mathcal{J}_F^\varphi)' - Tg\ (\mathcal{J}_G^\varphi)']dx = \int_a^b [Tf - Tg]\ \varphi' dx, \quad \forall \varphi \in C_c^\infty(\mathcal{I}) \tag{6.45}$$

so that the thesis is achieved by applying the Hölder inequality and Proposition 6.1.11. □

Proof of Proposition 6.1.14. i) Let us observe that

$$\int_a^b [\mathcal{H}(Tf)\ (\mathcal{J}_F^\varphi)' - \mathcal{H}(Tg)\ (\mathcal{J}_G^\varphi)']dx = \int_a^b [\mathcal{H}(Tf) - \mathcal{H}(Tg)]\ \varphi' dx, \quad \forall \varphi \in C_c^\infty(\mathcal{I})$$

then we proceed as in Proposition 6.1.13, considering the Lipschitz property of $\mathcal{H}$.

ii) We consider the equivalence

$$\begin{aligned} &\int_a^b [\mathcal{H}(Tf)\ (\mathcal{G}^{F,\psi})' - \mathcal{H}(Tg)\ (\mathcal{G}^{G,\psi})']dx = \int_a^b [\mathcal{H}(Tf)(\psi \cos F)' - \mathcal{H}(Tg)(\psi \cos G)']dx \\ &= \int_a^b [\mathcal{H}(Tf) - \mathcal{H}(Tg)](\psi \cos F)' dx + \int_a^b \mathcal{H}(Tg)\ (\psi \cos F - \psi \cos G)' dx \quad \forall \psi \in C_c^\infty(\mathcal{I}). \end{aligned} \tag{6.46}$$

Since $(\psi \cos F - \psi \cos G)' = \psi'(\cos F - \cos G) - \psi[(f - g)\sin F + g(\sin F - \sin G)]$, the thesis follows by the Lipschitzianity of the trigonometric functions and by proceeding as in the proofs above. □

Proof of Proposition 6.1.15. The functions $\mathcal{J}_n^\varphi$ are Lipschitz continuous, with

$$\|\mathcal{J}_n^\varphi\|_\infty \le \|\varphi\|_\infty, \qquad \|(\mathcal{J}_n^\varphi)'\|_\infty \le \|\varphi'\|_\infty.$$

Hence, by the Dominated Convergence Theorem, it is enough to show that $\mathcal{J}_n^\varphi \to \mathcal{J}^\varphi$ and $(\mathcal{J}_n^\varphi)' \to (\mathcal{J}^\varphi)'$ almost everywhere in $\mathcal{I}$.

The pointwise convergence of $\{\mathcal{J}_n^\varphi\}$ to $\mathcal{J}^\varphi$ is a direct consequence of Lemma 6.5.1.

To prove the a.e. convergence of $\{(\mathcal{J}_n^\varphi)'\}$ to $(\mathcal{J}^\varphi)'$, it will be convenient to distinguish between the two cases (a) and (b) in Lemma 6.5.1.

Let x_0 be as in case (a), and assume that all the function $\mathcal{J}_n^\varphi$ are differentiable at x_0 (this condition is satisfied at almost every point). For every n, if $x_0 \in K_{f_n}$ (i.e. $a_n = b_n$) then $(\mathcal{J}_n^\varphi)'(x_0) = \varphi'(x_0)$, otherwise there exists a point $x_n \in (a_n, b_n)$ such that

$$(\mathcal{J}_n^\varphi)'(x_0) = \frac{\varphi(b_n) - \varphi(a_n)}{b_n - a_n} = \varphi'(x_n).$$

Since $a_n, b_n \to x_0$, we finally get $(\mathcal{J}_n^\varphi)'(x_0) \to \varphi'(x_0) = (\mathcal{J}^\varphi)'(x_0)$.

Let x_0 be as in case (b). Then, for n large enough,

$$(\mathcal{J}_n^\varphi)'(x_0) = \frac{\varphi(b_n) - \varphi(a_n)}{b_n - a_n} \to \frac{\varphi(b_0) - \varphi(a_0)}{b_0 - a_0} = (\mathcal{J}^\varphi)'(x_0),$$

and the proof is complete. □

6.6 Proofs of existence and uniqueness results

To simplify the notations we define the functionals

$$\chi(u) := \frac{u'}{\sqrt{1+(u')^2}}, \qquad \gamma(u) := \sqrt{1+(u')^2} \tag{6.47}$$

and we state a preliminary

Lemma 6.6.1. *The functionals $\chi, \gamma : C^1[0,L] \to C^0[0,L]$ are locally Lipschitz continuous.*

Proof. Given $v, w \in C^1[0,L]$, we apply the Lagrange Theorem, so that there exists $\varrho := \varrho(x) \in \big(v', w'\big)$ such that

$$\big|\chi(v)-\chi(w))\big| = \frac{|v'-w'|}{\sqrt{(1+\varrho^2)^3}} \le |v'-w'|, \qquad \big|\gamma(v)-\gamma(w))\big| = \frac{|\varrho||v'-w'|}{\sqrt{1+\varrho^2}} \le |v'-w'|.$$

□

Proof of Theorem 6.3.2. Let $n \ge 1$ an integer. The local existence of a solution (w_n^k, θ_n^k) for all $k = 1, \dots, n$ and $t \ge 0$ depends on the regularity of the right hand side terms of (6.28). We introduce the vectors $W = [w_n^1, \dots, w_n^n]$, $\Theta = [\theta_n^1, \dots, \theta_n^n]$ and $e(x) = [e_1(x), \dots, e_n(x)]$ belonging to $\mathbb{R}^n$; we study the nonlinearities related to one cable, the other being similar.

If the functions

$$F_k(W,\Theta) := \big[H\overline{\xi} + \frac{AE_c}{L_c}\Gamma\big(W\cdot e + \ell\sin(\Theta\cdot e)\big]\int_0^L \chi\Big([W\cdot e + \ell\sin(\Theta\cdot e) + y]^{**}\Big)\,(\mathcal{J}_\alpha^{e_k})'dx,$$
$$G_k(W,\Theta) := \big[H\overline{\xi} + \frac{AE_c}{L_c}\Gamma\big(W\cdot e + \ell\sin(\Theta\cdot e)\big]\int_0^L \chi\Big([W\cdot e + \ell\sin(\Theta\cdot e) + y]^{**}\Big)\,(\mathcal{G}_\alpha^{\Theta\cdot e, e_k})'dx,$$

are locally Lipschitz continuous with respect to W and Θ for all $k = 1, \dots, n$, we have the existence and uniqueness of a solution of (6.28) on some interval $[0, t_n)$ with $t_n \in (0, T]$.

Thanks to Lemma 6.6.1, Proposition 6.1.14-i) and (6.17), for every compact subset $X \subset \mathbb{R}^n$ there exists $C_0 > 0$ such that, for every $W_1, W_2, \Theta_1, \Theta_2 \in X$ we have

$$\begin{aligned}
&\big|F_k(W_1,\Theta_1) - F_k(W_2,\Theta_2)\big| = \Big|\big[H\overline{\xi} + \frac{AE_c}{L_c}\Gamma\big(W_1\cdot e + \ell\sin(\Theta_1\cdot e)\big)\big]\cdot\\
&\cdot\int_0^L\Big[\chi\Big([W_1\cdot e + \ell\sin(\Theta_1\cdot e)+y]^{**}\Big)[(\mathcal{J}_\alpha^{e_k})_1]' - \chi\Big([W_2\cdot e + \ell\sin(\Theta_2\cdot e)+y]^{**}\Big)[(\mathcal{J}_\alpha^{e_k})_2]'\Big]dx\\
&+\frac{AE_c}{L_c}\Big\{\int_0^L\Big[\gamma\Big([W_1\cdot e + \ell\sin(\Theta_1\cdot e)+y]^{**}\Big) - \gamma\Big([W_2\cdot e + \ell\sin(\Theta_2\cdot e)+y]^{**}\Big)\Big]dx\Big\}\cdot\\
&\cdot\Big\{\int_0^L\chi\Big([W_2\cdot e + \ell\sin(\Theta_2\cdot e)+y]^{**}\Big)[(\mathcal{J}_\alpha^{e_k})_2]'dx\Big\}\Big| \le C_0\|e_k'\|_\infty\big(|W_1-W_2| + |\Theta_1-\Theta_2|\big)\|e\|_{W^{1,1}},
\end{aligned} \tag{6.48}$$

so that $F_k(W,\Theta)$ is locally Lipschitz continuous for all $k = 1, \dots, n$. With some additional computations due to the presence of the trigonometric functions, see Proposition

6.1.14-ii), the same arguments can be applied to obtain the locally Lipschitz continuity of $G_k(W,\Theta)$.

Our purpose is now to find a uniform bound for the sequence (w_n,θ_n). We omit for the moment the spatial dependence of the approximated solutions. We test the first equation in (6.26) by $\dot{w}_n$, the second by $\dot{\theta}_n$ and we sum the two equations. Hence, we obtain

$$\begin{aligned}
&\frac{M}{2}\frac{d}{dt}\|\dot{w}_n\|_2^2+\frac{EI}{2}\frac{d}{dt}\|w_n\|_{H^2}^2+\frac{M\ell^2}{6}\frac{d}{dt}\|\dot{\theta}_n\|_2^2+\frac{EJ}{2}\frac{d}{dt}\|\theta_n\|_{H^2}^2+\frac{GK}{2}\frac{d}{dt}\|\theta_n\|_{H^1}^2-\int_0^L Mg\dot{w}_n dx\\
&=-[H\bar{\xi}+\frac{AE_c}{L_c}\Gamma(w_n+\ell\sin\theta_n)]\int_0^L\frac{[(w_n+\ell\sin\theta_n+y)^{**}]_x}{\sqrt{1+\{[(w_n+\ell\sin\theta_n+y)^{**}]_x\}^2}}(\mathcal{J}_\alpha^{\dot{w}_n}+\ell\mathcal{G}_\alpha^{\theta_n,\dot{\theta}_n})_x dx\\
&\quad-[H\bar{\xi}+\frac{AE_c}{L_c}\Gamma(w_n-\ell\sin\theta_n)]\int_0^L\frac{[(w_n-\ell\sin\theta_n+y)^{**}]_x}{\sqrt{1+\{[(w_n-\ell\sin\theta_n+y)^{**}]_x\}^2}}(\mathcal{J}_\beta^{\dot{w}_n}-\ell\mathcal{G}_\beta^{\theta_n,\dot{\theta}_n})_x dx.
\end{aligned}\tag{6.49}$$

Let us define the energy of the system for the approximate solution (w_n,θ_n) as

$$\begin{aligned}
\mathcal{E}_n(t):=&\frac{M}{2}\|\dot{w}_n\|_2^2+\frac{EI}{2}\|w_n\|_{H^2}^2+\frac{M\ell^2}{6}\|\dot{\theta}_n\|_2^2+\frac{EJ}{2}\|\theta_n\|_{H^2}^2+\frac{GK}{2}\|\theta_n\|_{H^1}^2-Mg\int_0^L w_n dx\\
&+H\bar{\xi}\int_0^L(\sqrt{1+\{[(w_n+\ell\sin\theta_n+y)^{**}]_x\}^2}+\sqrt{1+\{[(w_n-\ell\sin\theta_n+y)^{**}]_x\}^2})dx\\
&+\frac{AE_c}{2L_c}\big([\Gamma(w_n+\ell\sin\theta_n)]^2+[\Gamma(w_n-\ell\sin\theta_n)]^2\big).
\end{aligned}$$

Since we are in the finite dimensional setting it holds the assumption (6.9), so that we apply Corollary 6.1.3 and Theorem 6.1.8, finding the energy conservation. This is the point where we take advantage of the final dimensional nature of the problem. Hence from (6.49) we have $\dot{\mathcal{E}}_n(t)=0$, that is

$$\begin{aligned}
\mathcal{E}_n(t)=\mathcal{E}_n(0)=&\frac{M}{2}\|w_n^1\|_2^2+\frac{EI}{2}\|w_n^0\|_{H^2}^2+\frac{M\ell^2}{6}\|\theta_n^1\|_2^2+\frac{EJ}{2}\|\theta_n^0\|_{H^2}^2+\frac{GK}{2}\|\theta_n^0\|_{H^1}^2-Mg\int_0^L w_n^0 dx\\
&+H\bar{\xi}\int_0^L(\sqrt{1+\{[(w_n^0+\ell\sin\theta_n^0+y)^{**}]'\}^2}+\sqrt{1+\{[(w_n^0-\ell\sin\theta_n^0+y)^{**}]'\}^2})dx\\
&+\frac{AE_c}{2L_c}\bigg(\int_0^L[\sqrt{1+\{[(w_n^0+\ell\sin\theta_n^0+y)^{**}]'\}^2}]dx-L_c\bigg)^2\\
&+\frac{AE_c}{2L_c}\bigg(\int_0^L[\sqrt{1+\{[(w_n^0-\ell\sin\theta_n^0+y)^{**}]'\}^2}]dx-L_c\bigg)^2.
\end{aligned}\tag{6.50}$$

We observe that in $\mathcal{E}_n(t)$ only the gravitational term has undefined sign. In order to estimate this term we apply the same passages as in Section 5.4.1 (see step 2), so that from (6.50) we infer the existence of $\eta>0$ such that

$$\eta(\|\dot{w}_n\|_2^2+\|w_n\|_{H^2}^2+\|\dot{\theta}_n\|_2^2+\|\theta_n\|_{H^2}^2+\|\theta_n\|_{H^1}^2)\le\mathcal{E}_n(0)+MgL,\tag{6.51}$$

for any $t\in[0,t_n)$ and $n\ge1$. Thanks to (6.51) we obtain $t_n=T$, ensuring the global existence and uniqueness of the solution (w_n,θ_n) on $[0,T]$. Moreover, since the total energy of (6.26) is conserved in time, the solution cannot blow up in finite time and the global existence is obtained for an arbitrary $T>0$, including $T=\infty$. □

Proof of Theorem 6.3.5. To simplify the notation we denote by $L^p(V)$ the Lebesgue space $L^p((0,T);V(0,L))$ for $1 \le p \le \infty$, by $Q = (0,T)\times(0,L)$ and by $C > 0$ all the generic positive constants.

We observe that $\sup_n |\mathcal{E}_n(0)| + MgL < \infty$ is independent of n and t, since w_n^0 and θ_n^0 belong to $C^1[0,L]$, ensuring the convexification procedure in Section 6.1.1. Then from (6.51) we infer the boundedness of $\{w_n\}, \{\theta_n\}$ in $L^\infty(H^2)$ and of $\{\dot w_n\}, \{\dot\theta_n\}$ in $L^\infty(L^2)$, implying, up to a subsequence, the weak* convergence respectively to w, θ and to $\dot w$, $\dot\theta$ in the previous spaces. In particular from the boundedness of $\{w_n\}, \{\theta_n\}$ and $\{\dot w_n\}, \{\dot\theta_n\}$ we also have weak convergence respectively in $L^2(H^2)$ and $L^2(Q)$; then, due to the compact embedding $H^1(Q) \subset L^2(Q)$, we obtain the strong convergence

$$w_n \to w, \quad \theta_n \to \theta \qquad \text{in} \qquad L^2(Q), \tag{6.52}$$

from which $\sin\theta_n \to \sin\theta$ in $L^2(Q)$, since $\|\sin\theta_n - \sin\theta\|_{L^2(Q)} \le \|\theta_n - \theta\|_{L^2(Q)} \to 0$ as $n \to \infty$ (similarly $\cos\theta_n \to \cos\theta$).

About the nonlocal term Γ, defined in (6.17), thanks to Lemma 6.6.1, Proposition 6.1.11, Hölder and Poincaré inequalities, we see that there exists $C > 0$ such that

$$\begin{aligned}|\Gamma(w_n \pm \ell\sin\theta_n) - \Gamma(w \pm \ell\sin\theta)| &\le (\|(w_n - w)_x\|_1 + \|\theta_n - \theta\|_{W^{1,1}}) \\ &\le C(\|w_n - w\|_{L^\infty(H^2)} + \|\theta_n - \theta\|_{L^\infty(H^2)}) \to 0,\end{aligned}$$

up to a subsequence, implying $\Gamma(w_n \pm \ell\sin\theta_n) \to \Gamma(w \pm \ell\sin\theta)$.

Let us now consider the functional χ, defined in (6.47), and note that $|\chi(u)| < 1$ for all $u \in H^2(0,L) \subset C^1[0,L]$. Then, we have that $\chi^2\big([w_n \pm \ell\sin\theta_n + y]^{**}\big) < 1$ and

$$\|\chi\big([w_n \pm \ell\sin\theta_n + y]^{**}\big)\|^2_{L^2(Q)} = \int_0^T\int_0^L \frac{\{[(w_n \pm \ell\sin\theta_n + y)^{**}]_x\}^2}{1 + \{[(w_n \pm \ell\sin\theta_n + y)^{**}]_x\}^2} dxdt < LT.$$

Hence $\chi\big([w_n \pm \ell\sin\theta_n + y]^{**}\big)$ converges weakly, up to a subsequence, to $\chi\big([w \pm \ell\sin\theta + y]^{**}\big)$ in $L^2(Q)$ and it is possible to pass to the limit in the first equation in (6.26), since $\|(\mathcal{J}_\alpha^{e_k})'\|_\infty \le \|e_k'\|_\infty$. To do the same for the second equation in (6.26) we use (6.46) and the bounds

$$\begin{aligned}\|\chi\big([w_n \pm \ell\sin\theta_n + y]^{**}\big)\cos\theta_n\|^2_{L^2(Q)} &< LT, \\ \|\chi\big([w_n \pm \ell\sin\theta_n + y]^{**}\big)\theta_{nx}\sin\theta_n\|^2_{L^2(Q)} &\le T\|\theta_n\|^2_{L^\infty(H^1)},\end{aligned}$$

which imply the weak convergence of these terms in $L^2(Q)$, up to a subsequence.

Next, for any $n \ge 1$ we put

$$\begin{aligned}w_n^0 &:= \sum_{k=1}^n (w^0, e_k)_2\, e_k = \frac{L^4}{\pi^4}\sum_{k=1}^n \frac{(w^0, e_k)_{H^2}}{k^4}\, e_k, \\ \theta_n^0 &:= \sum_{k=1}^n (\theta^0, e_k)_2\, e_k = \sum_{k=1}^n \frac{EJ(\theta^0, e_k)_{H^2} + GK(\theta^0, e_k)_{H^1}}{\left(EJ\frac{k^4\pi^4}{L^4} + GK\frac{k^2\pi^2}{L^2}\right)}\, e_k, \\ w_n^1 &:= \sum_{k=1}^n (w^1, e_k)_2\, e_k, \qquad \theta_n^1 := \sum_{k=1}^n (\theta^1, e_k)_2\, e_k,\end{aligned}$$

so that

$$w_n^0 \to w^0,\ \ \theta_n^0 \to \theta^0 \ \text{ in } \ H^2, \qquad w_n^1 \to w^1,\ \ \theta_n^1 \to \theta^1 \ \text{ in } \ L^2$$

as $n \to \infty$.

Therefore we pass to the limit the problem (6.26)-(6.27), so that there exists an approximable solution of (6.23)-(6.24), $(w, \theta) \in X_T^2$ in the sense of Definition 6.3.4. □

Conclusions

In this work we introduced three isolated models for suspension bridges; we presented the general framework of study of this kind of problems, discussing the isolated system assumption, that is fundamental for our models. In all the cases we considered two degrees of freedom, the vertical displacement and the torsional rotation of the deck. Hence, we introduced systems of nonlinear PDEs, avoiding assumptions on small rotations of the deck and complying with the real geometry of the problem. The system is studied at first in terms of existence ad uniqueness of a solution; then, adopting the Galerkin procedure, we reduced the PDEs to a finite-dimensional approximated ODEs system. A general framework to study the torsional stability has been developed with particular attention with respect to the real observations recorded for suspension bridges, primarily at the TNB.

We introduced a first model for suspension bridges with fixed cables and deformable hangers, focusing on the main problems related to the modeling of the hangers' restoring force, source of nonlinearity. Motivated by the witnesses of the TNB collapse and some results in literature, we concentrated our attention on the 2-nd torsional mode interacting with the longitudinal modes from 2 to 10.

We presented the problem studying three different nonlinearities: the positive part nonlinearity, a cubic perturbation of the positive part and a smooth nonlinearity, all simulating the slackening of the hangers. For each case we performed numerical experiments exciting initially different longitudinal modes and observing from which of them the 2-nd torsional mode absorbed more energy.

The results show that, applying the same initial condition ($\overline{w}_j^0 = 2\text{m}$), there are longitudinal modes more prone to develop torsional instability and others that produce imperceptible torsional movements. For each slackening nonlinearity we recorded instability phenomena, confirming that different analytical choices provide, in general, a similar trend for the system.

The importance of the structural parameters is shown through some parametric analysis; these results can give some hints for future choices in the bridges design to avoid the oversizing of the structures, also in an economic saving perspective. For instance our model confirms that a closed deck's cross section gives better torsional performance

arranging the structural element of the deck in the optimal configuration.

We applied our model inserting the mechanical features of two existing suspension bridges (Halsafjorden and Vincent Thomas bridges); for these cases we do not record phenomena of torsional instability, confirming the general validity of the model.

A second model for suspension bridge inspired by the Melan equation is proposed, assuming deformable cables and rigid hangers. The presence of two cables linked to a single deck produces a problem more complex than the original Melan equation (single cable-beam system) and gives two strongly coupled equations of the motion. In this model we included not only the torsional effects on the deck due to de Saint Venant theory, but also those more precise introduced by Vlasov theory.

Adopting the Galerkin procedure we proved the existence of a solution, while we obtained its uniqueness testing the equations with the Green function applied to the time derivative of the solutions; we proposed the complete proof since it is non-standard due to the presence of the nonlinearities.

We presented some numerical experiments on this system, considering 10 longitudinal modes interacting with 4 torsional modes. The results show that, exciting distinct longitudinal modes, there are different thresholds of torsional instability; this fact reveals that the origin of the instability is structural, as [3,5,10]. An analysis of sensitivity with respect to the mechanical parameters involved in the system is performed; we considered the parameters of the TNB as "basic situation" and then, modifying them, we analyzed how the response of the system changes in terms of torsional instability.

The thesis is completed with a third model in which both the hangers and the cables are deformable. This was previously considered in [4] through a four DOF model, but here we have only focused on the vertical displacements and the torsional rotations of the deck, thereby dealing with a two DOF model. For the model considered it appears out of reach to obtain a precise explanation of the origin of torsional instability in terms of Poincaré maps as in [3]. However, our numerical results still show the same qualitative phenomenon: after exceeding a certain energy threshold the system becomes unstable and sudden torsional oscillations appear.

The analysis of this new model for suspension bridges requires the study of the variation of an energy functional depending on the convexification of the concerned functions. The computation of the Gateaux derivatives of the functional is quite involved and, apart of "spoiling" the action of the smooth test functions, it does not exist in some situations. After a full energy balance, in Section 6.3 we derived the weak form of the system of nonlinear nonlocal partial differential inclusions.

The typical behavior of civil structures enabled us to consider approximable solutions as representative enough of our problem, thereby reducing to a system of ordinary differential equations, through the Galerkin procedure. We then proved existence of weak approximable solutions. This enabled us to study the problem numerically, considering 10 longitudinal modes interacting with 4 torsional modes and we found a threshold of torsional instability for each longitudinal mode excited. We compared these thresholds with those of instability of the correspondent model without convexification. Our numerical results show that, for structures displaying only low modes of vibration (e.g. 1-st, 2-nd, 3-rd), we may assume inextensible hangers, reducing the computational costs and obtaining safe instability thresholds. On the other hand, if the

structure vibrates on higher modes (e.g. 9-th, 10-th) as the TNB, this assumption may provide overestimated thresholds. Here the slackening of the hangers increases dangerously the torsional instability; this fact should be a warning for the designers of bridge structures, that are able to exhibit, in realistic situations, large vibration frequencies. Let us recall that the wind velocity determines the excited mode, see [2, pp.21-27], and that an explicit rule has been recently found in [14]. It turns out that the longitudinal modes that were torsionally unstable at the TNB were the 9-th and 10-th, precisely the ones for which we found lower thresholds of instability in the new model with convexification (that is, with hangers slackening).

The study of models for suspension bridges also requires deep theoretical tools possibly of general interest; we refer to the calculus of the variations of convexified functions in Section 6.1 and to the existence and uniqueness problem. In Section 6.6 we proved that a solution exists and is unique in the finite dimensional setting, without knowing how many solutions the system of partial differential inclusions (6.23) has. Other open issues are reported in Section 6.3.3.

The thesis focused mainly on the study of torsional instability phenomena in isolated models for suspension bridge; in order to refine further the models a next step may be the study of the stability with respect to the interaction between internal resonance and aeroelastic phenomena; in this case we should introduce the structural damping and, surely, we should modify the approach to the problem. This may be a possible development in forthcoming researches.

Bibliography

[1] A.M. Abdel-Ghaffar, *Dynamic analysis of suspension bridge structures*, Technical Report 76-01, California Institute of Technology (1976).

[2] O.H. Ammann, T. von Kármán, G.B. Woodruff, *The failure of the Tacoma Narrows Bridge*, Federal Works Agency (1941).

[3] G. Arioli, F. Gazzola, *A new mathematical explanation of what triggered the catastrophic torsional mode of the Tacoma Narrows Bridge collapse*, App. Math. Modelling **39**, 901–912 (2015).

[4] G. Arioli, F. Gazzola, *On a nonlinear nonlocal hyperbolic system modeling suspension bridges*, Milan J. Math. **83**, 211–236 (2015).

[5] G. Arioli, F. Gazzola, *Torsional instability in suspension bridges: the Tacoma Narrows Bridge case*, Communications Nonlinear Sci. Numerical Simulation **42**, 342–357 (2017).

[6] J. P. Aubin, A. Cellina, *Differential inclusions. Set-valued maps and viability theory*, Springer-Verlag, Berlin, (1984).

[7] J.M. Ball, *Initial-boundary value problems for an extensible beam*, J. Math. Anal. Appl. **42**, 61-90 (1973).

[8] G. Bartoli, P. Spinelli, *The stochastic differential calculus for the determination of structural response under wind*, J. Wind Engineering and Industrial Aerodynamics **48**, 175–188 (1993).

[9] E. Berchio, A. Ferrero, F. Gazzola, *Structural instability of nonlinear plates modelling suspension bridges: mathematical answers to some long-standing questions*, Nonlin. Anal. Real World Appl. **28**, 91–125 (2016).

[10] E. Berchio, F. Gazzola, *A qualitative explanation of the origin of torsional instability in suspension bridges*, Nonlinear Analysis TMA **121**, 54-72 (2015).

[11] J. Berkovits, P. Drábek, H. Leinfelder, V. Mustonen, G. Tajčová, *Time-periodic oscillations in suspension bridges: existence of unique solutions*, Nonlinear Anal. Real World Appl. **1**, 345–362 (2000).

[12] K.Y. Billah, R.H. Scanlan, *Resonance, tacoma narrows bridge failure, and undergraduate physics textbooks,* Am. J. Phys. **59**, 118–124 (1991).

[13] F. Bleich, C.B. McCullough, R. Rosecrans, G.S. Vincent, *The mathematical theory of suspension bridges*, U.S. Dept. of Commerce, Bureau of Public Roads, Washington DC (1950).

[14] D. Bonheure, F. Gazzola, E. Moreira dos Santos, *Periodic solutions and torsional instability in a nonlinear nonlocal plate equation*, preprint (2018).

[15] J.M.W. Brownjohn,*Observations on non-linear dynamic characteristics of suspension bridges*, Earthquake Engineering & Structural Dynamics **23**, 1351–1367 (1994).

[16] D. Bucur, *Regularity of optimal convex shapes*, J. Convex Anal. **10**, no.2, 501–516 (2003).

[17] V.I. Burdina, *Free vibrations of solutions of a system of differential equations,* Dokl. Akad. Nauk. SSSR **92**, 603–606 (1953).

[18] G. Buttazzo, V. Ferone, B. Kawohl, *Minumum problems over sets of concave functions and related questions*, Math. Nachr. **173**, 71–89 (1995).

[19] M. Cannone, S. Friedlander, *Navier: blow-up and collapse*, Amer. Math. Soc. Notices **50** (1), 7–13 (2003).

[20] A. Capsoni, R. Ardito, A. Guerrieri, *Stability of dynamic response of suspension bridges*, J. Sound and Vibration **393**, 285–307 (2017).

[21] A. Cellina, *A view on differential inclusions*, Rend. Semin. Mat. Univ. Politec. Torino **63**, 197–209 (2005).

[22] C. Chicone, *Ordinary differential equations with applications,* Springer Science & Business Media, New York (1999).

[23] F.H. Clarke, *Optimization and nonsmooth analysis,* Jhon Wiley & Sons, New York (1983).

[24] M.G. Crandall, L. Tartar, *Some relations between nonexpansive and order preserving mappings*, Proc. Amer. Math. Soc. **78** , no. 3, 385–390 (1980).

[25] G. Crasta, A. Falocchi, F. Gazzola, *A new model for suspension bridges involving the convexification of the cables* , preprint.

[26] I. Ekeland, R. Temam, *Convex analysis and variational principles*, North-Holland, Amsterdam (1976).

[27] A. Falocchi, *Torsional instability and sensitivity analysis in a suspension bridge model related to the Melan equation*, Communications Nonlinear Sci. Numerical Simulation **67**, 60–75 (2019).

[28] A. Falocchi, *Torsional instability in a nonlinear isolated model for suspension bridges with fixed cables and extensible hangers*, IMA Journal of Applied Mathematics **83**, 1007–1036 (2018).

[29] F. B. Farquharson, *Aerodynamic stability of suspension bridges: with special reference to the Tacoma Narrows Bridge, Part I: investigations prior October 1941,* Investigation conducted by the Structural Research Laboratory, University of Washington Press, Seattle, (1949).

[30] A. Ferrero, F. Gazzola, *A partially hinged rectangular plate as a model for suspension bridges*, Disc. Cont. Dyn. Syst. A **35**, 5879–5908 (2015).

[31] K. Frampton, *Modern Architecture: a critical history. Forth edition revised, expanded and updated,* Thames and Hudson, London, (2007).

[32] M. Garrione, F. Gazzola, *Loss of energy concentration in nonlinear evolution beam equations*, J. Nonlinear Sci. **27**, 1789–1827 (2017).

[33] C. Gasparetto, F. Gazzola, *Resonance tongues for the Hill equation with Duffing coefficients and instabilities in a nonlinear beam equation*, Comm. Contemp. Math. **20**, 1750022 (22 pp.) (2018).

[34] F. Gazzola, *Mathematical models for suspension bridges*, MS&-A Vol.15, Springer (2015).

[35] F. Gazzola, M. Jleli, B. Samet, *On the Melan equation for suspension bridges*, Journal of Fixed Point Theory and Applications 16(1-2):159188, (2014).

[36] F. Gazzola, R. Pavani, Y. Wang, *Variational formulation of the Melan equation*, Mathematical Methods in the Applied Sciences, (2018).

[37] F. Gazzola, G. Sperone, *Thresholds for hanger slackening and cable shortening in the Melan equation for suspension bridges*, Nonlin. Anal. Real World Appl. **39**, 520–536 (2018).

[38] F. Gazzola, Y. Wang, *Modeling suspension bridges through the von Kármán quasilinear plate equations*, Progress in Nonlinear Differential Equations and Their Applications, In: Contributions to Nonlinear Differential Equations and Systems, a tribute to Djairo Guedes de Figueiredo on occasion of his 80th birthday, 269–297 (2015).

[39] F. Genna, A. Franchi, *Lezioni di scienza delle costruzioni,* Esculapio (1995).

[40] G. Holubová, A. Matas, *Initial-boundary value problem for nonlinear string-beam system*, J. Math. Anal. Appl. **288**, 784–802 (2003).

[41] D. Imhof, *Risk assessment of existing bridge structures*, Phd Dissertation, University of Cambridge (2004).

[42] H.M. Irvine, *Cable structures*, MIT Press Series in Structural Mechanics, Massachusetts (1981).

[43] A. Larsen, *Aerodynamics of the Tacoma Narrows Bridge - 60 years later*, Structural Engineering International **4**, 243-248 (2000).

[44] A.C. Lazer, P.J. McKenna, *Large-amplitude periodic oscillations in suspension bridges: some new connections with nonlinear analysis*, SIAM Rev. **32**, 537–578 (1990).

[45] W. Li, M. Zhang, *A Lyapunov-type stability criterion using L^α norms*, Proc. Amer. Math. Soc. **130**, 3325–3333 (2002).

[46] J.L. Luco, J.Turmo, *Effect of hanger flexibility on dynamic response of suspension bridges*, J. Engineering Mechanics **136**, 1444–1459 (2010).

[47] W. Magnus, S. Winkler, *Hill's equations*, Dover, New York (1979).

[48] J. Malík, *Sudden lateral asymmetry and torsional oscillations in the original Tacoma suspension bridge,* J. Sound Vib. **332**, 3772–3789 (2013).

[49] C. Marchionna, S. Panizzi, *An instability result in the theory of suspension bridges*, Nonlinear Analysis **140**, 12–28 (2016).

[50] E. Mathieu, *Mémoire sur le mouvement vibratoire d'une membrane de forme elliptique*, J. Math. Pures Appl. **13**, 137-203 (1868).

[51] P.J. McKenna, *Large torsional oscillations in suspension bridges revisited: fixing an old approximation*, Am. Math. Mon. **106**, 1–18 (1999).

[52] P.J. McKenna, C. Ó Tuama, *Large torsional oscillations in suspension bridges visited again: vertical forcing creates torsional response*, Am. Math. Mon. **108**, 738–745 (2001).

[53] P.J. McKenna, W. Walter, *Nonlinear oscillations in a suspension bridge*, Arch. Rat. Mech. Anal. **98**, 167–177 (1987).

[54] N.W. McLachlan, *Theory and application of Mathieu functions*, Dover publications, New York (1964).

[55] J. Melan, *Theory of Arches and Suspension Bridges, Vol. 2*, Myron Clark Publ. Comp. London, (1913).

[56] C.L. Navier, *Mémoire sur les ponts suspendus*, Imprimerie Royale, Paris (1823).

[57] Norwegian Public Roads Administration, www.vegvesen.no.

[58] A. Picon, *Navier and the introduction of suspension bridges in France*, Construction History **4**, 21–34 (1988).

[59] B.G. Pittel, V.A. Yakubovich, *Application of the theory of parametric resonance to explain the collapse of the Tacoma narrows bridge*, (Russian), Uspekhi Mat. Nauk. **15**, 183–184 (1961).

[60] R.H. Plaut, *Snap loads and torsional oscillations of the original Tacoma Narrows Bridge*, Journal of Sound and Vibration **309**, 613-636 (2008).

[61] R.H. Plaut, F.M. Davis, *Sudden lateral asymmetry and torsional oscillations of section models of suspension bridges*, J. Sound Vib. **307**, 894–905 (2007).

[62] W. Podolny, *Cable-suspended bridges*, in *Structural steel designer's handbook: AISC, AASHTO, AISI, ASTM, AREMA and ASCE-07 Design standards*, ed. by R.L. Brockenbrough, F.S. Merritt, 5th edn., McGraw-Hill, New York, (2011).

[63] H. Poincaré, *Les méthods nouvelles de la mécanique céleste*, Dover publication, New York (1957).

[64] W.A. Provis, *Observations on the effects produced by wind on the suspension bridge over the Menai Strait, more especially as relates to the injuries sustained by the roadways during the storm of January, 1839; together with brief notices of various suggestions for repairing the structure.* Trans. Inst. Civil Eng. **3**, 357–370 (1842).

[65] Y. Rocard, *Dynamic instability: automobiles, aircraft, suspension bridges*, Crosby Lock-wood, London (1957).

[66] R.T. Rockafellar, Convex Analysis, Princeton Univ. Press, Princeton, NJ, (1970).

[67] R.H. Scanlan, *Developments in low-speed aeroelasticity in the civil engineering field.*, AIAA J. **20**, 839–844 (1982).

[68] R.H. Scanlan, *The action of flexible bridges under wind, I: flutter theory, II: buffeting theory*, J. Sound Vib. **60**, 187–199 & 201-211 (1978).

[69] P.A. Seaburg, C.J. Carter, *Torsional analysis of structural steel members*, American Institute of Steel Construction, Inc., (2003).

[70] B. Semper, *Finite element approximation of a fourth order integro-differential equation*, Appl. Math. Lett. **7**, 59-62 (1994).

[71] F.C. Smith, G.S. Vincent, *Aerodynamic stability of suspension bridges: with special reference to the Tacoma Narrows Bridge, Part II: mathematical analysis.* Investigation conducted by the Structural Research Laboratory, University of Washington Press, Seattle, (1950).

[72] D.B. Steimann, *Letter to the editor*, ENR **14**, 41–59 (1941).

[73] Tacoma Narrows Bridge collapse, http://www.youtube.com/watch?v=3mclp9QmCGs (1940).

[74] R. Temam, *Infinite-dimensional dynamical systems in mechanics and physics*, Applied Mathematical Sciences 68, Springer (1988).

[75] T. Theodorsen, *General theory of aerodynamic instability and the mechanism of flutter*, National Advisory Committee for Aeronautics, Report no. 496 (1935).

[76] V.Z. Vlasov, *Thin-walled elastic bars*, (Russian) Fizmatgiz, Moscow (1959).

[77] T. von Kármán, M.A. Biot, *Mathematical methods in engineering: An introduction to the mathematical treatment of engineering problems*, McGraw-Hill, New York, (1940).

[78] V.A. Yakubovich, V.M. Starzhinskii, *Linear differential equations with periodic coefficients,* (Russian original: Izdat, Nauka, Moscow, 1972), Wiley,New York (1975).

[79] N.E. Zhukovskii, *Finiteness conditions for integrals of the equation* $d^2y/dx^2+py=0$ (Russian), Mat. Sb. **16**, 582–591 (1892).